

ANALYSIS OF ROLL-FORGING PROCESS

**A THESIS SUBMITTED TO
THE GRADUATE SCHOOL OF NATURAL AND APPLIED SCIENCES
OF
MIDDLE EAST TECHNICAL UNIVERSITY**

**BY
HAKAN KARACAOVALI**

**IN PARTIAL FULFILLMENT OF THE REQUIREMENTS
FOR
THE DEGREE OF MASTER OF SCIENCE
IN
MECHANICAL ENGINEERING**

SEPTEMBER 2005

Approval of the Graduate School of Natural and Applied Sciences

Prof Dr. Canan ÖZGEN
Director

I certify that this thesis satisfies all the requirements as a thesis for the degree of Master of Science.

Prof. Dr. Kemal İDER
Head of Department

This is to certify that we have read this thesis and that in our opinion it is fully adequate, in scope and quality, as a thesis for the degree of Master of Science.

Prof.Dr. Haluk DARENDELİLER
Co-Supervisor

Prof. Dr. Mustafa İlhan GÖKLER
Supervisor

Examining Committee Members

Prof. Dr. R. Orhan Yıldırım (METU,ME) _____

Prof. Dr. Mustafa İlhan GÖKLER (METU,ME) _____

Prof. Dr. Haluk DARENDELİLER (METU,ME) _____

Prof. Dr. Suha Oral (METU,ME) _____

Prof. Dr. Can Çoğun (Gazi University,ME) _____

I hereby declare that all information in this document has been obtained and presented in accordance with academic rules and ethical conduct. I also declare that, as required by these rules and conduct, I have fully cited and referenced all material and results that are not original to this work.

Name, Last name :Hakan, KARACAOVALI

Signature :

ABSTRACT

ANALYSIS OF ROLL-FORGING PROCESS

KARACAOVALI, Hakan

M.S., Department of Mechanical Engineering

Supervisor: Prof. Dr. Mustafa İlhan GÖKLER

Co-supervisor: Prof. Dr. Haluk DARENDELİLER

September 2005, 85 pages

Roll-forging is a metal forming process and mainly used for preform forging of long parts prior to press or hammer forging in the industry. Variable cross sections through the length of billet can be obtained by roll-forging to acquire an adequate distribution of material to the next forging stages. In the design of process and dies used in roll-forging, there are some empirical techniques in literature. However these techniques only provide approximate reduction ratio and elongation during the process and the geometry of the workpiece at the end of each stage cannot be determined exactly by using these techniques.

In this study, multistage roll-forging process has been analyzed by using a finite element analysis software to examine material flow, temperature, stress and strain distribution at each roll-forging step. The geometries at the intermediate stages have been determined. Computer results have been compared to experimental results and good agreement has been observed.

Keywords: Roll-forging, Finite Element Analysis, Preforms in Forging

ÖZ

HADDELI DÖVME İŞLEMİ ANALİZİ

KARACAOVALI, Hakan

Yüksek Lisans, Makine Mühendisliği Bölümü

Tez Yöneticisi: Prof. Dr. Mustafa İlhan GÖKLER

Ortak Tez Yöneticisi: Prof. Dr. Haluk DARENDELİLER

Eylül 2005, 85 sayfa

Haddeli dövme bir metal şekillendirme işlemidir ve endüstride, çoğunlukla uzun parçaların, preste veya çekiçte dövülmesinden önce ön şekillendirilmesi için kullanılır. Sonraki dövme işlemlerinde uygun malzeme dağılımı elde etmek için, haddeli dövme ile iş parçası boyunca değişen kesitler elde edilebilir. Haddeli dövme işleminin ve kullanılan kalıpların tasarımında literatürde ampirik hesap teknikleri bulunmaktadır, ancak bu teknikler kesit küçültme oranı ve uzama için yaklaşık sonuçlar vermektedir ve her bir aşama sonunda, iş parçası geometrisi tam olarak belirlenmemektedir.

Bu çalışmada, çok aşamalı haddeli dövme işleminin her bir aşamasındaki malzeme akışı, sıcaklık, gerilim ve gerinim dağılımını incelemek için sonlu elemanlar analiz yazılımı kullanılarak benzetim yapılmış ve ara aşamalardaki iş parçası geometrileri belirlenmiştir. Bilgisayar sonuçları, deneysel sonuçlar ile karşılaştırılmış ve tutarlı sonuçların elde edildiği gözlenmiştir.

Anahtar Kelimeler: Haddeli Dövme, Sonlu Elemanlar Analizi, Dövmede ön şekillendirme

To My Parents

ACKNOWLEDGMENTS

The author wish to express his deepest gratitude to his supervisor Prof. Dr. Mustafa İlhan Gökler and co-supervisor Prof. Dr. Haluk Darendeliler for their guidance, advices, criticisms, encouragements and insight throughout the research.

The author also would like to thank Cevat Kömürçü and other Aksan Steel Forging Company staff for their helps, suggestions, comments and for providing the roll-forging equipment during the experiment.

The author also thanks to METU-BİLTİR Center and staff for technical support and assistances and for allowing usage of facilities in the center.

Finally, the author wishes to express his sincere thanks to his family for their infinite support and to his friends who encouraged and assured him continuously along this study.

TABLE OF CONTENTS

PLAGIARISM.....	iii
ABSTRACT.....	iv
ÖZ.....	v
DEDICATION.....	vi
ACKNOWLEDGMENTS.....	vii
TABLE OF CONTENTS.....	viii
LIST OF TABLES.....	x
LIST OF FIGURES.....	xi
LIST OF SYMBOLS.....	xiv
CHAPTERS	
I. INTRODUCTION.....	1
1.1 Forging and Classifications.....	1
1.2 Roll-Forging.....	7
1.3 Literature Survey.....	11
1.4 Scope of the Thesis.....	13
II. FINITE ELEMENT METHOD.....	14
2.1. Non-Linear Finite Element Analysis.....	14
2.1.1. Formulations.....	15
2.1.2. Coupled Analysis.....	15
2.1.3. Remeshing/Rezoning.....	16
2.1.4. Friction Model.....	17
2.2. MSC.SuperForm Code.....	18
2.2.1. Thermo-Mechanical Coupling.....	20
2.2.2. Contact.....	21
2.2.3. Remeshing.....	22
III. EXPERIMENTAL STUDY.....	23
3.1. Roll-Forging Machine Used.....	23
3.2. Preparation of the Billet and Forging Rolls for the Experiment.....	29
3.3. Conducting the Experiment.....	29

3.4. Test Results.....	30
IV. FINITE ELEMENT ANALYSIS OF ROLL-FORGING.....	32
4.1. Introduction	32
4.2. FEA of Roll-Forging of the Workpiece by Symmetric Dies.....	40
4.3. FEA of Roll-Forging without Using the Symmetry Assumption.....	52
V. CONCLUSIONS.....	77
5.1 Conclusion	77
5.2 Recommendations for future work	78
REFERENCES.....	80
APPENDIX.....	83
A: FEATURES OF THE ROLL-FORGING MACHINE USED IN THE STUDY..	83
B: MECHANISM ANALYSES OF SECOND ROBOT ARM.....	84

LIST OF TABLES

Table 3.1 Main Features of Roll-Forging Machine	24
Table 3.2 Dimensions of Roll-Forged Workpieces.....	30
Table 4.1 Model Parameters of Stages 1-4	41
Table 4.2 Summaries of Analysis Results of Stages 1-4	41
Table 4.3 Model Parameters of Stages 1- 4	53
Table 4.4 Summaries of Analysis Results of the Stages 1-4.....	53
Table A.1 Features of Roll-Forging Machine used in the Study	83

LIST OF FIGURES

Figure 1.1 (a)Open-die forging , (b) closed-die forging	2
Figure 1.2 Forging Equipments; (a) Hammer, (b) Screw press, (c)Mechanical press, (d) Hydraulic forging press, (e)Horizontal upset forging press	6
Figure 1.3 Typical cross-wedge rolling machine.....	6
Figure 1.4 Various forgings with operations; (a) roll-forging, (b) blocking, (c) finish forging and trimming	8
Figure 1.5 Roll-forging dies and products	9
Figure 1.6 Process of roll-forging	10
Figure 1.7 Roll-forging machine with automatic workpiece handling system	10
Figure 2.1 Fluid structure interactions (Physically Different Domain)	16
Figure 2.2 Metal extrusion with plastic flow coupled with thermal field.....	16
Figure 2.3 Mesh rezoning	17
Figure 2.4 Coulomb friction model.....	18
Figure 2.5 Overview of thermo-mechanical coupled analysis.....	21
Figure 3.1 Layout of the 1600 tones forging production line	24
Figure 3.2 Three main units of the roll-forging machine.....	29
Figure 3.3 Functions of the tong of roll-forging machine.....	26
Figure 3.4 Placement of hydraulic pistons for transverse and rotational movement of tong.....	27
Figure 3.5 Simplified mechanism of the second robot arm	28
Figure 3.6 Hydraulic system placed on linkage F.....	29
Figure 3.7 Samples geometries of the workpiece at the end of each stage of roll- forging operation a) Initial workpiece, b) Stage 1, c) Stage 2, (d) Stage 3, (e) Stage 4.....	31
Figure 4.1 Technical drawing of roll-forging dies in stage 1.....	33
Figure 4.2 Technical drawing of roll-forging dies in stage 2.....	34
Figure 4.3 Technical drawing of roll-forging dies in stage 3.....	35
Figure 4.4 Technical drawing of roll-forging dies in stage 4.....	36
Figure 4.5 (a)Node numbering of element 7 and (b) gaussian iteration points	37

Figure 4.6 Template mesh.....	38
Figure 4.7 Flow diagrams of C45 in various strain rates	38
Figure 4.8 Temperature dependent thermal and mechanical properties of C45	39
Figure 4.9 3D symmetric model of roll-forging process.....	40
Figure 4.10 Equivalent plastic strain and temperature distribution on the symmetric workpiece in stage1	43
Figure 4.11 Equivalent plastic strain and temperature distribution on the symmetric workpiece in the stage 2.....	44
Figure 4.12 Equivalent plastic strain and temperature distribution on the symmetric workpiece in the stage 3	45
Figure 4.13 Equivalent plastic strain and temperature distribution on the symmetric workpiece in the stage 4.....	46
Figure 4.14 Equivalent von Mises stress distribution on the workpiece in stages 1..	47
Figure 4.15 Equivalent von Mises stress distribution on the workpiece in stage 2 ...	48
Figure 4.16 Equivalent von Mises stress distribution on the workpiece in stage 3 ...	48
Figure 4.17 Equivalent von Mises stress distribution on the workpiece in stage 4 ...	49
Figure 4.18 Conversion of symmetrical workpiece to non-symmetrical workpiece .	50
Figure 4.19 Photograph of the experiment sample and captured view of simulated geometry of (a) Stage 1, (b) Stage 2	50
Figure 4.20 Misalignment of workpiece and dies.....	51
Figure 4.21 3D model of roll-forging process	52
Figure 4.22 Equivalent plastic strain distribution on the workpiece in stage1	54
Figure 4.23 Equivalent plastic strain distribution on the workpiece in stage 2	55
Figure 4.24 Equivalent plastic strain distribution on the workpiece in stage 3	56
Figure 4.25 Equivalent plastic strain distribution on the workpiece in stage 4	57
Figure 4.26 Equivalent plastic strain distribution inside the workpiece in stages 1-4	58
Figure 4.27 Temperature distribution on the workpiece in stage 1.....	59
Figure 4.28 Temperature distribution on the workpiece in stage 2.....	60
Figure 4.29 Temperature distribution on the workpiece in stage 3.....	60
Figure 4.30 Temperature distribution on the workpiece in stage 4.....	61
Figure 4.31 Temperature distribution inside the workpiece in stages 1-4	62
Figure 4.32 Equivalent von Mises stress distribution on the workpiece in stage 1 ...	63

Figure 4.33 Equivalent von Mises stress distribution on the workpiece in stage 2 ...	64
Figure 4.34 Equivalent von Mises stress distribution on the workpiece in stage 3 ...	65
Figure 4.35 Equivalent von Mises stress distribution on the workpiece in stage 4 ...	66
Figure 4.36 Equivalent von Mises stresses inside of workpiece in stage 1	67
Figure 4.37 Distribution of von Mises stresses inside of workpiece in stage 2	68
Figure 4.38 Distribution of von Mises stresses inside of workpiece in stage 3	69
Figure 4.39 Distribution of von Mises stresses inside of workpiece in stage 4	70
Figure 4.40 Comparison of experimental and simulated geometry of workpiece in stage 1	71
Figure 4.41 Comparison of experimental and simulated geometry of workpiece in stage 2	72
Figure 4.42 Comparison of experimental and simulated geometry of workpiece in stage 3	73
Figure 4.43 Comparison of experimental and simulated geometry of workpiece in stage 4	74
Figure 4.44 Volume distribution through the length of the workpiece at the end of each stage	76
Figure B.1 Analysis result for one rotation of the roll shaft in 0.857 sec.	85

LIST OF SYMBOLS

\underline{a}	: Nodal point unknown
a_u	: Unknown nodal displacement
a_s	: Specified nodal displacement
\underline{b}	: Body load
E_t	: Total percent elongation
E_i	: Percent elongation at the end of i^{th} stage
\underline{f}^e	: Loads experienced by the elements
f_a	: Applied nodal loads
f_t	: Tangential force
f_n	: Normal reaction.
f_r	: Nodal point reaction forces
\underline{F}	: Concentrated load
\underline{K}^e	: Element stiffness matrix
L_f	: Length of the workpiece at the end of stage
L_s	: Length of the workpiece at the start of stage
L_i	: Initial length of the workpiece
$\underline{N}(\underline{x})$: Shape function
\underline{t}	: Tangential vector in the direction of the relative velocity
\underline{t}	: Surface loads
v_r	: Relative sliding velocity.
$\underline{u}(\underline{x})$: Nodal displacement
Γ^e	: Element Surface
Δ	: Misalignment between surfaces of workpiece and dies
$\underline{\varepsilon}(\underline{x})$: Strain field
μ	: Friction coefficient
σ_n	: Normal stress
σ_f	: Tangential (friction) stress
Ω^e	: Element volume

CHAPTER I

INTRODUCTION

1.1 Forging and Classifications

Forging is a metal forming process in which the deformation takes place under compressive stresses [1]. The wide range of alloys and sizes, combined with excellent mechanical and physical properties has made forgings as a feasible choice for nearly all product areas. The most common applications are in automotive, aerospace, metalworking, power generation industry and mining [2].

Forging process is mainly classified according to die used, which are open-die forging and closed-die forging [3] as seen in Figure 1.1. In open-die forging, the material is allowed to expand freely. Open-die forging is a simple and flexible process, it is slow and resulting size and shape of workpiece is dependent on the skill of the operator. Closed-die forging or impression die forging, is the shaping of hot metal completely within the walls or cavities of die that come together to enclose the workpiece on all sides [3]. The closed dies are made of upper and lower die components, which mate at the parting plane. The parting plane is located at the largest cross-section of the workpiece. The forging stock is generally round or square bar. Bar is cut to length to provide the volume of metal needed to fill the die cavities. In impression die forging, complex shapes can be forged in one or more steps.

Closed die forging can be classified as forging with flash and flashless forging. The flash is an excessive material, which flows out along the parting plane at the end of the operation. Flash generally serves as a part of the die. It chills quicker during the process and causes the increase of pressure inside the die, which results in filling of material to narrow sections of die cavities. Defining the amount of flash is an important fact for the die designers as it is trimmed as scrap at the end of the operation. Scrap is a waste of material and directly affects the part cost. Flashless forging is used to reduce the cost. It is performed in totally enclosed impressions.

The process is used to produce a near-net or net shape forging. The dies make no provision for flash. Actually, a thin fin or ring of flash may form in the clearance between the upper punch and die, but it is easily removed by blasting or tumbling operations, and does not require a trim die [4]. The absence of flash is an advantage for flashless forging over the conventional impression die process, but the process imposes additional requirements. For example, the volume of metal in the workpiece must be controlled within very narrow limits to achieve complete filling of the cavity without developing extreme pressures. Preforming steps must be very well controlled to accomplish the precise weight control in the final die [5].

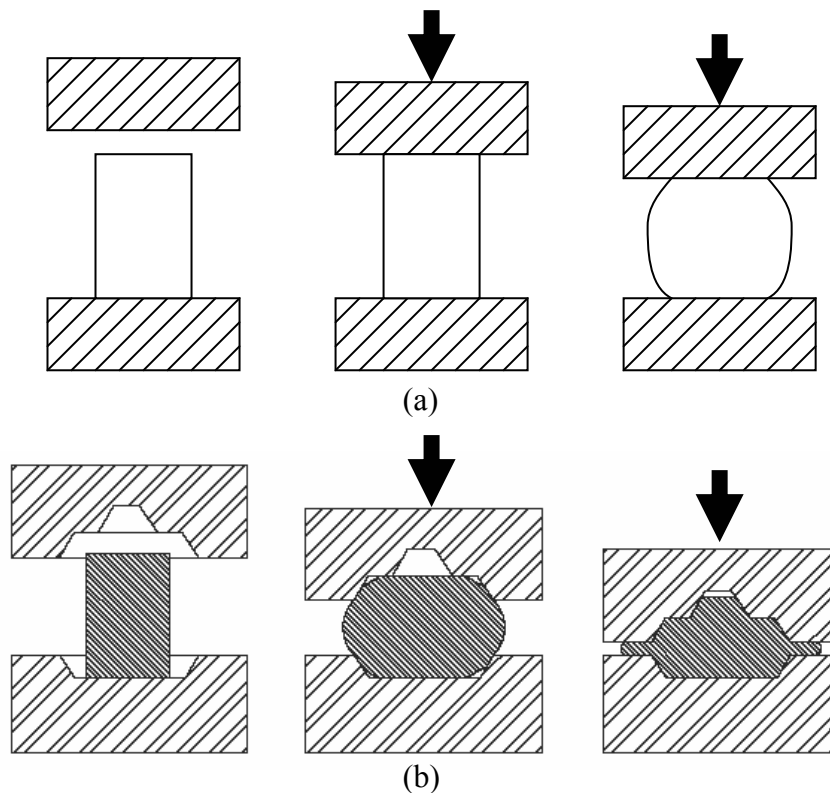


Figure 1.1 (a) Open-die forging, (b) closed-die forging

Forging can also be categorized into three groups according to the forging temperature; cold forging, hot forging and warm forging. Cold forging, which is performed at room temperature, has many advantages; no required heating, precise dimensions (i.e. tight tolerances), improved part strength, better surface finish, material conservation. On the other hand the disadvantages are; high forming

pressures, higher number of preforming steps, required annealing steps during process and low formability [6]. Heavier and more powerful equipments are required in cold forging compared to hot or warm forging [7].

The advantages of hot forging which takes place over the recrystallization temperature of material, are the possibility to forge complex shapes, good formability, low forming pressures, forging parts of higher weight and volume. The disadvantages are the formation of scale, decreased accuracy (larger tolerances) [6] etc. Die costs are comparatively less in this process.

If the forging is performed somehow below but near the recrystallization temperature of forged material then the operation is named as warm forging. Compared to hot forging, the warm regime has less energy consumption (decrease energy in preheating the workpiece), produce less scaling, provide better dimensional control, less scrap, and longer tool life (there is less thermal shock and thermal fatigue). However, warm forging is still a developing field. Material behavior is less characterized at these temperatures. Lubricants have not been fully developed for the operation. Nevertheless, the pressure of energy conservation concerns will definitely favor the increased use of warm working [7]. Compared to cold forging, warm forging offers the advantages of reduced loads on tooling and equipment and increased material ductility. For high-carbon steels, it may be possible to eliminate the need to anneal the material prior to forging. Also, subsequent heat treatment operation may be eliminated. Disadvantages are high tooling costs and tooling must withstand forging pressures as well as high temperatures [6].

Forging processes are also classified according to the equipment used and principle of operation [3]; hammer forging and screw press forging (energy-restricted), mechanical press forging (stroke-restricted), hydraulic press forging (force-restricted) and upset-forging. These forging equipments are shown in Figure 1.2. Historically hammers have been the most widely used type of equipment for forging. They are the least expensive and most flexible type of forging equipment. Hammers are capable of developing large forces and have short die contact time. In operation

of hammer forging, the workpiece is placed on lower die. The ram moves downward, exerting a force on the anvil and causing the workpiece to deform. More than one blow are very common on hammers.

Mechanical presses employ flywheel energy, which is transferred to the workpiece by a network of gears, cranks, eccentrics or levers. The ram stroke is shorter than that of hammer forging or hydraulic press forging. The ram speed is the greatest in the middle of the stroke and force is greatest at the bottom of the stroke. Compared to hammer forging, mechanical press forging, results in accurate close-tolerance parts and higher production rates. Mechanical presses permit automatic feed and transfer mechanism to feed, pick up and move the part from one die to the next. Because the dies used with mechanical presses are subject to squeezing forces instead of impact forces, harder die materials can be used in order to extend die life. Dies can also be less massive in mechanical press forging. Mechanical presses have higher initial cost than hammer presses [3].

Hydraulic presses are used for both open- and closed-die forging. In hydraulic presses, after rapid approach speed, the ram (with upper die attached) moves at a slower speed while exerting a squeezing force on work metal. Deformation rate can be controlled or varied during the stroke if required. This is especially important when forging metals that are susceptible to rupture at high deformation rates. The slower action of a hydraulic press increases contact time between the dies and the workpiece and this results in shortened die life because of heat transfer from the hot work metal to the dies when forging materials at high temperatures (such as nickel base alloys and titanium alloys). The initial cost of the hydraulic press is higher than that of mechanical press.

Screw presses are energy-restricted machines, and they use energy stored in a flywheel to provide the force for forging. The rotation energy or inertia of the flywheel is converted to linear motion by a threaded screw attached to the flywheel on one end and to the ram on the other end. Screw presses are used for both open- and closed-die forging. They usually have more energy available per stroke than

mechanical presses with similar tonnage ratings, permitting them to accomplish more work per stroke. Die height adjustment is not critical, and press cannot jam.

Upset forging involves increasing the diameter of the end or central portion of a bar of metal by compressing its length. Parts are upset-forged both hot and cold on special high-speed machines in which the workpiece is moved from station-to-station. Some machines can forge bars up to 250 mm in diameter [7]. In the upset-forging process, segments of heated metal can be sheared from the bar as it moves into position in the die, which permits continuous production of a number of pieces from a single coil or length of feedstock. Upset-forging machines are used to forge heads on bolts and other fasteners, valves, coupling, and many other small components.

Most of the forgings require more than one forging step due to process limitations. Hence preform forging may be necessary, in which stock is shaped to a predetermined size and contour prior to subsequent die forging operations to save material and number of hits in subsequent forging in closed dies. Drawing, fullering, flattening, edging, bending, cross-wedge rolling, roll-forging or upsetting may be used as preforming process [8].

Cross-wedge rolling is a technique for forging axisymmetric preforms, which is very productive but has a limited application since it can only produce axisymmetric preforms [9]. Cross-wedge rolling machine operate with low noise and vibrations, and they are easy for automization and it does not require lubrication and cooling. Cross-wedge rolling is also used to produce blanks for machining and on automatic lathes and plunge-type grinding machines. Cross-wedge rolling is highly flexible to continue with other forging process. All materials are cross rollable, if they are forgeable in hot, warm, cold forging.

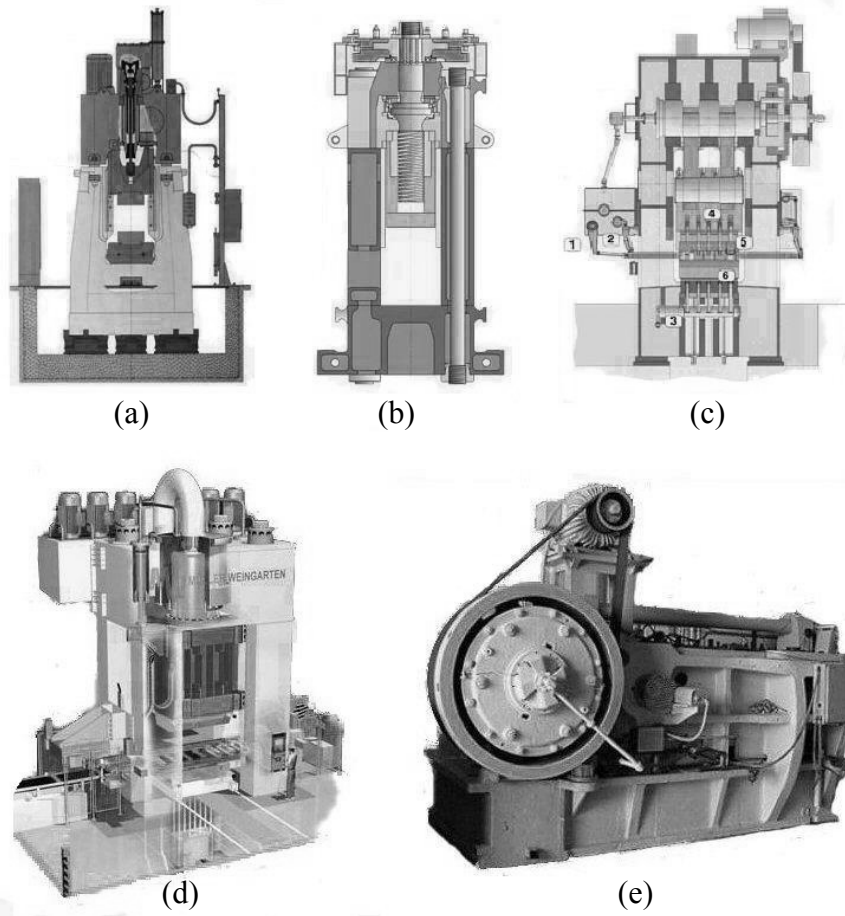


Figure 1.2 Forging Equipments; (a) Hammer, (b) Screw press, (c) Mechanical press, (d) Hydraulic forging press, (e) Horizontal upset forging press [10]

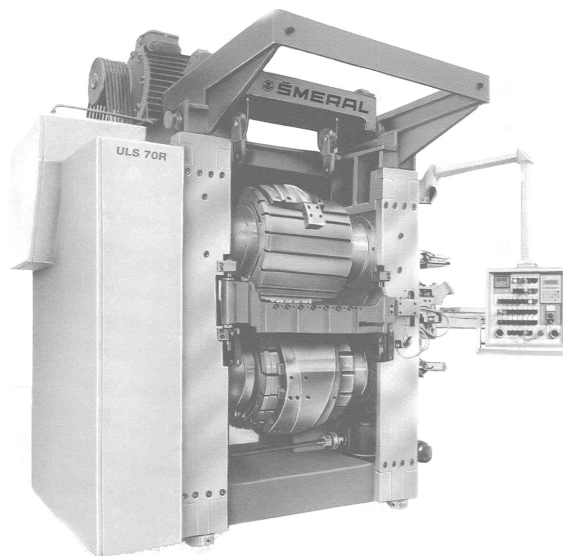


Figure 1.3 Typical cross-wedge rolling machine [11]

1.2 Roll-Forging

Roll-forging is a process by which a varying section along the longitudinal direction of workpiece can be obtained by using rolling dies and is also called reducer-rolling. It has remarkable advantages such as high productivity; high utilization rate of material, good labor conditions, long life of the rolling dies etc [9]. In addition, due to the rational stream-line-distribution of metal fibers and uniformly distributed metallographic structure, roll-forging products exhibit better mechanical properties and reliability than those manufactured by die-forging or machining [12]. Roll-forging may serve as both main operation and preform forging operation. Application in the first category generally involves the shaping of long, thin, usually tapered parts. Typical examples are airplane propeller blade half sections, tapered axle shafts, tapered leaf springs, table knife blades, hand shovels and spades, various agricultural tools such as chisels and trowels. Roll-forging is sometimes followed by the upsetting of one end of workpiece to form a flange, as in the forging of axel shafts. Application in the second category includes preliminary shaping of stock, preform, prior to forging in closed die in either a press or hammer, which generally eliminates a fullering or blocking operation. Crankshafts, connecting rods and other automotive parts are typical products that are first roll-forged to get preform and then blocked, finish forged and trimmed, respectively as shown in Figure 1.4 [3].

Roll-forging machines use specially designed dies with roll segments. The cavities in the roll segments can be designed to obtain both a continuous and sudden change of sections. There are three types of roll-forging dies; these are flat back, semi-cylindrical and fully cylindrical dies [3].

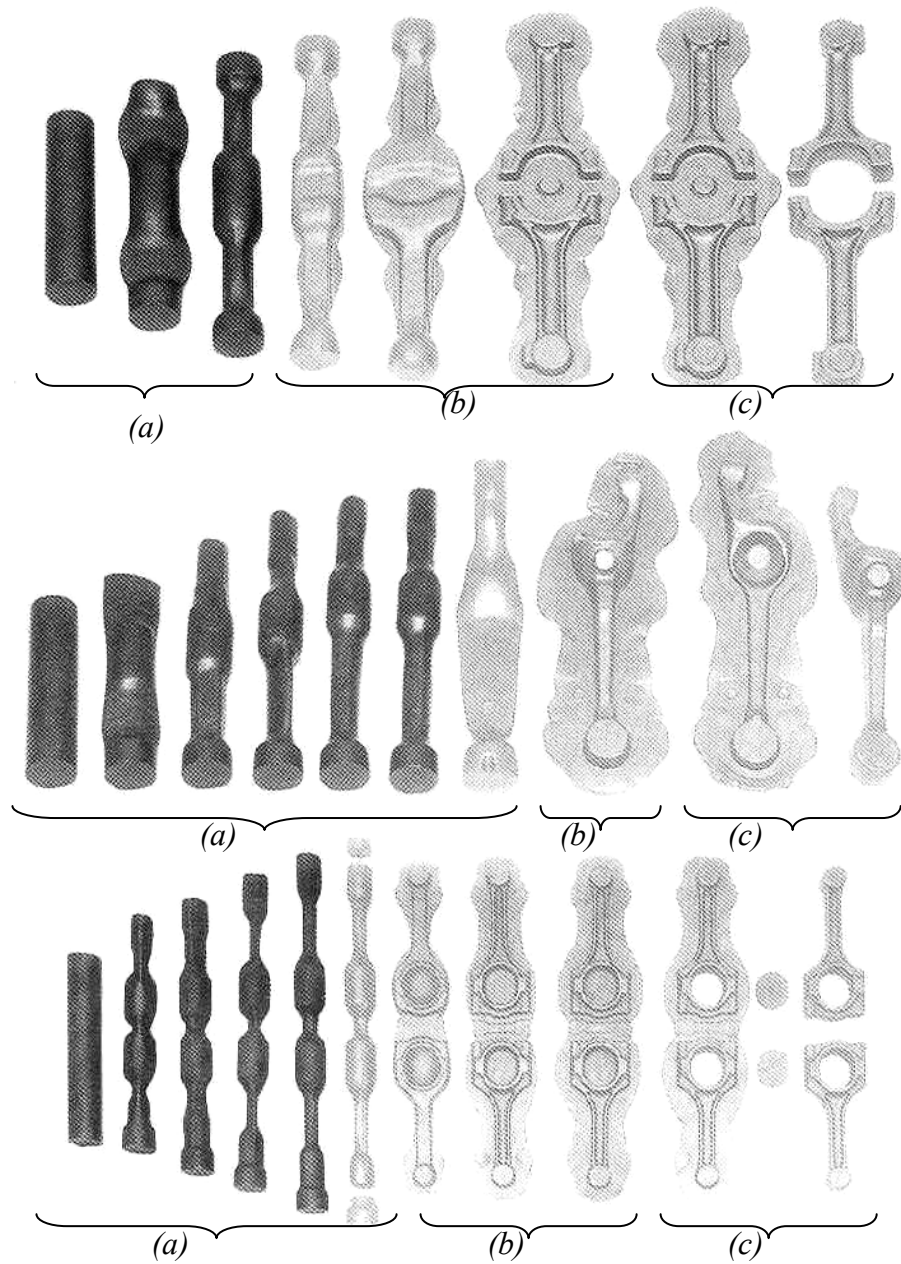


Figure 1.4 Various forgings with operations; (a) roll-forging, (b) blocking, (c) finish forging and trimming [13]

In Figure 1.5, flat back and semi-cylindrical dies and product can be seen. Flat back dies are primarily used for short length reductions. They are bolted to the roll shafts and can be easily changed. Semi-cylindrical dies are well suited to the forging of medium length workpieces. Most are true half cylinders (180°), although some, particularly in large sizes, may encompass up to 220° of a circle to provide sufficient

roll-forging machines are equipped with automatic workpiece handling systems to increase productivity as seen in Figure 1.7.

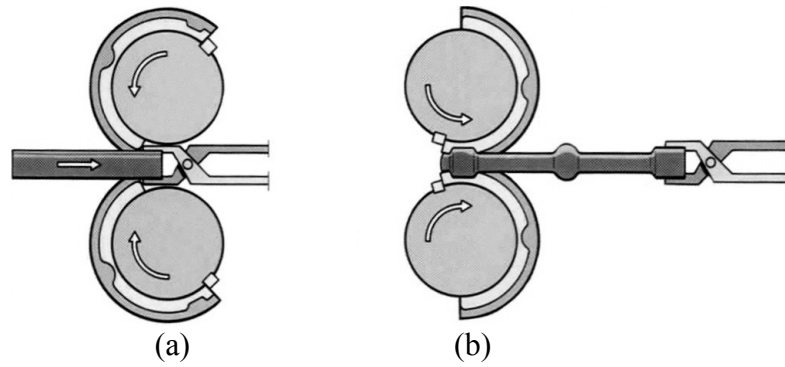


Figure 1.6 Process of roll-forging

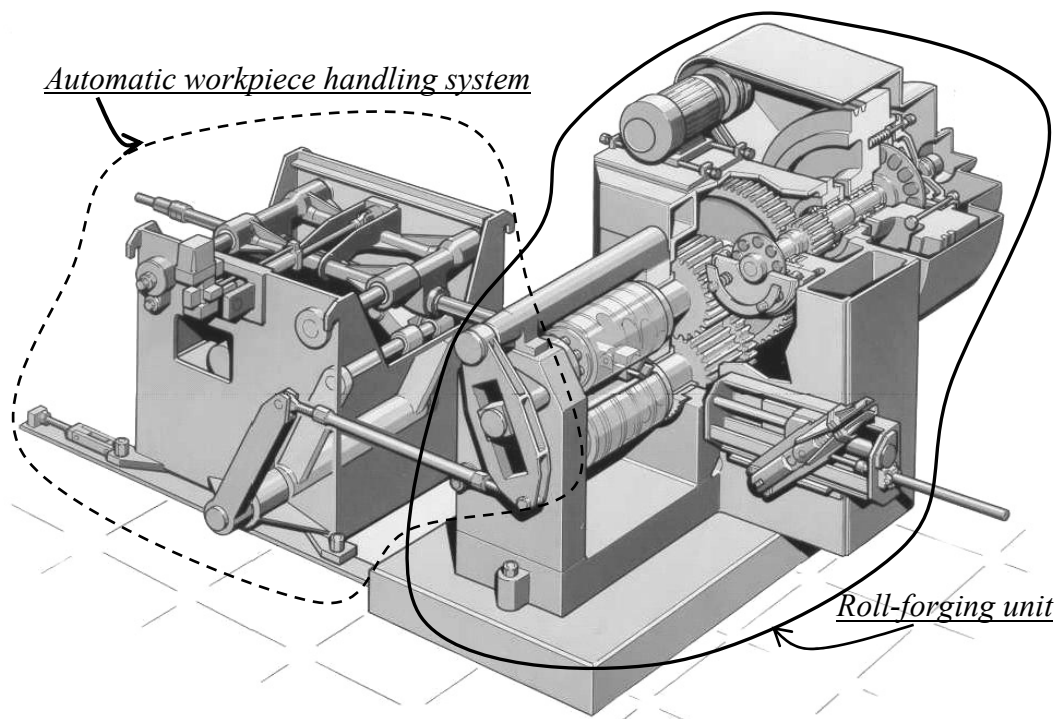


Figure 1.7 Roll-forging machine with automatic workpiece handling system [13]

1.3 Literature Survey

A high portions of forgings have a long straight axis [14]; including such items as connecting rods, spanners; etc. Forging of this type requires several preforming stages in order to produce the finished forging from the bar stock used [15]. According to Chan and Knight [16], if the cross section area of forging varies appreciably, material must be redistributed along the length by drawing down the bar at various points. On this issue, Biswas and Knight [17] have advised that preform is satisfactory if the material distribution is close to final product as much as possible with smoother curves and larger radii in profile in order to promote good material flow in the final die and thereby extend its life.

Biswas and Knight have developed a computer program for roll-forging die design, which embodies the various preform design rules formulated that based of experience [14]. Another CAD software (VeraCAD) has been developed by H. Eratz by using empirically based forging rules [18]. This software automatically calculate the mass distribution of part and gives optimum number of dies and operations.

Zhong-Yi Cai [12] has presented conjugate surface principal, which is an analytical approach to design of roll-forging dies of front axel rods of automobiles, for the design of roll-forging dies.

A number of studies have been conducted on preform forging in METU-BİLTİR Center [19-24]. Alper [19], developed a computer program for axisymmetric press forging, which designs the forging geometry and the die cavity for preform and finishing operation. Kutlu [20] studied on the design and analysis of preforms in hot forging for non-axisymmetric press forging. In his study, the importance of volume distribution along the length of part has been shown for reducing the wear of finishing die and process of forging of gear fork has been revised to reduce wear of dies and waste of material.

Karagözler [21] studied on the die cavity for preforms and finishing operations of the forgings with non-planar parting surfaces.

A study by Gülbahar [22], propose a method for design of preform dies of heavy vehicle steering joint to distribute material properly for a part and reduce the material wastage, number of applied strokes and production costs.

In the study of Doğan [23], the effects of tapered preform shapes on the final product in cold upset forging have been investigated by using the elastic-plastic finite element method. Kazancı [24] has shown that the upset forging can also be used for the preforming operation for some press forgings or hammers.

One of the easiest and fastest techniques to produce a preform is the roll-forging. By the aid of the roll-forging dies, material dislocation on the longitudinal axis can be realized easily. Cross section changes along the longitudinal (rolling) direction make the roll pass design difficult. The velocity of the forged product is greater at exit section than the circumferential velocity of roll. It is therefore necessary to determine the velocity increase of rolled workpiece at every section so that the circular arc length on roll segment can be reduced compared with the required length of rolled workpiece. To improve production efficiency and product quality, process designers must optimize the amount of elongation at each roll pass. Process design for roll-forging is highly dependent on the experience of designers and empirical rules based on numerous experiments. Such rules are mostly focused on flow mechanism of workpiece such as spread and elongation for various roll groove geometries without considering the effect of various process variables and material properties. It is important to predict heat transfer in the workpiece properly because the change of microstructure depending on temperature will affect the flow characteristics of material and roll pressure [25]. Because of reasons mentioned above, numerical analysis of process is adequate to reduce the number of trial and errors of design stage and to consider the effects of processing variables such as stress, strain and temperature distribution in the deformed workpiece, which increases the cost and results in waste of material when obtained by trial and error approach.

Roll-forging requires 3D analysis due to its nature and hence requires powered computer with high speed of computing. To the best knowledge of the author there is no study on 3D Finite Element Analysis (FEA) of roll-forging process.

1.4 Scope of the Thesis

The aim of this thesis study is to make use of benefits of FEA technique in the design of roll-forging process and dies used. Since the FEA technique tremendously reduces the requirement for experienced person or empirical formulations developed with several years of company experience. It is very important to input correct data such as initial condition, material properties, die and workpiece geometry, process time, die and tong velocities etc. in the finite element analysis. After the finite element analysis of process on computer, verification of the results is required to ensure the input of data correctly. Verification process requires the experimental study.

The scope of the study is to analyze the multistage roll-forging process based on the finite element analysis and experimental studies. In Chapter 2, Finite Element Method has been presented. Experimental study conducted in AKSAN Steel Forging Company and results have been demonstrated in Chapter 3. In Chapter 4, two Finite element models of the process by considering symmetry and non-symmetry cases and results of computer simulation have been presented. Finally, conclusions and recommendations for future study have been given in Chapter 5.

CHAPTER II

FINITE ELEMENT METHOD

The principles of Finite Element Method, which is used in the analysis of roll-forging process, are given in this chapter.

2.1. Non-Linear Finite Element Analysis

The Finite Element Method is a numerical technique, which is widely used for the solution of complex parts. In this method, bodies to be analyzed are divided into small finite number of material domains. These domains are called elements. By using the Finite Element Method, complex structural, heat transfer, electrical, solid mechanics, robotics and nuclear problems are easily solved [3].

When the stiffness matrix is dependent on the displacement, the system is called non-linear. The three major types of nonlinearities are material nonlinearity, geometric nonlinearity and boundary nonlinearity. Plasticity, creep and viscoelasticity results in material nonlinearities, large deformations, large strains and buckling cause geometric nonlinearities, and contact and follower force cause the boundary nonlinearities [26].

Nonlinear problems are inherently more complex to analyze than linear problems, and the "principle of superposition", which states that the resultant deflection, stress, or strain in a system due to several forces is the algebraic sum of their effects when separately applied, no longer applies.

Nonlinear analysis is usually more expensive than linear analysis. In general, the solutions of nonlinear problems always require incremental solution schemes and sometimes require iterations (or recycles) within each load/time increment to ensure that equilibrium is satisfied at the end of each step.

The commonly used iterative procedures are Newton-Raphson, Modified Newton-Raphson, Newton-Raphson with strain correction modification, and a secant procedure. Widely used one is the full Newton-Raphson (N-R) method, which assembles and solves the stiffness matrix in the every iteration. It has quadratic convergence properties, which means in subsequent iterations the relative error decreases quadratically and gives satisfactory results for most nonlinear problems.

2.1.1. Formulations

There are two fundamentally different approaches for the description of mechanical problems; the Eulerian method and the Lagrangian method. In the Eulerian method, the finite element mesh is fixed in space and the material flows through the mesh. This approach is particularly suitable for analysis of steady-state processes, such as the steady-state extrusion process [26] and in fluid mechanics, and has advantages when the constitutive equations depend on current strains, not strain rates. Another problem exists when treating free surfaces, particularly if there are distributed loads applied to these surfaces. These problems are more easily handled by the Lagrangian method. In the Lagrangian method, the finite element mesh is attached to the material and moves through space along with the material. There is no difficulty in establishing stress or strain histories at a particular material point and the treatment of free surfaces is natural and straightforward. There are two varieties of Lagrangian method: the total Lagrangian method and the updated Lagrangian method. In the total Lagrangian method, the mesh coordinates are not updated to the new positions. In the updated Lagrangian method, the coordinates of the mesh are updated after each increment.

2.1.2. Coupled Analysis

The definition of coupled systems includes the multiple domains and independent or dependent variables describing different physical systems. Coupled systems can be classified into two categories [27] as interface variables coupling problems and field variables coupling problems. In the interface variable coupling problems, the coupling occurs through the interfaces of the domain. The domains can be physically different (for example, fluid-solid interaction) or physically the same but with

different discretization (for example, mesh partition with explicit/implicit procedures in different domains) (Figure 2.1). In the field variables coupling problems, whether the domain is the same or different, the coupling occurs through the governing differential equations describing different physical phenomenon as in coupled thermo-mechanical problems (Figure 2.2). The types of coupled analysis can be listed as follows; fluid-solid, fluid thermal, fluid-solid-thermal interaction, piezoelectric, thermo-electrical (Joule heating), thermo-mechanical, electrical-thermal-mechanical (Joule Mechanical), fluid-soil (pore pressure), and electromagnetic problems.

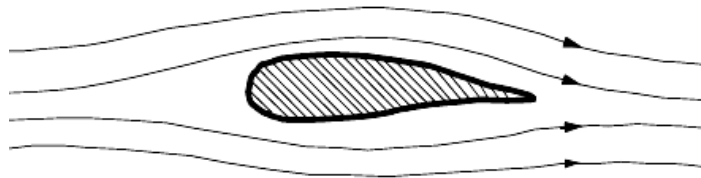


Figure 2.1 Fluid structure interactions (Physically Different Domain)[27]

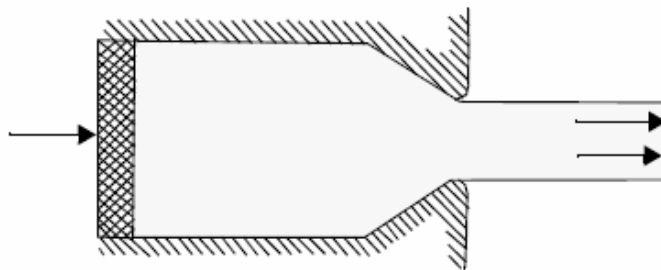


Figure 2.2 Metal extrusion with plastic flow coupled with thermal field [27]

2.1.3. Remeshing/Rezoning

In manufacturing simulations, the objective is to deform the workpiece from some initial (simple) shape to a final, often complex shape. The numerical deformation analysis of the material results in mesh distortion. For this reason, it is often required to perform a rezoning/remeshing step. At the remeshing step a new mesh is created; the current state of deformation, strains, stresses, etc. are transferred to the new mesh [26]. In Figure 2.3, example to a rezoning of 2D mesh is given.

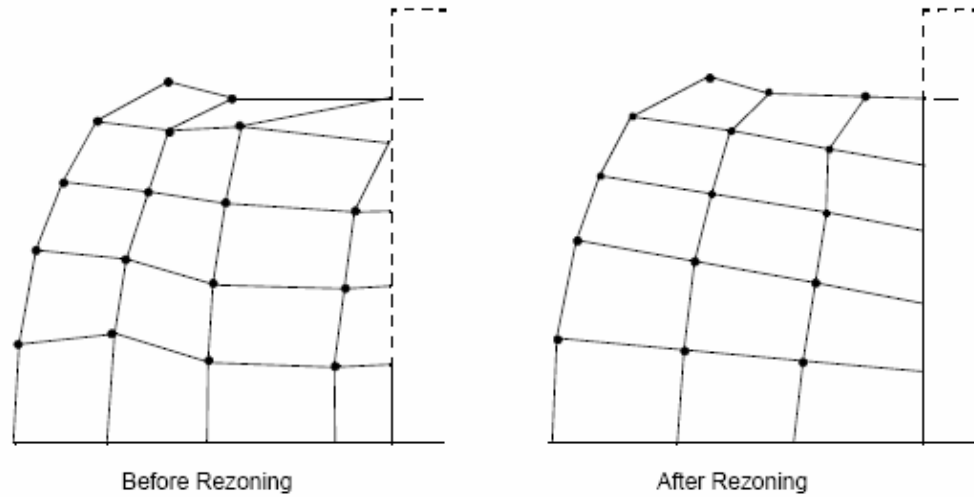


Figure 2.3 Mesh rezoning [26]

2.1.4. Friction Model

Friction is a complex physical phenomenon that involves the characteristics of the surface such as surface roughness, temperature, normal stress, and relative velocity. The most popular friction model is the Adhesive Friction or Coulomb Friction model. This model is one of the most widely model for most applications [28] and is illustrated in Figure 2.4.

The Coulomb model is:

$$\sigma_f \leq -\mu\sigma_n \cdot \mathbf{t} \quad (2.1)$$

where, σ_n is the normal stress, σ_f is the tangential (friction) stress, μ is the friction coefficient, \mathbf{t} is the tangential vector in the direction of the relative velocity determined as

$$\mathbf{t} = \frac{\mathbf{v}_r}{|\mathbf{v}_r|} \quad (2.2)$$

where, v_r is the relative sliding velocity. The Coulomb model can also be often written with respect to forces

$$f_t \leq -\mu f_n \cdot \mathbf{t} \quad (2.3)$$

where, f_t is the tangential force, f_n is the normal reaction. For a given normal stress, the friction stress has a step function behavior based upon the value of v_r or Δu .

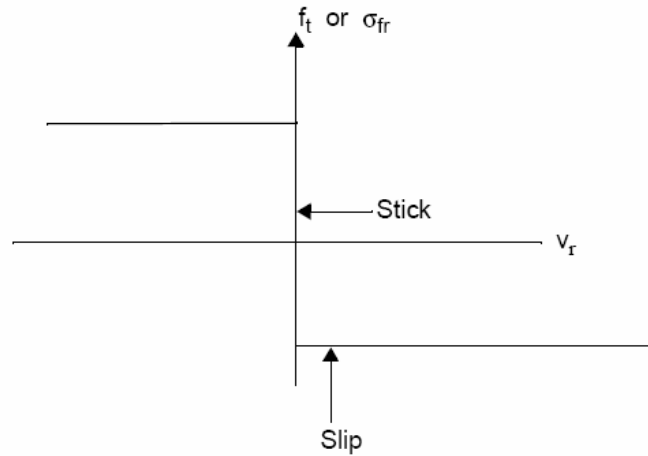


Figure 2.4 Coulomb friction model [26]

2.2. MSC.SuperForm Code

The MSC.SuperForm has been used in this study. The finite element method implemented in MSC.SuperForm has the following six steps [29].

Step 1 Shape Functions: The FEM expresses the unknown field, $u(\mathbf{x})$, in terms of the nodal point unknowns, \underline{a} , by using the shape functions, $\underline{N}(\underline{x})$, over the domain of the element, Ω^e , as,

$$\underline{u}(\underline{x}) = \underline{N}(\underline{x})\underline{a}^e \quad (2.4)$$

Step 2 Material Loop: The FEM expresses the dependent flux fields, $\underline{\varepsilon}(\underline{x})$, such as the strain (stress) or heat flux in term of the nodal point unknowns as,

$$\underline{\varepsilon}(\underline{x}) = \underline{L}[\underline{u}(\underline{x})] = \underline{B}\underline{a} \quad (2.5)$$

$$\underline{\sigma} = \underline{\sigma}(\underline{\varepsilon}) = \underline{D} \underline{\varepsilon}(\underline{x}) \quad (2.6)$$

Step 3 Element Matrices: The FEM equilibrates each element with its environment, which can be expressed as,

$$\underline{K}^e \underline{a}^e + \underline{f}^e = 0 \quad (2.7)$$

where the element matrices, \underline{K}^e and \underline{f}^e , have consistently lumped all physical significance of the element at its nodes,

Where:

$$\underline{K}^e = \int_{\Omega^e} \underline{B}^T \underline{D} \underline{B} dV \quad (2.8)$$

$$-\underline{f}^e = \int_{\Omega^e} \underline{N}(\underline{x})^T \underline{b} dV + \int_{\Gamma^e} \underline{N}(\underline{x})^T \underline{t} dS + \underline{F} \quad (2.9)$$

are the element matrices. \underline{K}^e represents physical properties such as stiffness or conductivity, and \underline{f}^e , represents loads experienced by the element, . These loads may be: body loads, \underline{b} , such as weight or internal heat generation in volume Ω^e ; surface loads, \underline{t} , such as pressure or convection on surface Γ^e ; or concentrated loads, \underline{F} .

Step 4 Assembly: The FEM assembles all elements to form a complete structure in such a manner to equilibrate the structure with its environment, which requires,

$$\underline{K} = \sum_e \underline{K}^e \quad (2.10)$$

$$\underline{f} = \sum_e \underline{f}^e \quad (2.11)$$

and to insure continuity of nodal point unknowns, $\underline{a} = \underline{a}^e$. Therefore, a finite number of system equations results as,

$$\underline{K}\underline{a} + \underline{f} = 0 \quad (2.12)$$

Step 5 Solve Equations: The FEM specifies the boundary conditions, namely, the nodal point values on the boundary and the system equations are partitioned as,

$$\begin{bmatrix} \underline{\mathbf{K}}_{uu} & \underline{\mathbf{K}}_{us} \\ \underline{\mathbf{K}}_{su} & \underline{\mathbf{K}}_{ss} \end{bmatrix} \begin{bmatrix} \underline{\mathbf{a}}_u \\ \underline{\mathbf{a}}_s \end{bmatrix} = - \begin{bmatrix} \underline{\mathbf{f}}_a \\ \underline{\mathbf{f}}_r \end{bmatrix} \quad (2.13)$$

where: $\underline{\mathbf{a}}_u$ are the unknown nodal values; $\underline{\mathbf{a}}_s$ are the specified nodal values; $\underline{\mathbf{f}}_a$ are the applied nodal loads; $\underline{\mathbf{f}}_r$ are the nodal point reactions. Hence the solution becomes,

$$\underline{\mathbf{a}}_u = -\underline{\mathbf{K}}_{uu}^{-1} (\underline{\mathbf{f}}_a + \underline{\mathbf{K}}_{us} \underline{\mathbf{a}}_s) \quad (2.14)$$

$$\underline{\mathbf{f}}_r = -(\underline{\mathbf{K}}_{su} \underline{\mathbf{a}}_u + \underline{\mathbf{K}}_{ss} \underline{\mathbf{a}}_s) \quad (2.15)$$

Step 6 Recover: The FEM recovers the stresses by substituting the unknown nodal values found in Step 5 back into Step 2 to find the dependent flux fields such as strain, stress and heat flux.

Simulation of the forging process is complicated by the large displacement and the large strains that the material is subjected to. Because of the large displacements, the relationship between the strain and the displacement becomes nonlinear. The influence of large strains results in nonlinear stress-strain relationship. There are two procedures available in MSC.SuperForm for solving these problems; Elastic-plastic and rigid-plastic method. In the elastic-plastic method, the equations of equilibrium are formulated by using the updated Lagrangian method, while in the rigid-plastic procedure; the updated Eulerian method is used.

2.2.1. Thermo-Mechanical Coupling

Many operations performed in the metal forming industry (such as casting, extrusion, sheet rolling, and stamping) can require a coupled thermo-mechanical analysis. The observed physical phenomena must be modeled by a coupled analysis if the following conditions pertain:

The body undergoes large deformations such that there is a change in the boundary conditions associated with the heat transfer problem.

Deformation converts mechanical work into heat through an irreversible process, which is large relative to other heat sources.

In either case, a change in the temperature distribution causes to the deformation of the body through thermal strains and influences the material properties [27]. In Figure 2.5 is an overview for physical effect attributing to coupling between heat transfer part and mechanical part.

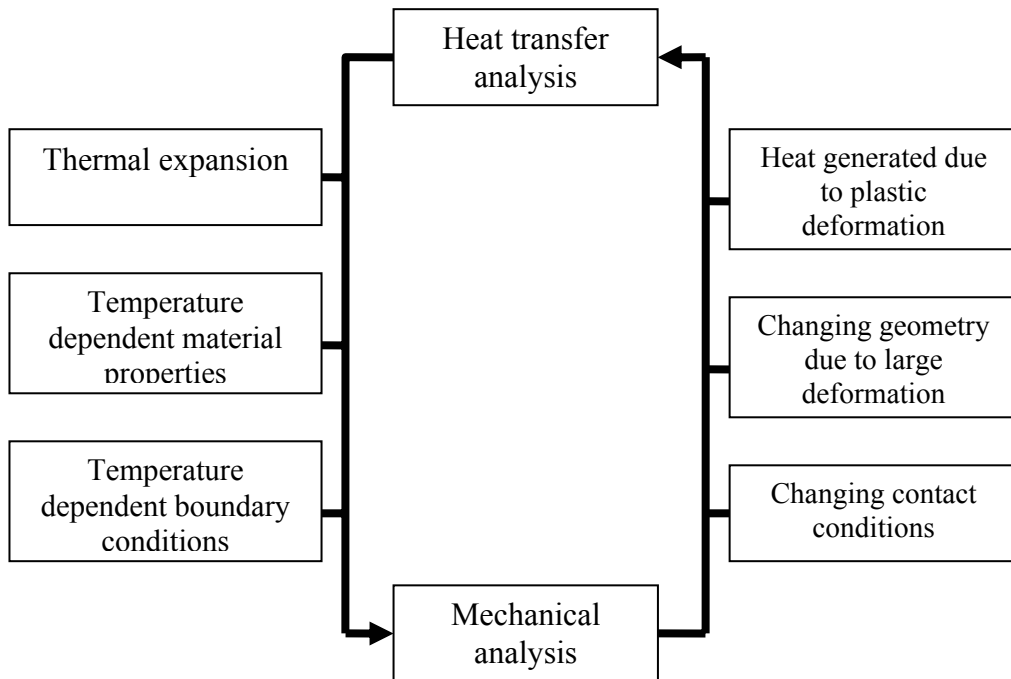


Figure 2.5 Overview of thermo-mechanical coupled analysis [28]

2.2.2. Contact

Through the contact algorithm, the boundary conditions are automatically generated. The analysis of contact behavior is complex because of the requirement to accurately track the motion of multiple geometric bodies, and the motion due to the interaction of these bodies after contact occurs. This includes representing the

friction between surfaces and heat transfer between the bodies if required. The numerical objective is to detect the motion of the bodies, apply a constraint to avoid penetration, and apply appropriate boundary conditions to simulate the frictional behavior and heat transfer. Furthermore, contact simulation has often required the use of special contact or gap elements [26]. MSC.SuperForm allows contact analysis to be performed automatically without the use of special contact elements. A robust numerical procedure to simulate these complex physical problems has been implemented in MSC.SuperForm.

2.2.3. Remeshing

Excessive finite element mesh deformation results in analysis errors. When needed MSC.SuperForm automatically remeshes the geometry and transfers all quantities from an existing mesh to a new mesh. The provided parameters that control the automatic remeshing process are increment, strain change and immediate [26]. Increment parameter ensures that the remeshing process occurs as often as indicated. Strain change parameter defines when the remeshing must be done once the total effective strain since the previous remeshing reaches a critical value. The default value is 0.40. Immediate parameter forces the mesh generation before the analysis step starts.

CHAPTER III

EXPERIMENTAL STUDY

In this chapter, working principals and features of the roll-forging machine used in the study are introduced and the experimental results of roll-forging process conducted in an industrial forging plant are presented.

3.1. Roll-Forging Machine Used

The roll-forging machine, which is used in the experiments, is from one of the forging production lines in Aksan Steel Forging Company located in Ankara. In this particular production line, named as the 1600 tones forging line, there are a silo, a billet transfer equipment, an induction heater, roll-forging machine, conveyor, mechanical forging press of 1600 tones and trimming press of 160 tones as seen in Figure 3.1. After the billets are cut into the size, they are supplied into the silo. The billet transfer equipment seizes the billet and supplies into the induction heater which ensures the heating of workpiece homogenously. The robot arms of roll-forging machine take and feed the heated bar between roll-forging dies. A series of roll-forging process is applied on the billet to obtain the preform shape. Further preform and finish forging operations are performed on the 1600 tones mechanical forging press. Parts are trimmed by using 160 tones mechanical trimming press.

Roll-forging machine in this line is ARWS model of SMS.Eumuco GmbH which is seen in Figure 1.3 and used for preform forging. It complies and reduces the duty of the mechanical press and extends the lifetime by eliminating the fullering. The main features of the roll-forging machine are given in Table 3.1 and in Appendix A. The roll-forging machine has three main units. These are; the first robot arm, roll-forging unit and the second robot arm. Dashed lines in Figure 3.2 designate those units.

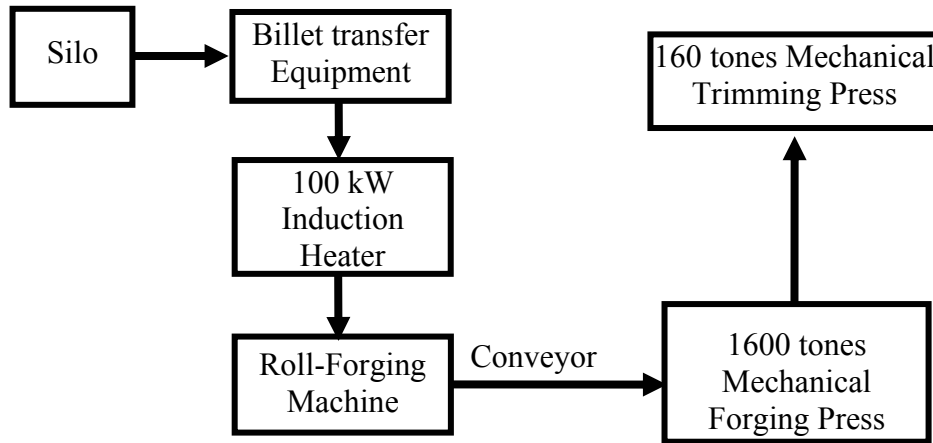


Figure 3.1 Layout of the 1600 tones forging production line

The first robot arm, which is actuated by pneumatic pistons, takes the hot workpiece coming from the induction furnace and transfers it to the second robot arm.

Table 3.1 Main Features of Roll-Forging Machine

Roll shaft diameter	240 mm
Maximum available die diameter	368 mm
Rotational velocity of roll shaft	79 rpm
Maximum diameter of workpiece	55 mm
Power of motor	15 kW

The deformation takes place in the roll-forging unit. It is composed of the main body which holds roll shaft, gear system, coupling system, flywheel, pulley, 15kW electric motor. Roll-forging dies are mounted on the roll shafts as seen in Figure 3.3. Maximum six couples of semi-cylindrical roll-forging dies can be mounted on roll shafts. Upper and lower roll shaft rotates in reverse directions by the help of gears. The flywheel is driven by the pulley and the electric motor. To rotate the roll shafts, a coupling system is used between the flywheel and the roll shafts. The flywheel and roll shaft are connected by coupling for one full cycle. Then after one cycle, the roll shaft and the flywheel decouple.

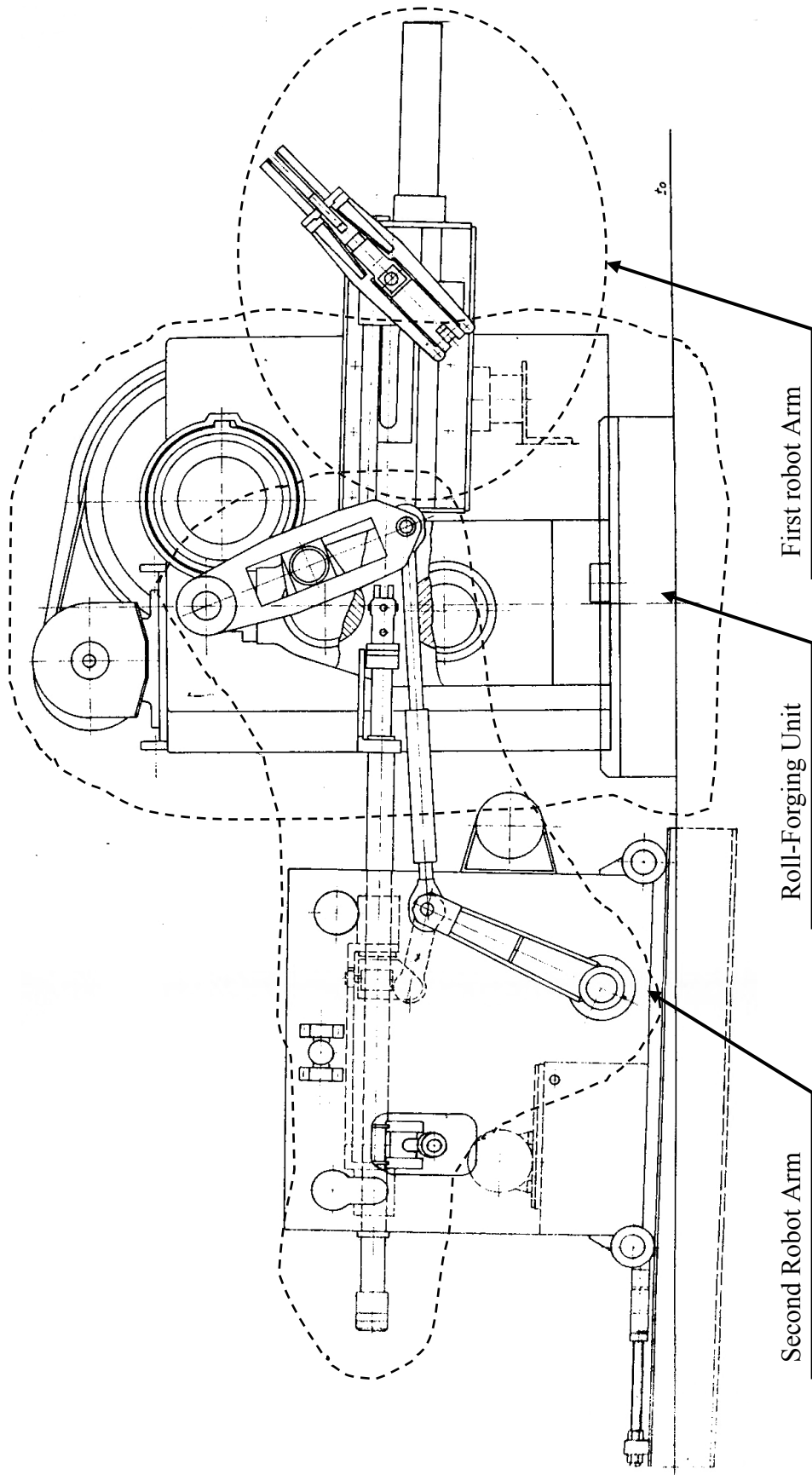


Figure 3.2 Three main units of the roll-forging machine [30]

The second robot arm holds the workpiece during the roll-forging process. (Figure 3.3). It also controls the rotation of billet in both clockwise and counterclockwise directions, since in multistage roll-forging processes it is necessary for workpiece to be rotated by 90 degrees about its centerline. When it is required to use more than one dies, it provides the tong motion on transverse to the longitudinal axis of the billet.

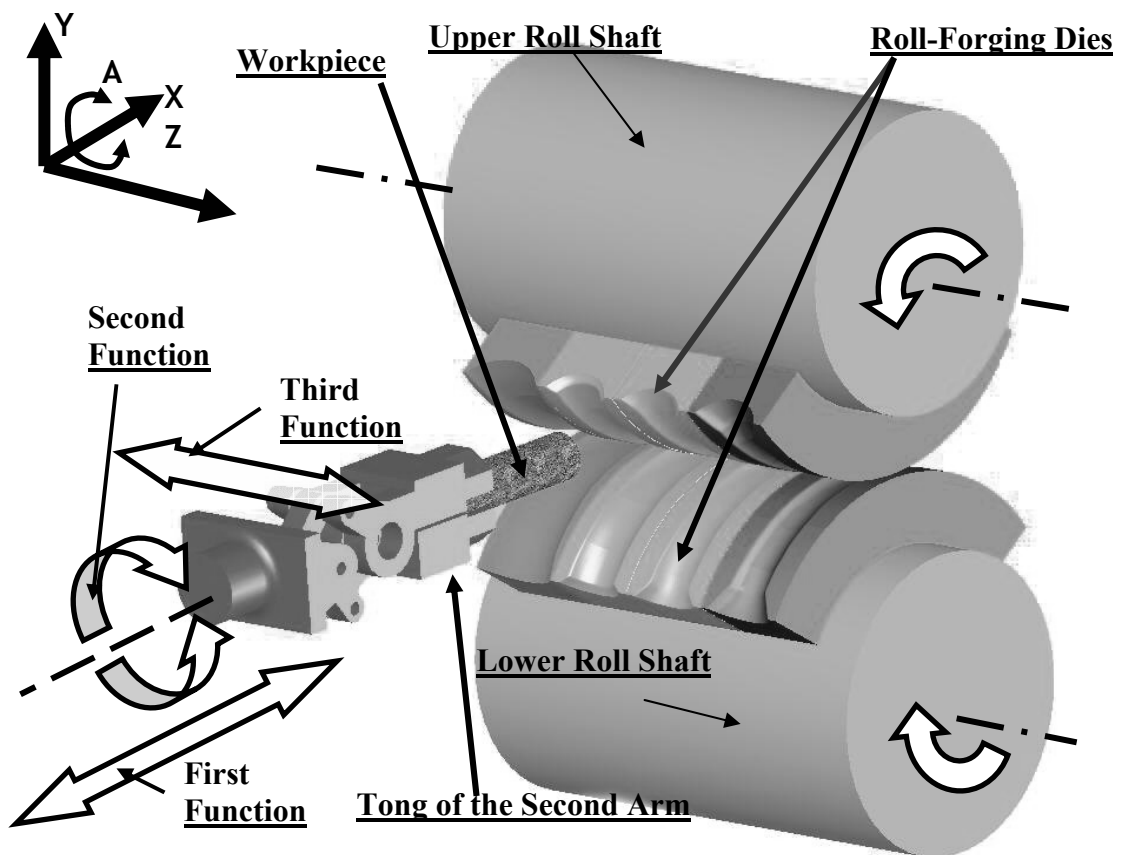


Figure 3.3 Functions of the tong of roll-forging machine

In Figure 3.4, the front view of the roll-forging machine and placement of hydraulic pistons for transverse and rotational movements of the tong of the second robot arm are illustrated.

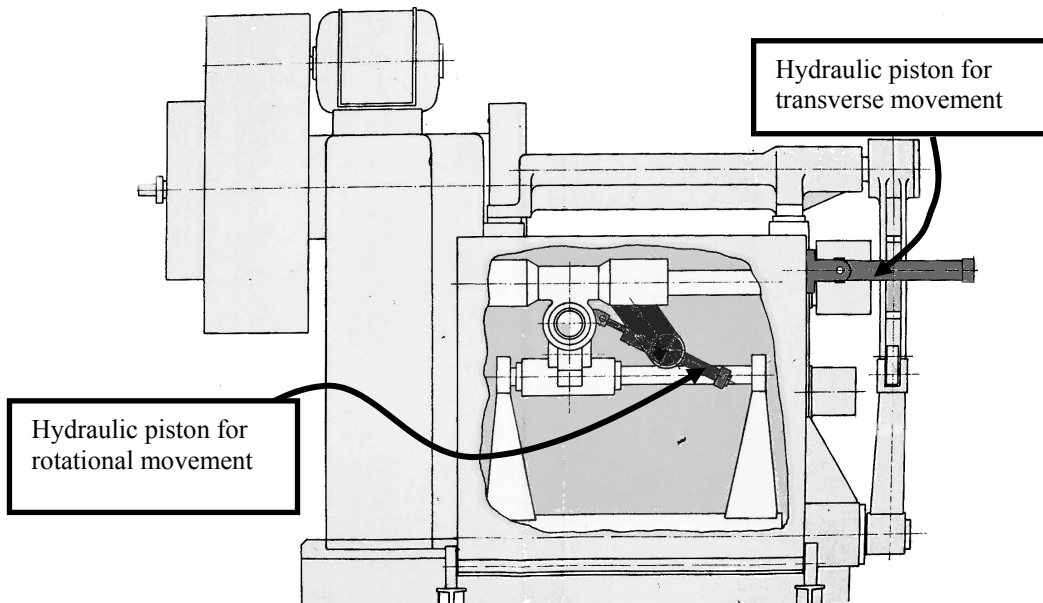


Figure 3.4 Placement of hydraulic pistons for transverse and rotational movement of tong [30]

The simplified mechanism is shown in Figure 3.5. The joints 2 and 7 are slider joints. On the other hand the joints 1,3,4,5,6 and 8 are cylindrical joints. The circles in Figure 3.5 represent the roll shafts. This mechanism is actuated by rotation of upper roll shaft designated on the figure. The linkage A rotates with the upper roll shaft. The linkage B moves as a pendulum while shaft is rotating. The linkages C, D, and E transmit motion of the linkage B to slider joint 7 and linkage F as linear reciprocating movement. The tong is attached to linkage F. At the start of cycle the tong approaches to the roll-forging dies and at a certain position it moves back to its initial position. The velocity and position analysis of the tong is given in Appendix B.

The linear velocity of tong changes with time and is not equal to tangential velocity roll-forging die surface. Linkage F is a flexible arm. It is possible to apply constant force to the workpiece by the tong.

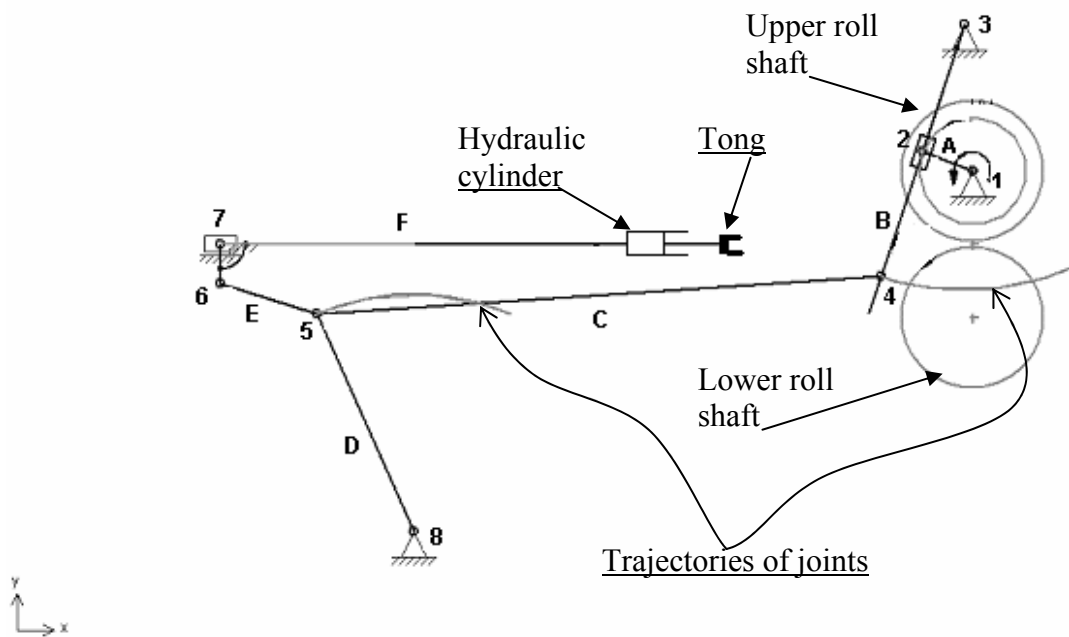


Figure 3.5 Simplified mechanism of the second robot arm

The hydraulic system of linkage F is given in detail in Figure 3.6. This system is composed of single acting hydraulic piston and pressure relief valve. When the workpiece gets into contact with roll-forging dies a reaction force is generated in inverse direction to the motion. As the oil pressure increases up to the set value of pressure relief valve, the oil in the hydraulic piston is transferred back to the oil tank by the help of pressure relief valve to prevent the further increase of pressure in the piston. So, the piston arm moves back. This system limits the pushing force of tong generated by the mechanism to hydraulic force of piston. Set value for this valve is 55 bars. Piston force under 55 bars does not cause a deformation on workpiece. By this system it is ensured that the workpiece is freely pulled by the roll-forging dies.

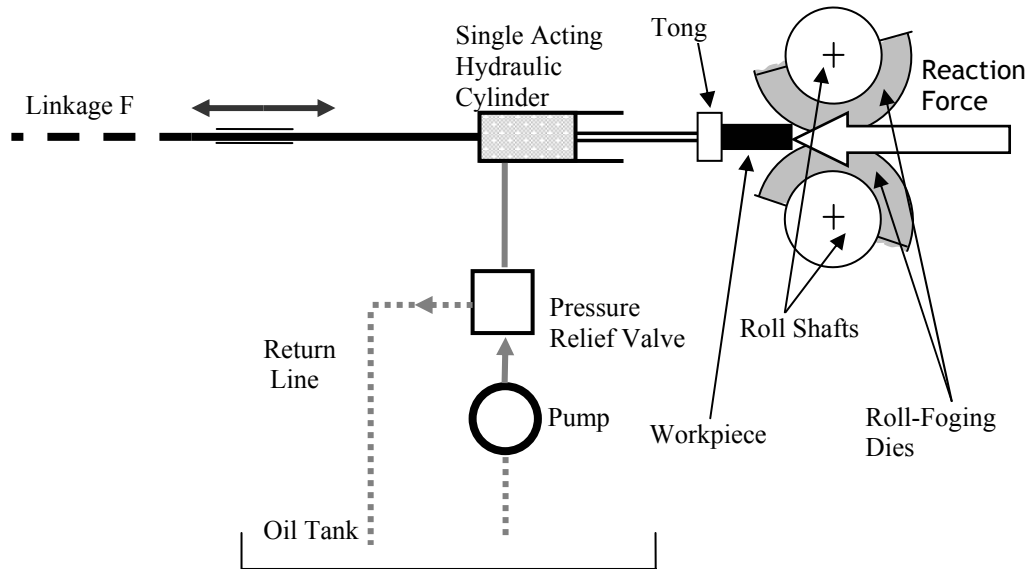


Figure 3.6 Hydraulic system placed on linkage F

3.2. Preparation of the Billet and Forging Rolls for the Experiment

The billet material was provided as C45 steel by Aksan Steel Forging Company. The initial billets were first cut to 164 mm in length from the stock bar of diameter 40mm by sawing operation. The billets were put into the induction heater. Since the proposed temperature range for C45 steel is 1150-1230 °C [31], the billets were heated up to 1150 °C. The roll-forging dies have been heated to 300 °C. For lubrication, 83 % water and 7 % graphite-base oil mixture has been used.

3.3. Conducting the Experiment

Operation consists of four stages. After each stage, the billet has been rotated by 90° about its centerline. These stages have been performed on four different roll-forging dies. The geometries after each stage are illustrated in Figure 3.7.

The initial billet is shown in Figure 3.7.a. After the first stage the head of the billet has been squeezed as seen in Figure 3.7.b. Before the second stage, workpiece has

been rotated by 90° in counterclockwise direction around its centerline. Deformed geometry of the billet after the second stage is shown in Figure 3.7.c. Before the third stage, the billet has been rotated by 90° in clockwise direction. Deformed geometry of the billet after the third stage is seen in Figure 3.7.d. After third stage workpiece is rotated in counterclockwise direction before the stage 4. Finally the workpiece takes the form as shown in Figure 3.7.e at the end of fourth stage. To obtain the geometry of billet in intermediate stages, samples have been collected after every stage.

3.4. Test Results

Since the width and height of cross sections of the workpiece varies through its length, a few dimensions such as length and the maximum width and height of cross section of the parts have been measured after each stage and is given in Table 3.2. The geometries of the parts after experiments are also shown together with the simulated geometries in the Chapter 4.

Table 3.2 Dimensions of Roll-Forged Workpieces

	Length (mm)	Maximum Width (mm)	Minimum Height (mm)
Stage 1	176	46.2	28
Stage 2	205	39	24
Stage 3	229	35.5	21.6
Stage 4	259	32	18.8

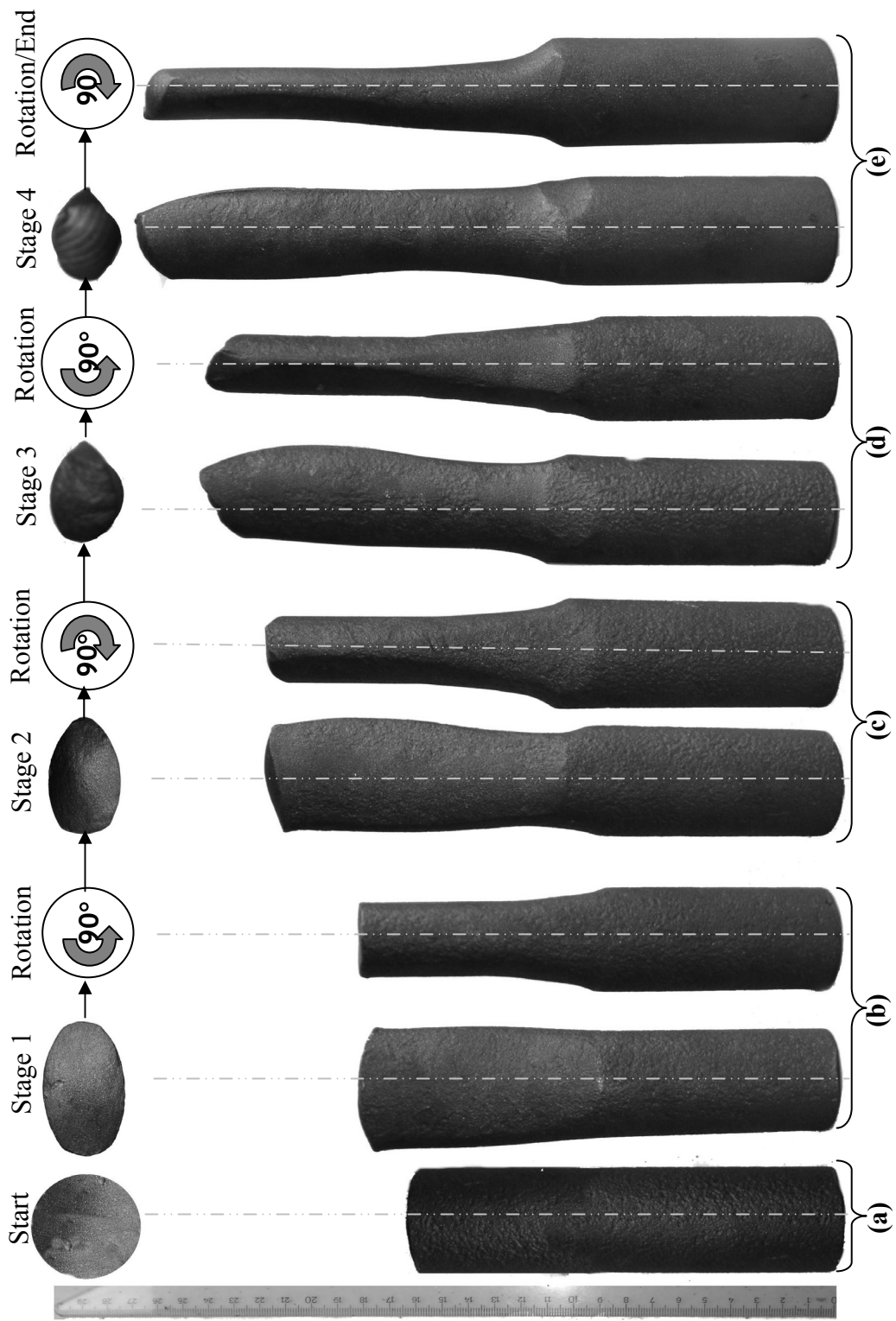


Figure 3.7 Samples geometries of the at the end of each stage of roll-forging operation a) Initial workpiece, b) Stage 1, c) Stage 2, (d) Stage 3, (e) Stage 4

CHAPTER IV

FINITE ELEMENT ANALYSIS OF ROLL-FORGING

4.1. Introduction

In the simulation of roll-forging, a well-known metal forming simulation tool, MSC.SuperForm [29], was used. MSC.SuperForm is a software specially designed for metal-forming applications based on a general purpose finite element software MSC.Marc [27]. In this chapter, the four stages of roll-forging process for the sample parts described in Chapter 3 are analyzed. Technical drawings of roll-forging dies of stages 1-4 are seen in Figures 4.1-4.4, respectively. As seen from the figures, the sections are not identical and therefore, the cross section of the workpiece changes through its length. This property of the roll-forging dies differs the process from profile rolling. Tool geometries used in FEM have been imported to MSC.SuperForm model in IGES format. The dies are modeled as rigid. Heat transfer between the workpiece and these dies has been taken into account. To make a reliable analysis, it is essential to input the actual process variables such as tong approach velocity and angular position of the roll-forging dies. The roll-forging dies rotate at constant speed 7.33 rad/s. To calculate the tong position and velocity, the mechanism has been analyzed by using a mechanism analysis software. Results of the analysis have been transferred to finite element model to input the tong approach velocity. Details have been given in Appendix B.

Since the operation occurs at elevated temperature and the deformation rate is high, heat transfer to die and environment and heat generation due to high deformation causes changes in material properties. Hence, thermo-coupled model is applied. At the first stage, initial temperature of all of the elements is taken as 1150 °C. In remaining three stages, the “prestate” is used as an initial condition. “Prestate” allows the transfer of the stress, the equivalent plastic strain and the temperature, from one analysis to another.

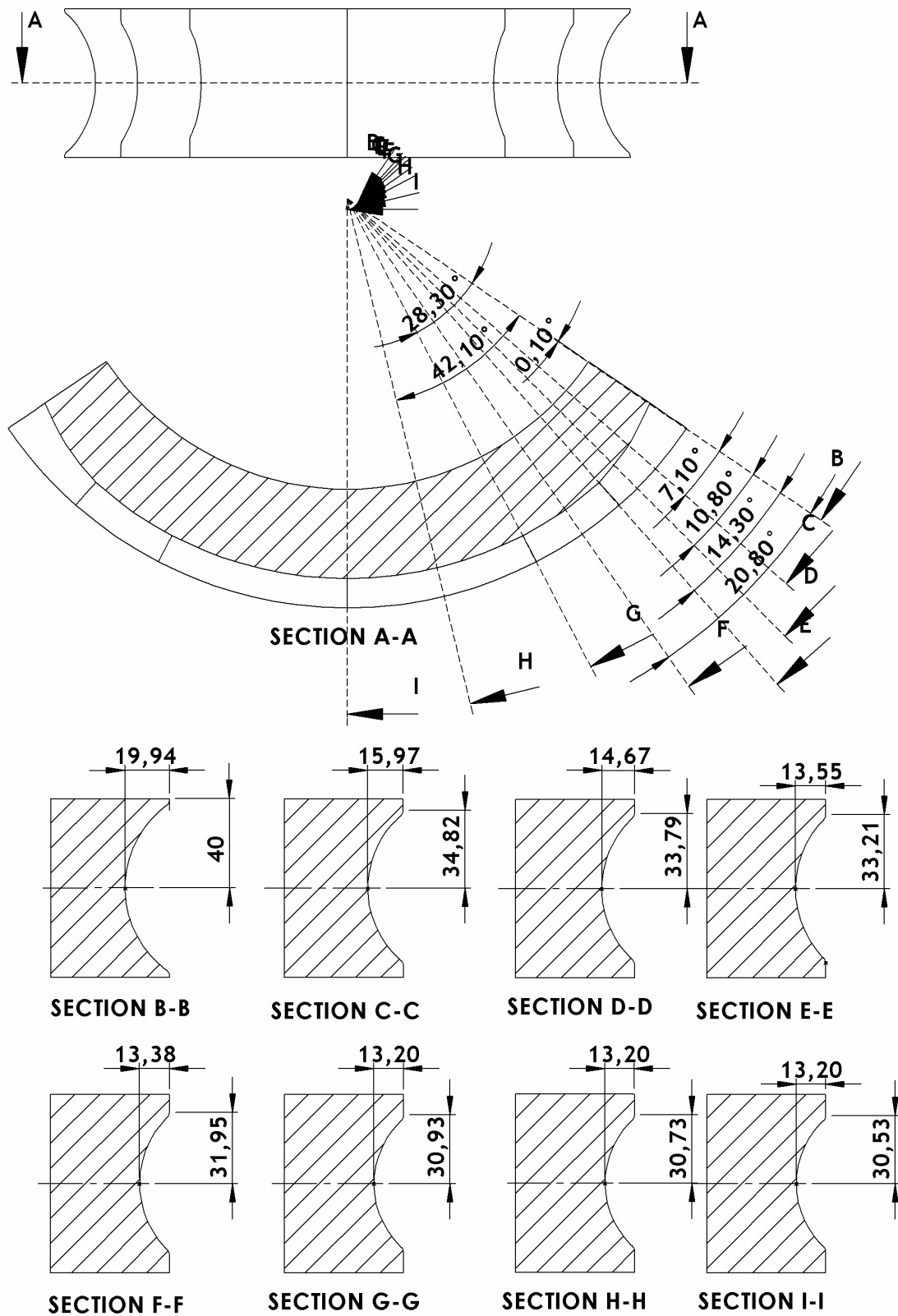


Figure 4.1 Technical drawing of roll-forging dies in stage 1

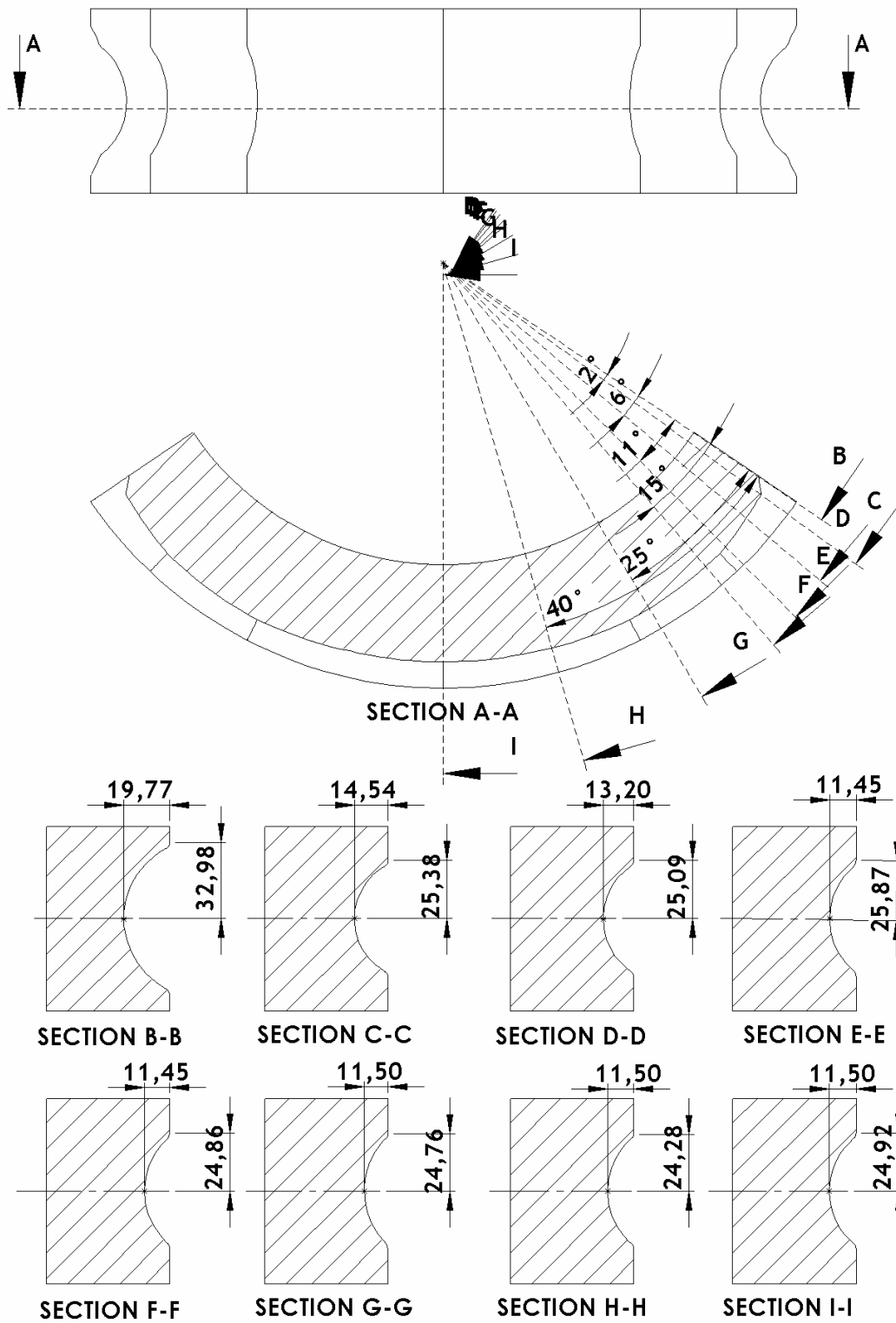


Figure 4.2 Technical drawing of roll-forging dies in stage 2

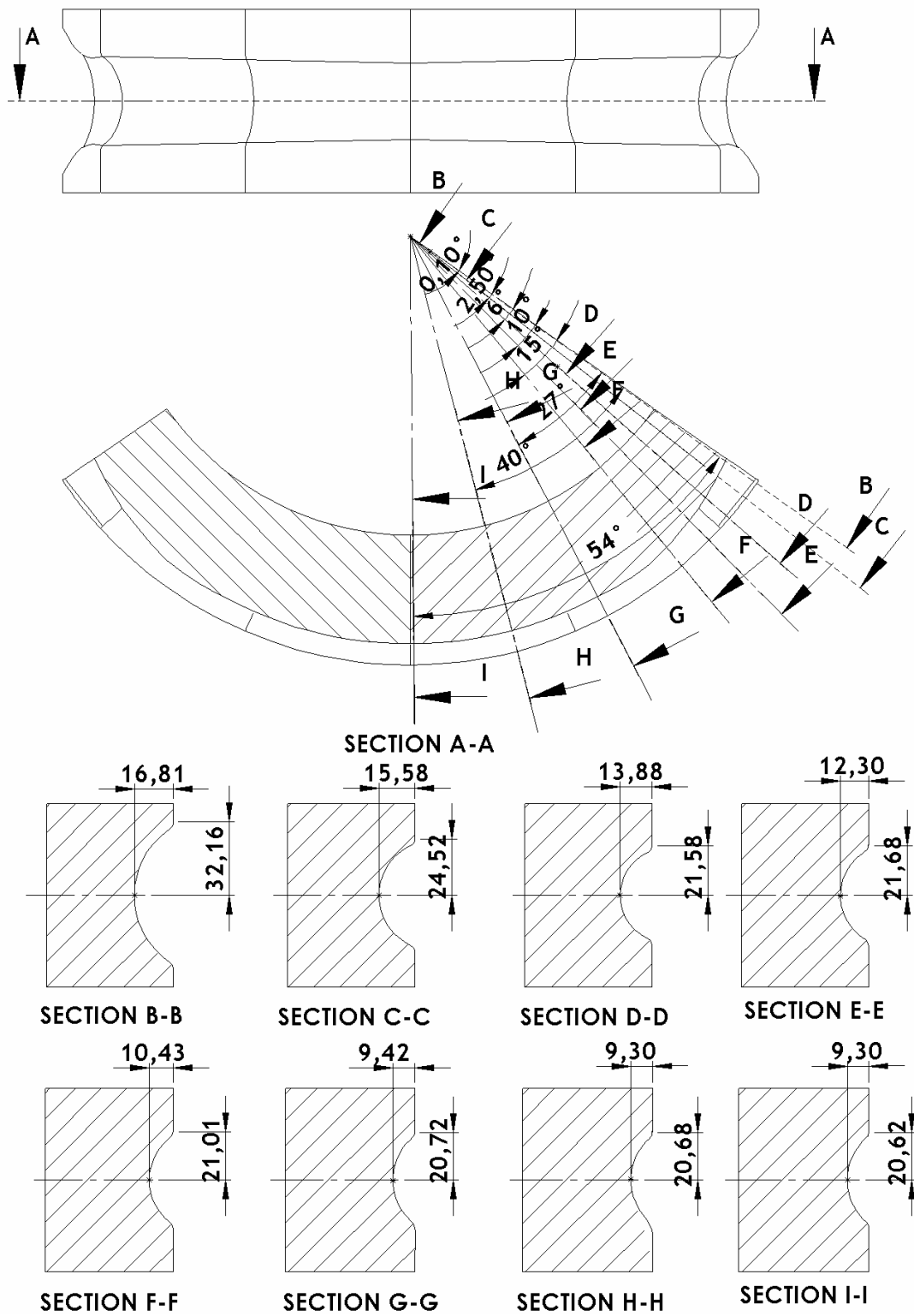


Figure 4.3 Technical drawing of roll-forging dies in stage 3

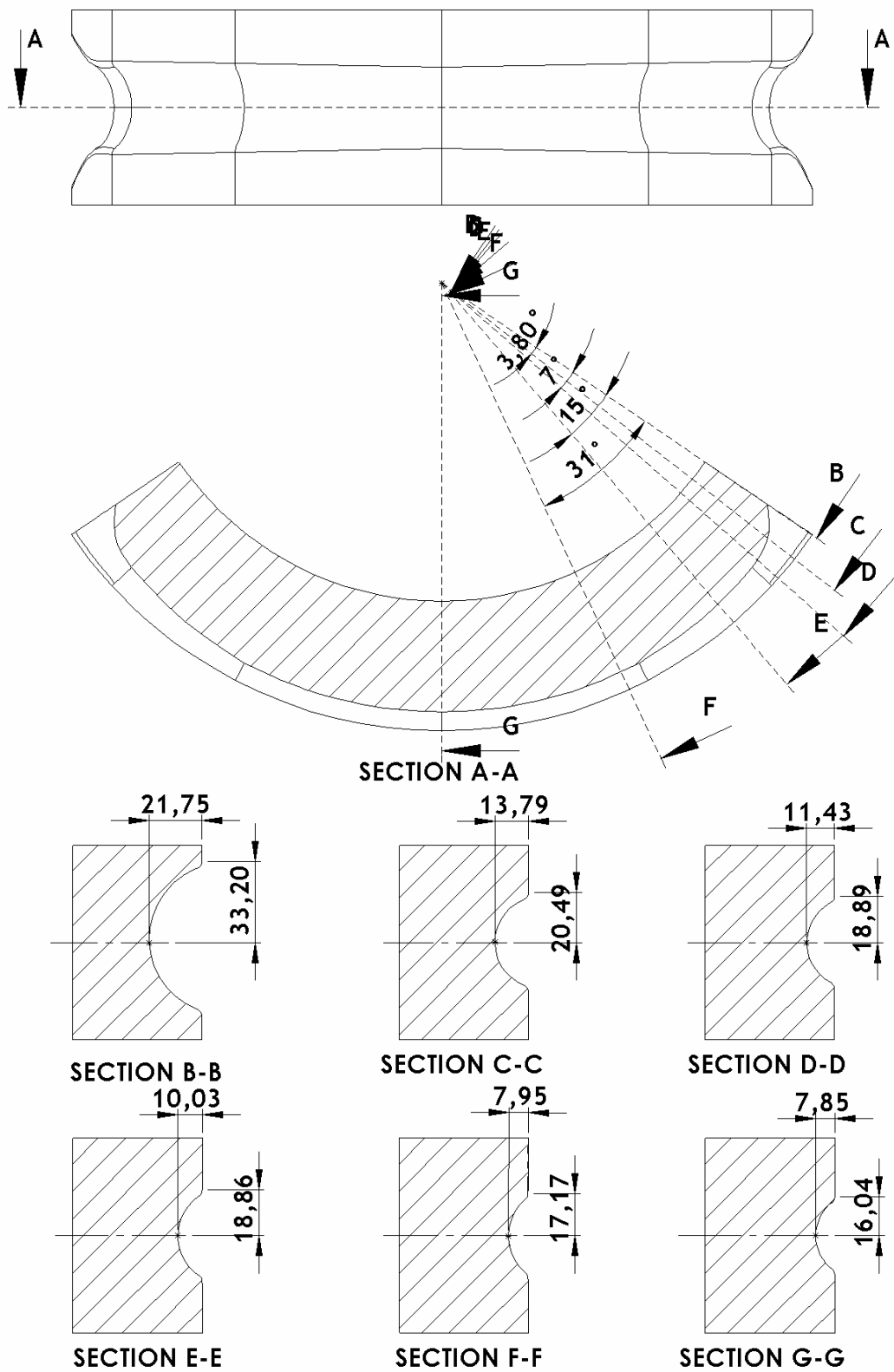


Figure 4.4 Technical drawing of roll-forging dies in stage 4

The workpiece is meshed by using element type 7 [26], which is hexahedral eight noded brick element as seen in Figure 4.5. There are three degrees of freedom associated with each node. Element 7 is a lower order displacement based element. MSC.SuperForm automatically sets the constant dilatation procedure for this element. This improves the results in analyses, which are incompressible or nearly incompressible, such as large strain plasticity [26]. Coulomb friction law is used and the friction coefficient between roll and billet is taken as 0.85 considering the friction data that is suggested in SuperForm Database [32].

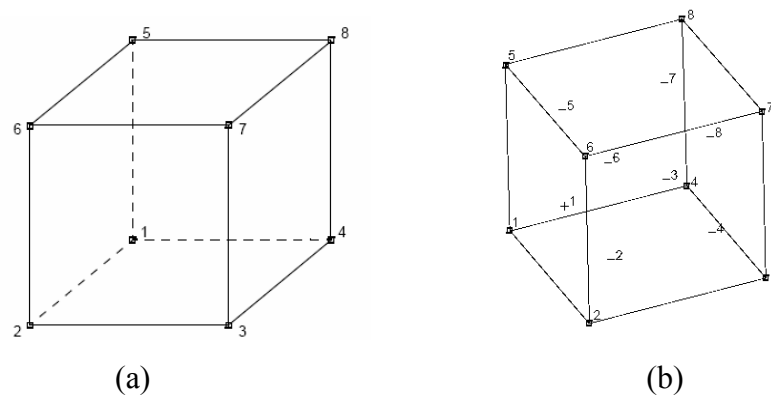


Figure 4.5 (a) Node numbering of element 7 and (b) gaussian iteration points [26]

Remeshing has been activated by using the strain change since the excessive strains in the elements cause inaccuracy in the calculations. The remeshing method used in the analysis is overlay hexahedral, where hexahedral brick elements are automatically generated in the deforming body. In this study, template grid has been used, which requires a template mesh to be used during the meshing (Figure 4.6). Since the remeshing technique is used in the analysis, MSC.SuperForm does not allow using of boundary condition other than contact condition, since applying a boundary condition to a node, edge, face, or element of the workpiece will result in loss of data after automatic remeshing has occurred. The exception to this is volumetric loads, such as gravity or centrifugal, which will be automatically applied to the new mesh.

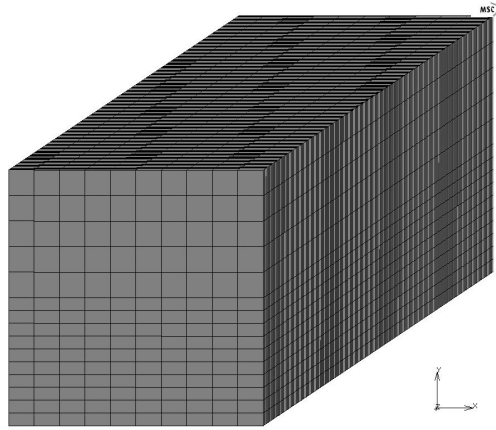


Figure 4.6 Template mesh

C45 material has been used in the analysis. Flow diagrams of C45 at various temperatures and various strain rates and temperature dependent mechanical and thermal properties are shown in Figures 4.7-4.8. Meanwhile at room temperature, yield strength of C45 is 310 Mpa and ultimate tensile strength is 565 Mpa. The mass density, Young modulus of elasticity and Poisons ratio are $7.85E-9$ Mg/mm³, 200 GPa, 0.3 respectively.

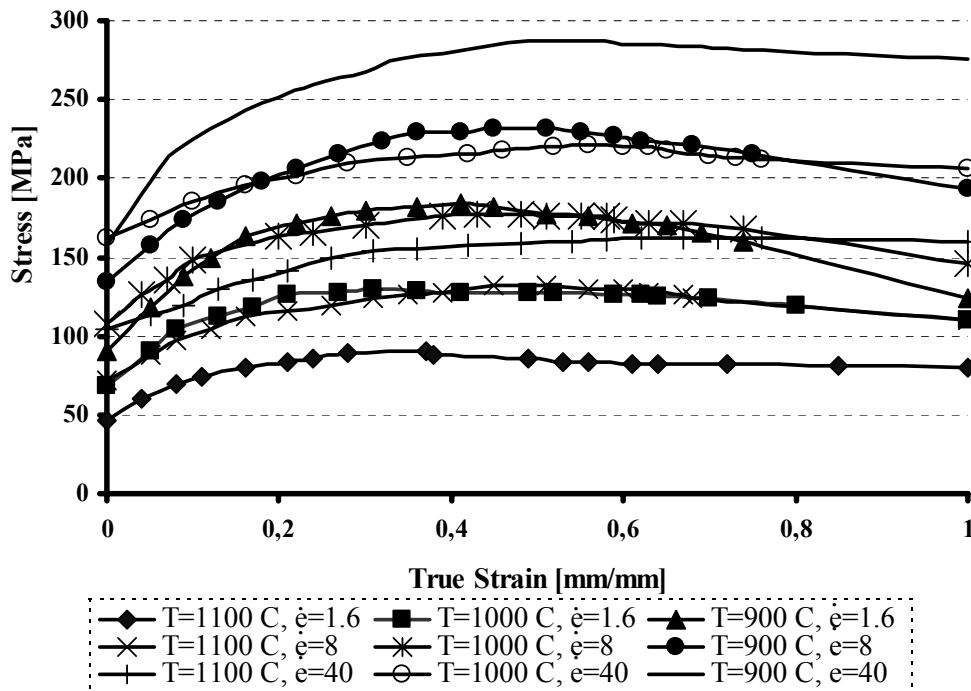


Figure 4.7 Flow diagrams of C45 in various strain rates [33]

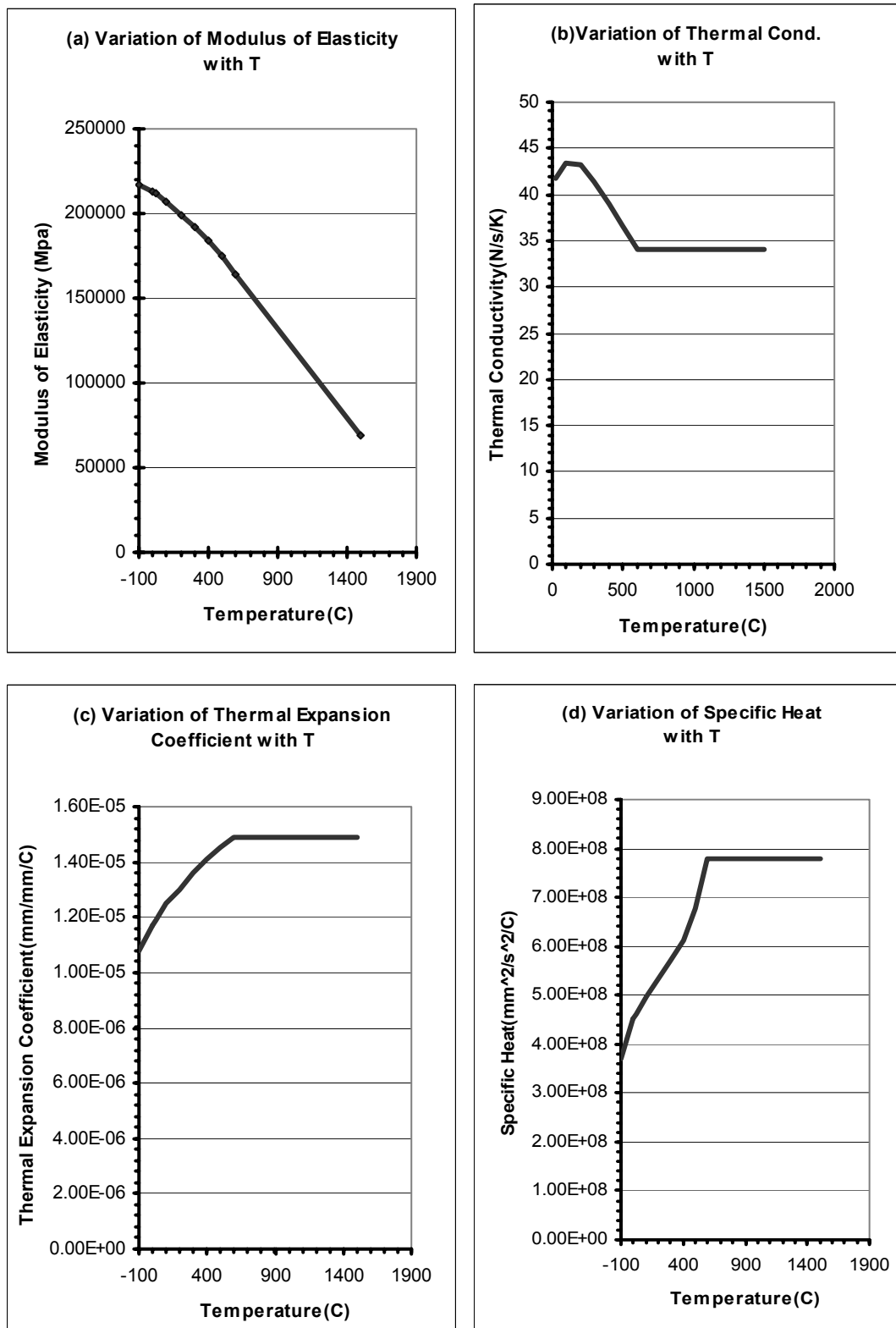


Figure 4.8 Temperature dependent thermal and mechanical properties of C45[33]

4.2. FEA of Roll-Forging of the Workpiece by Symmetric Dies

In this section, Finite Element Analysis of roll-forging process for the workpiece by using the symmetric die sets is presented. As seen in Figures 4.1-4.4, the dies are symmetrical about the section line A-A and in the analysis, the half of the dies were modeled to simplify the model. Analysis consists of four subsequent stages which have been performed by using different roll-forging dies. The geometric model of the process is given in Figure 4.9. There is no heat transfer and friction between symmetry surfaces and the workpiece. The nodes of workpiece, which are in the symmetry planes, are only allowed to move in the symmetry planes. The workpiece in the model is a quarter of a cylinder with 164 mm in length and 20 mm in radius as seen in Figure 4.9. The workpiece has initially 1312 elements. Environment temperature is taken as 27 °C and film coefficient to environment is 0.17 N/(s.K.mm). Die temperature is taken as 300 °C and contact heat transfer coefficient is 30 N/(s.K). Analysis time for each stage is 0.21 sec. and there is 50 increments at every stage. Strain change parameter for remeshing is 0.45.

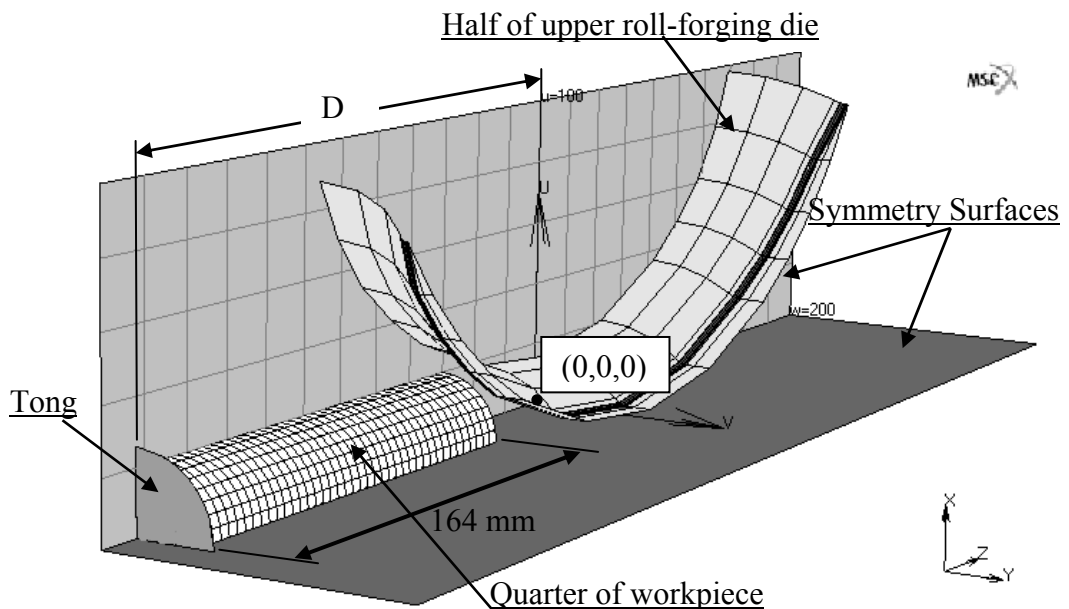


Figure 4.9 3D symmetric model of roll-forging process

The model parameters of every stages are identical to each other except the parameters that are listed in Table 4.1. Summary of the analysis results are given in Table 4.2.

Table 4.1 Model Parameters of Stages 1-4

	Stage 1	Stage 2	Stage 3	Stage 4
Initial number of elements	1312	3840	3823	3823
Initial temperature: [°C]	1150	Prestate	Prestate	Prestate
D value [mm]	226	242	267	274

Table 4.2 Summaries of Analysis Results of Stages 1-4

	Stage 1	Stage 2	Stage 3	Stage 4
Maximum equivalent plastic strain	0.63	1.81	3.04	3.56
Maximum temperature [°C]	1165	1181	1200	1210
Minimum temperature [°C]	990	910	910	910
Analysis time [h:min:s]	00:08:38	00:14:33	00:10:39	00:41:52
Length of workpiece at the end of stage [mm]	175	202	226	254
Percent elongation E_i [%]	6.7	15.4	11.9	12.4
Total percent elongation E_t [%]	6.7	22.4	37	54

The length of workpiece has been increased from 164 to 175mm at the end of the first stage. The percent elongation at this stage is calculated from the following equation,

$$E_i = 100 \cdot \frac{L_f - L_s}{L_s} \quad (4.1)$$

where, L_f is the length of the workpiece at the end of the stage, L_s is the length of the workpiece at the start of the stage. The total percent elongation is used to calculate the elongation of the workpiece after every stage with respect to the initial length of the workpiece and is given in Equation 4.2.

$$E_i = 100 \cdot \frac{L_f - L_i}{L_i} \quad (4.2)$$

where, L_i is the initial length of the billet. Percent and total elongation of the workpiece are identical to each other in the first stage and is 6.7 %. The analysis of stage 1 takes 8 minutes and 38 seconds. At the end of analysis, number of elements has increased to 3840 due to remeshing.

In Figure 4.10, the equivalent plastic strain and temperature variation of the workpiece are shown for the first stage. The maximum strain value for this stage is 0.632 mm/mm. As seen in the 17th increment, the minimum temperature is observed on the surface, which is in contact with roll-forging die and is 910 °C. However, on the 50th increment, the surface temperature raises over 1000 °C, due to high amount of plastic deformation. Most of the deformation energy is converted to heat and the simulation parameters are set such that the 90 % of deformation energy was converted to heat energy.

In Figures 4.11-4.13, the equivalent plastic strain and temperature variation of symmetric workpiece are presented for stages 2-4. It is seen that the equivalent plastic strain and temperature of nodes have been transferred from the previous stage and taken as initial condition in the subsequent stages in the analysis.

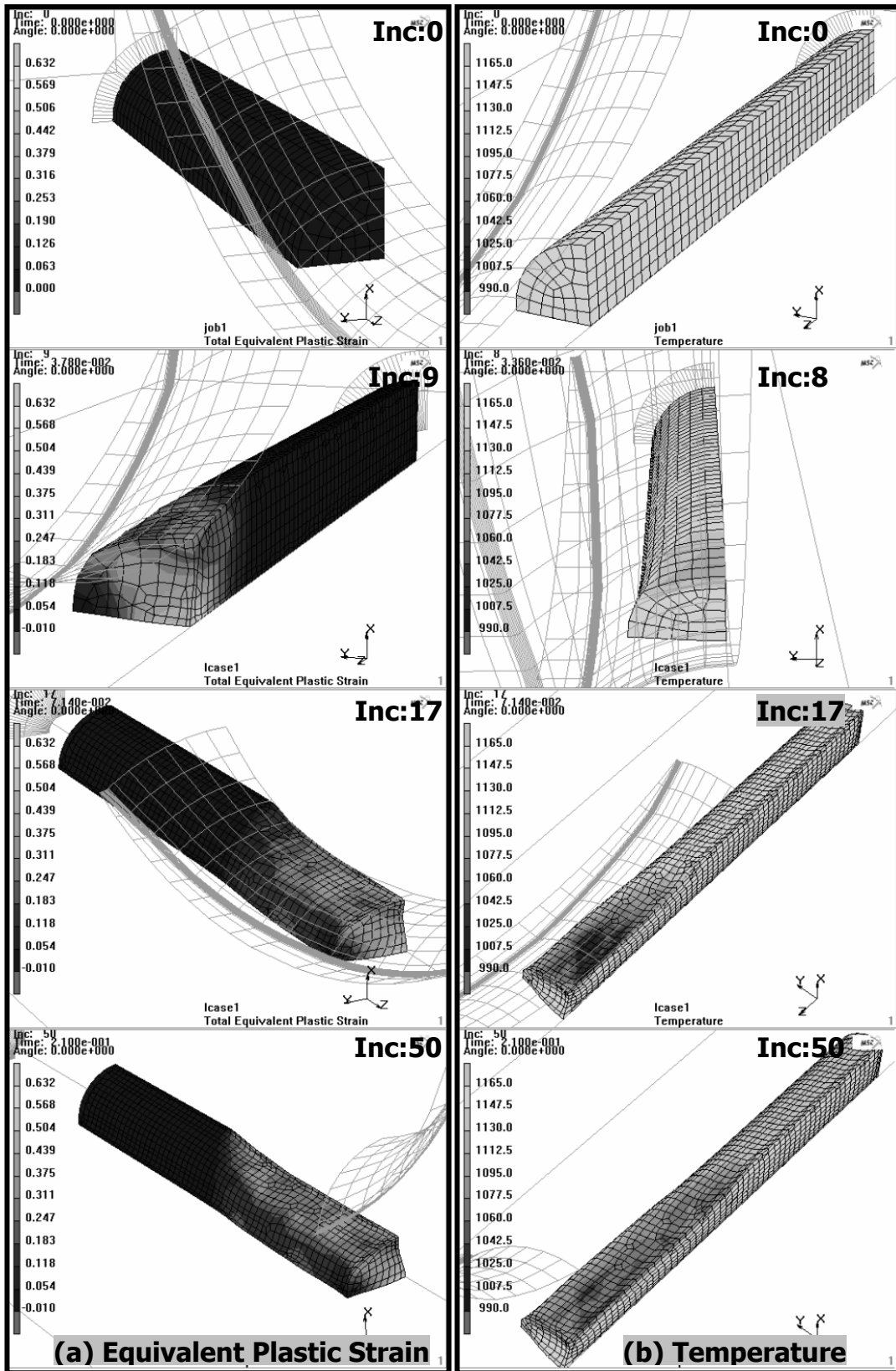


Figure 4.10 Equivalent plastic strain and temperature distribution on the symmetric workpiece in stage 1

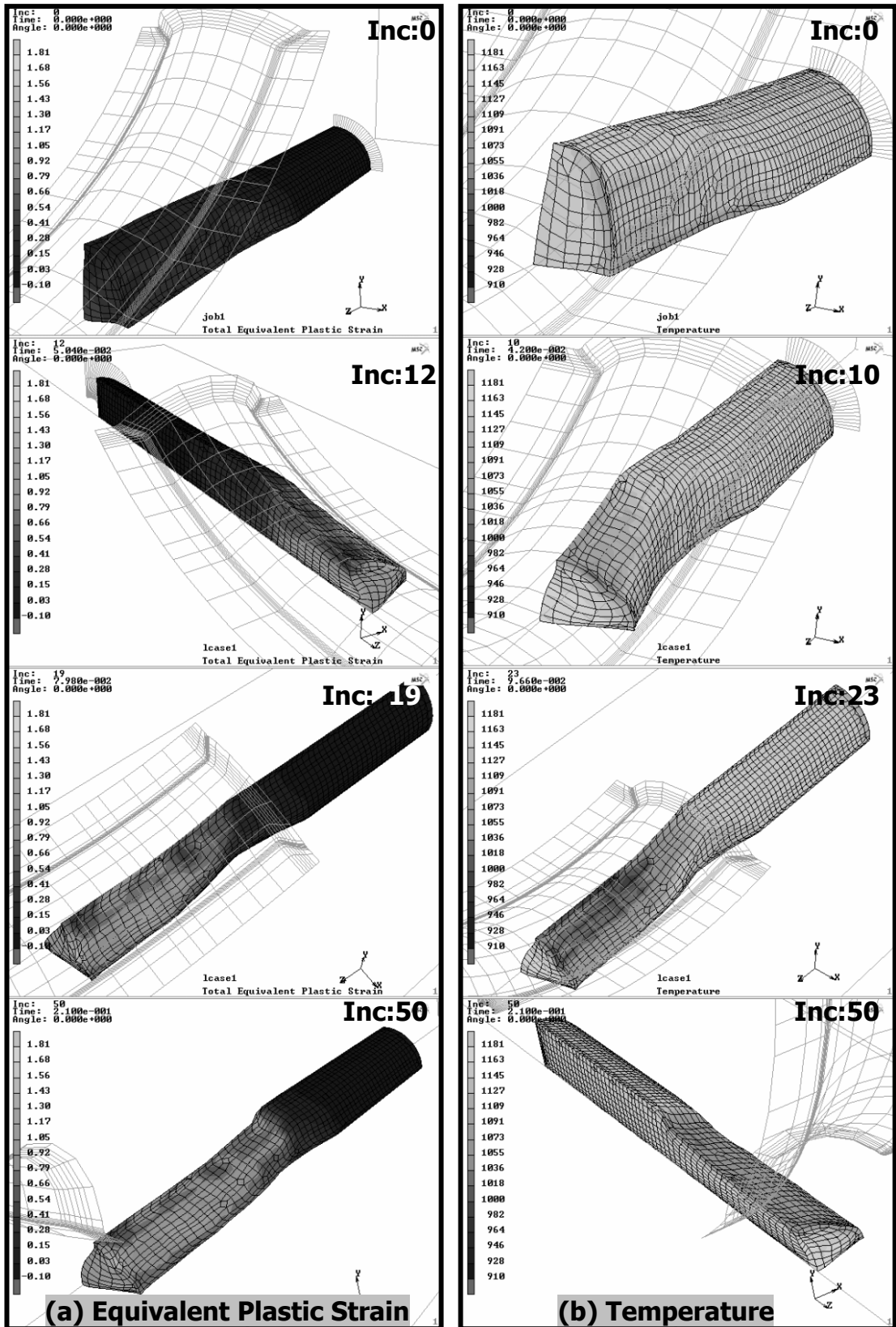


Figure 4.11 Equivalent plastic strain and temperature distribution on the symmetric workpiece in the stage 2

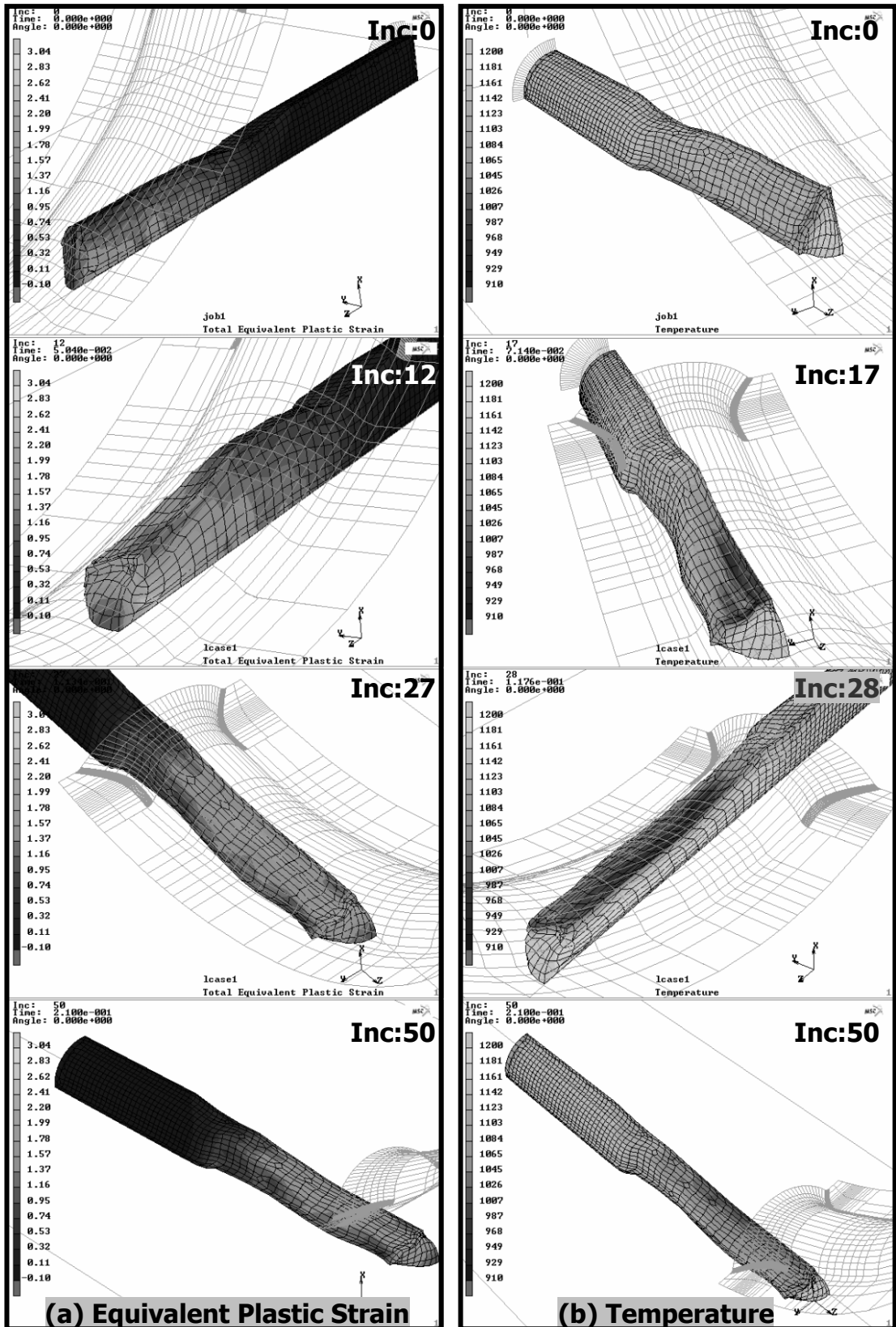


Figure 4.12 Equivalent plastic strain and temperature distribution on the symmetric workpiece in the stage 3

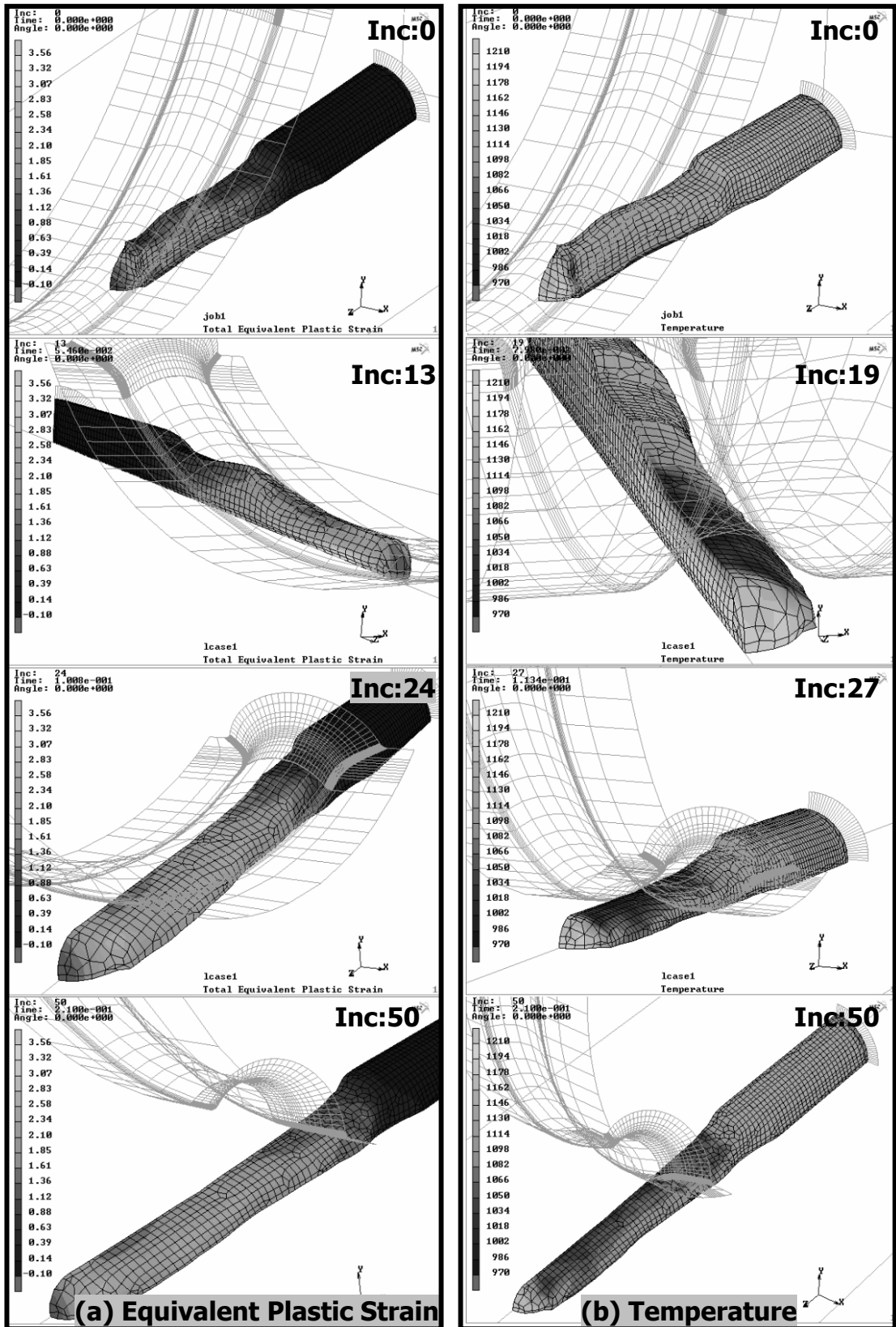


Figure 4.13 Equivalent plastic strain and temperature distribution on the symmetric workpiece in the stage 4

In Figure 4.14, the equivalent von Mises stress distributions are shown for the first stage. As seen in figure, the maximum stress is observed around the contact zone and its value is about 162 MPa. Residual stress distribution on the workpiece after the decoupling of dies and workpiece is given at 50th increment.

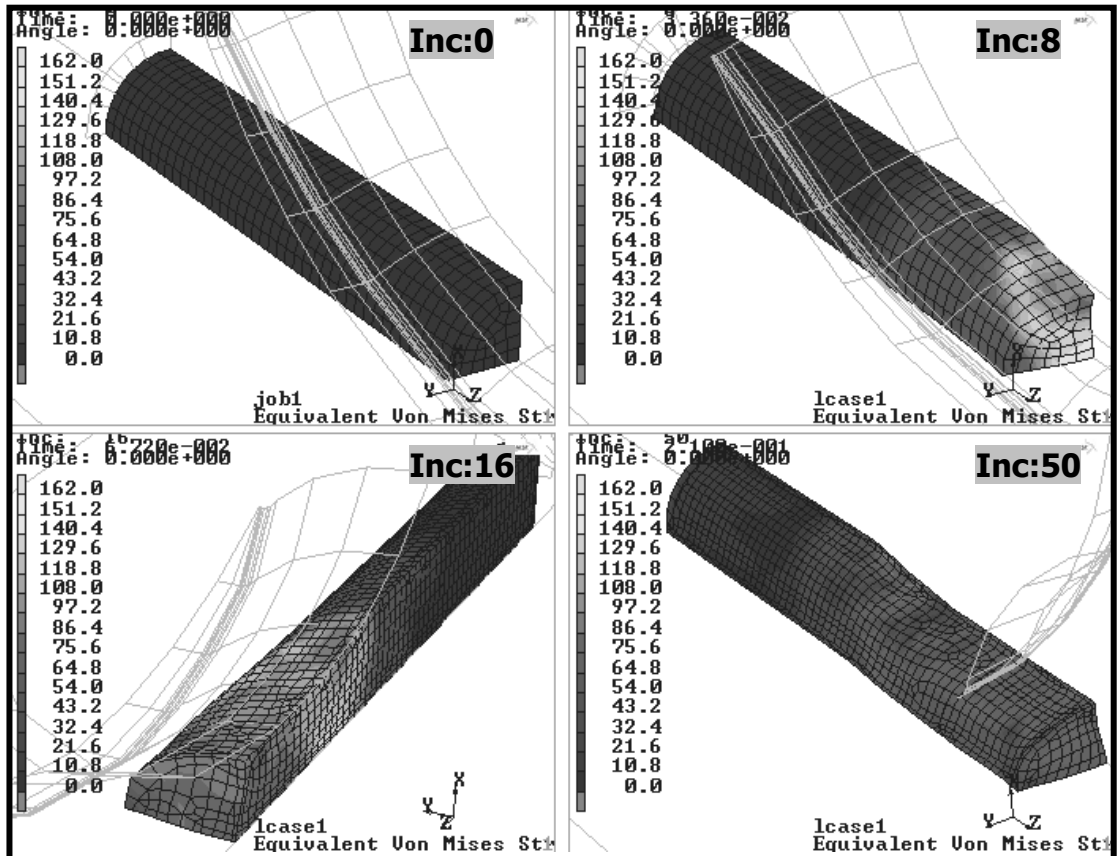


Figure 4.14 Equivalent von Mises stress distribution on the workpiece in stages 1

In Figures 4.15-4.17, the equivalent von Mises stress distributions on the workpiece for stages 2,3 and 4 are given for various increments. As seen in the figures that the deformation stresses are around 150 MPa for Stage 2 and 165 MPa for Stage 3 and Stage 4. Strain hardening is not observed as expected, since the process is performed in hot conditions.

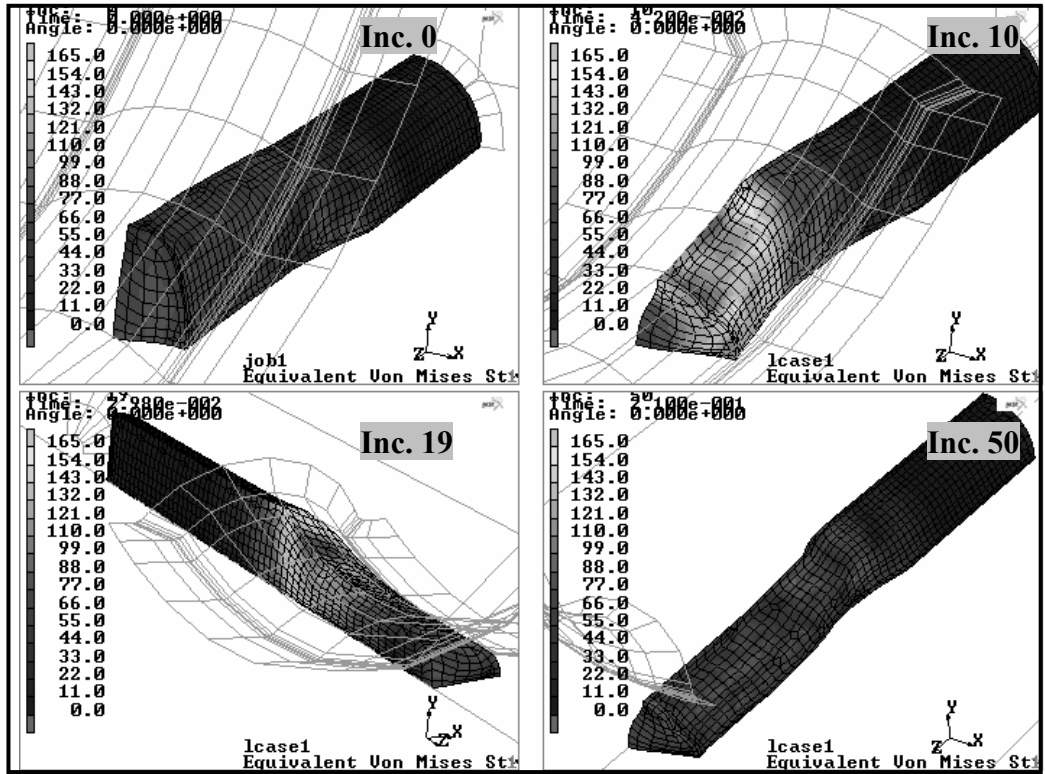


Figure 4.15 Equivalent von Mises stress distribution on the workpiece in stage 2

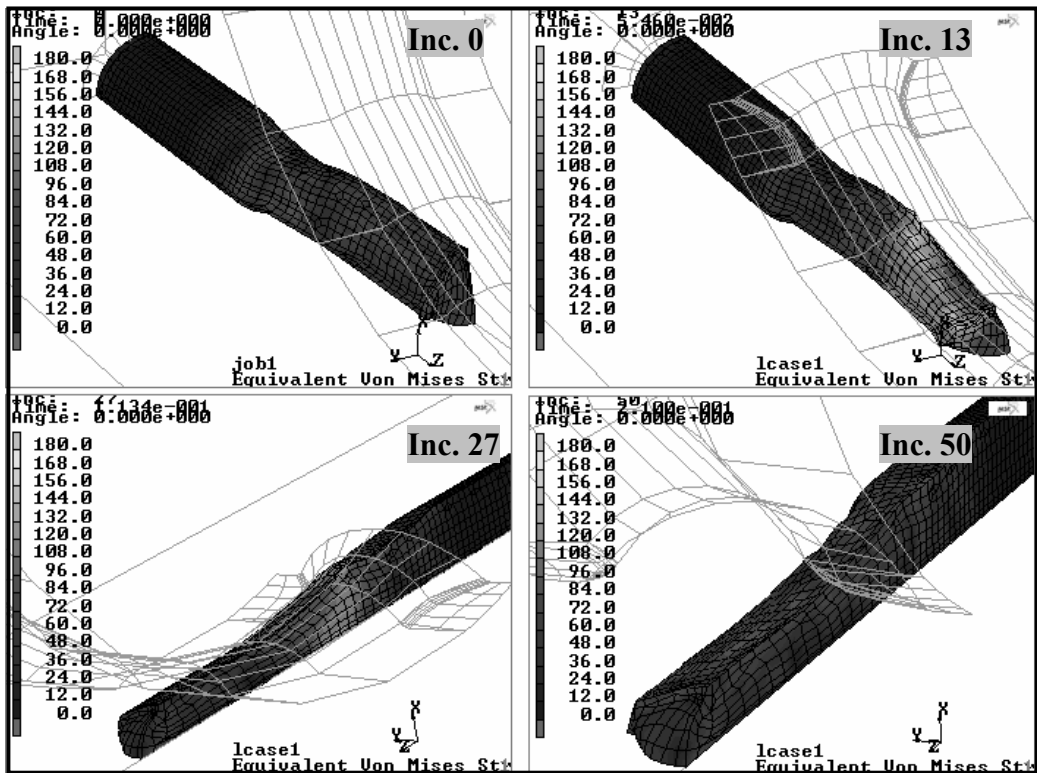


Figure 4.16 Equivalent von Mises stress distribution on the workpiece in stage 3

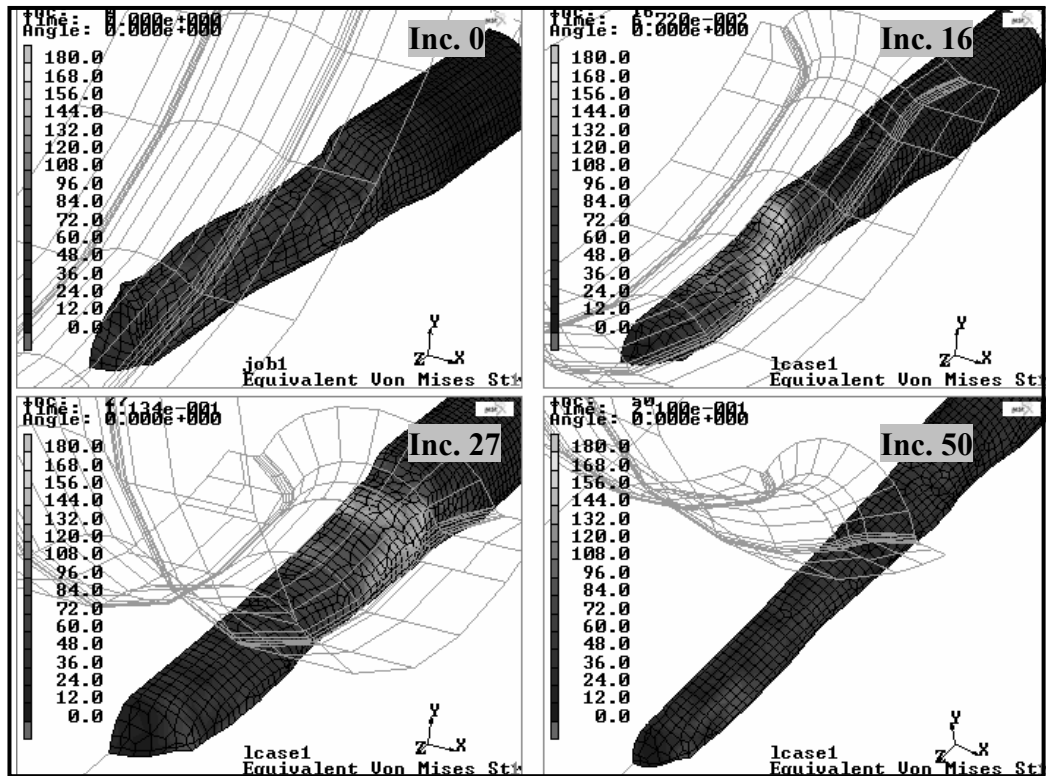


Figure 4.17 Equivalent von Mises stress distribution on the workpiece in stage 4

To compare the FEA simulation results with experiments, whole of the workpiece has been obtained from the quarter part analyzed as shown in Figure 4.18. As seen in Figure 4.18.b, using symmetry about the xz surface, half of the workpiece has been obtained. Then the whole workpiece has been obtained by using the symmetry about yz surface as seen in Figure 4.18.c. To be able to compare the results, the workpiece geometries are compared with the experimental result as seen in Figure 4.19. The geometries of the first two stages have been given to illustrate the geometric differences of experimental and simulation results.

It was observed that there are some differences between the experimental results and simulation results of symmetric model. The samples obtained in experimental study are not symmetric with respect to the longitudinal axis of workpiece.

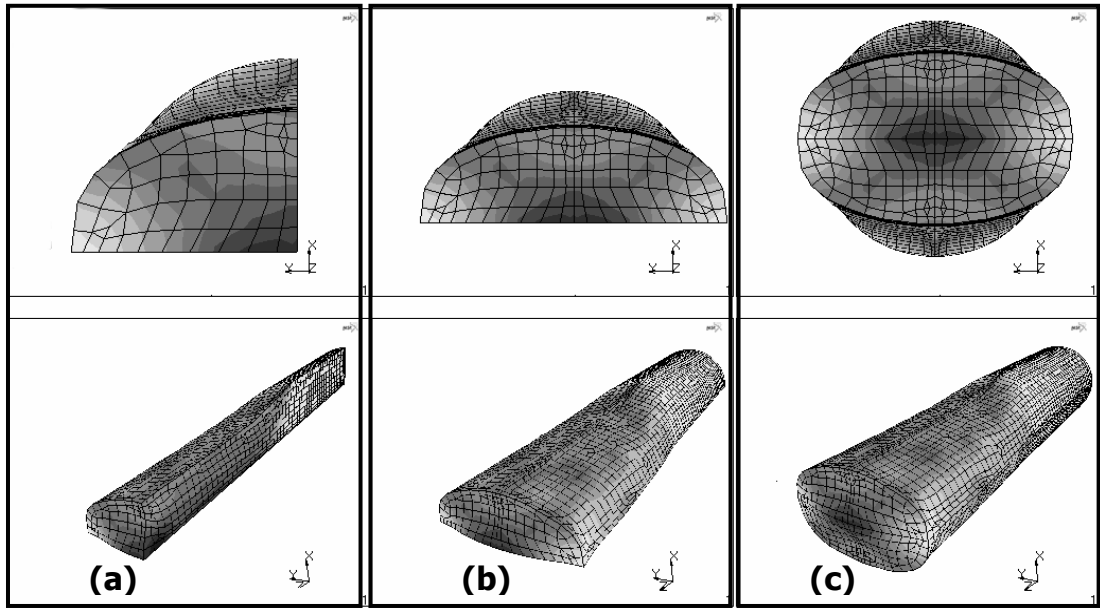


Figure 4.18 Conversion of symmetrical workpiece to non-symmetrical workpiece

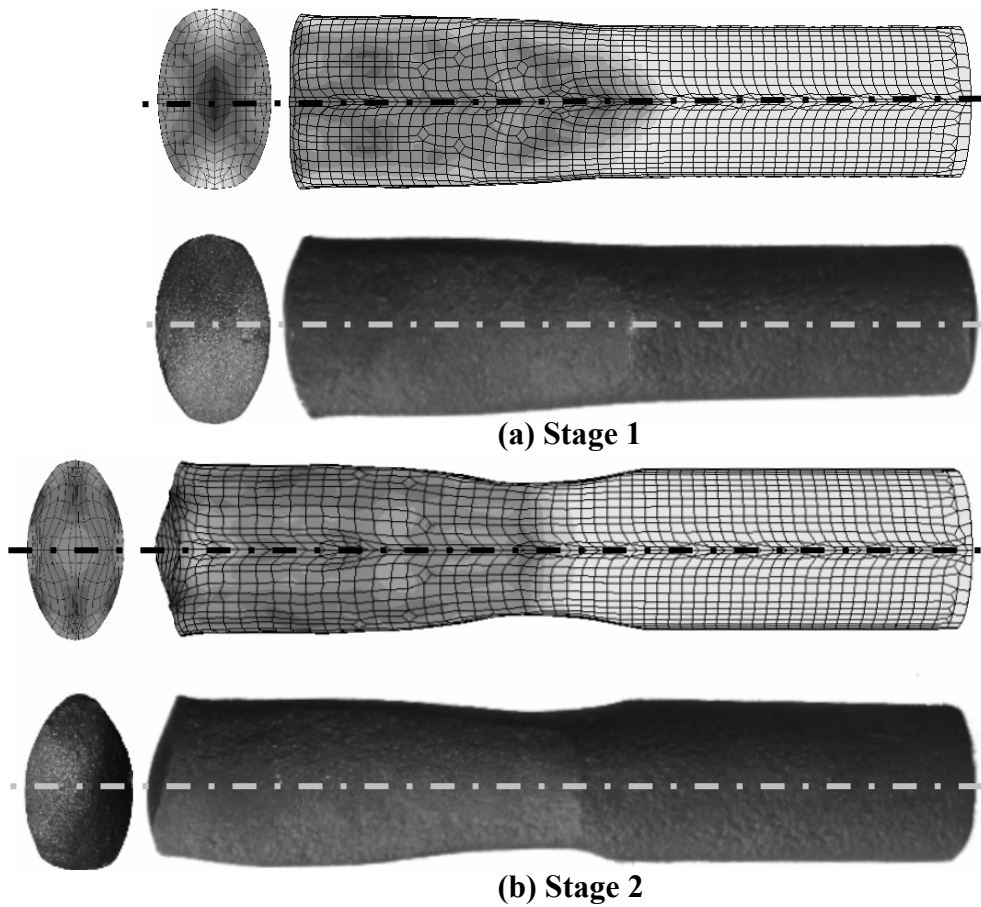


Figure 4.19 Photograph of the experiment sample and captured view of simulated geometry of (a) Stage 1, (b) Stage 2

To investigate the reasons of these differences roll-forging dies and tong on the particular roll-forging machine have been examined and it has been understood that the upper and lower parts of the roll-forging dies are not aligned properly. As seen in Figure 4.20, the symmetry axis of the workpiece and dies are not aligned. In Figure 4.20, “ Δ ” shows the misalignment between surfaces of workpiece and dies. This deviation violates the symmetrical loading conditions and results in non-symmetrical material distribution.

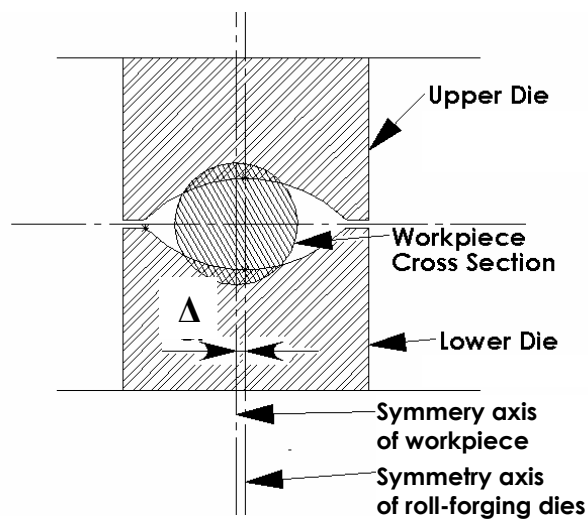


Figure 4.20 Misalignment of workpiece and dies

4.3. FEA of Roll-Forging without Using the Symmetry Assumption

To simulate the actual case the dies are modeled exactly in the same way they fixed to the roll-forging machine. As a result, whole of the initial billet has been modeled. 3-D geometric model of the roll-forging process, has been prepared as shown in Figure 4.21. As seen in Figure, only the contact surfaces of the dies are shown. The tong was simplified consisting of five planar surfaces. Four of them grip the workpiece to prevent rotation due to unsymmetrical loading conditions and one of the surface was placed at the back of the workpiece and pushes the workpiece with a desired velocity towards the roll-forging dies. Die and groove details such as angular cut sections have already been given in Figures 4.1-4.4.

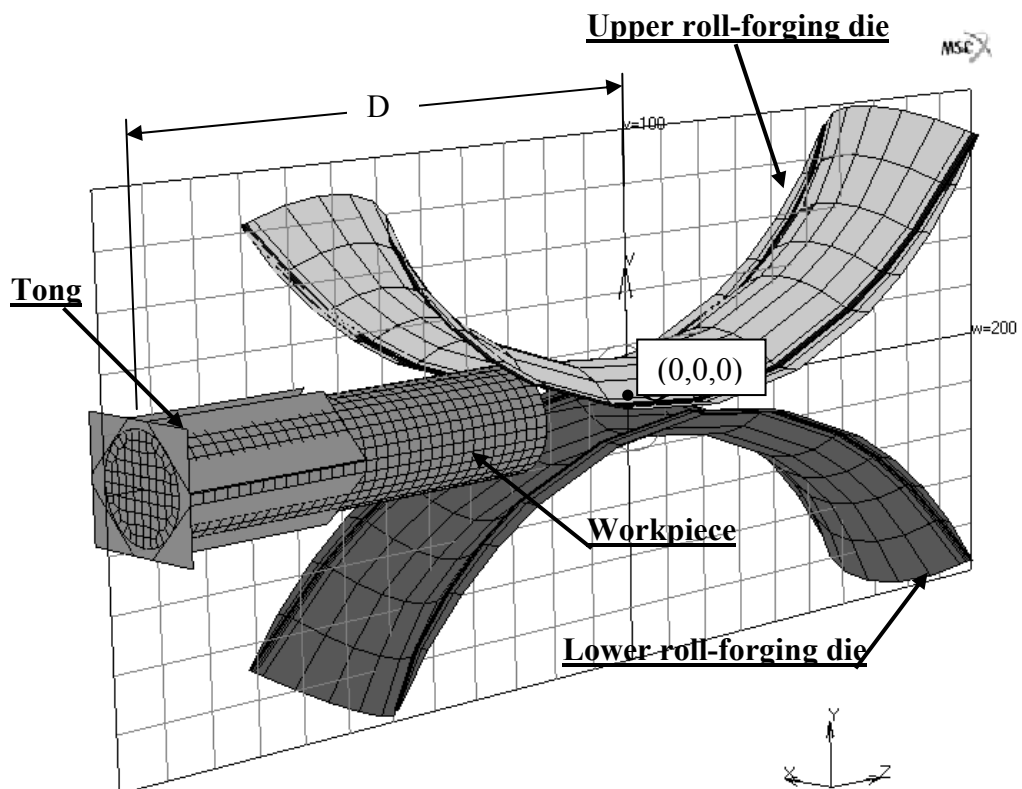


Figure 4.21 3D model of roll-forging process

The model parameters for each stage are identical except the parameters that are listed in Table 4.3. By the help of the prestate option of the MSC.SuperForm, residual stress, temperature and equivalent plastic strain distribution of workpiece at the end of any stage, have been transferred to the proceeding stage as an initial condition. In Table 4.4, the results are given. Analysis takes about 3-7 hours. It is seen that the number of elements increases the analysis time tremendously.

Table 4.3 Model Parameters of Stages 1- 4

	Stage 1	Stage 2	Stage 3	Stage 4
Initial number of elements	2772	5656	5549	5666
Initial temperature	1150	Prestate	Prestate	Prestate
D value [mm]	226	242	267	274
Δ value [mm]	1.3	2	0.3	0

Table 4.4 Summaries of Analysis Results of the Stages 1-4

	Stage 1	Stage 2	Stage 3	Stage 4
Maximum equivalent plastic strain	0.49	1.54	2.1	2.8
Maximum temperature [°C]	1160	1175	1185	1189
Minimum temperature [°C]	950	927	923	920
Maximum Von Mises Stress [Mpa]	140	170	164	160
Analysis time [h:min:sec]	03:13:07	07:16:43	06:22:34	06:10:50
Number of remeshing operation	1	16	11	13
Length of the workpiece at the end of the stage [mm]	176.4	205	232	262
Percent elongation [Ei]	7.3	16.5	13.2	12.9
Total percent elongation [Et]	7.3	25	41.5	59.8

In Figures 4.22-4.25, the deformed geometries and equivalent plastic strain distribution on the workpiece for stages 1-4 have been shown at various increments during the analysis. As seen in Figure 4.22, the maximum value of equivalent plastic strain is 0.488 mm/mm. The equivalent plastic strain distribution on the longitudinal

section of the workpiece is shown in Figure 4.26. It is seen from figure that the most of the deformation has occurred around the longitudinal axis of the workpiece.

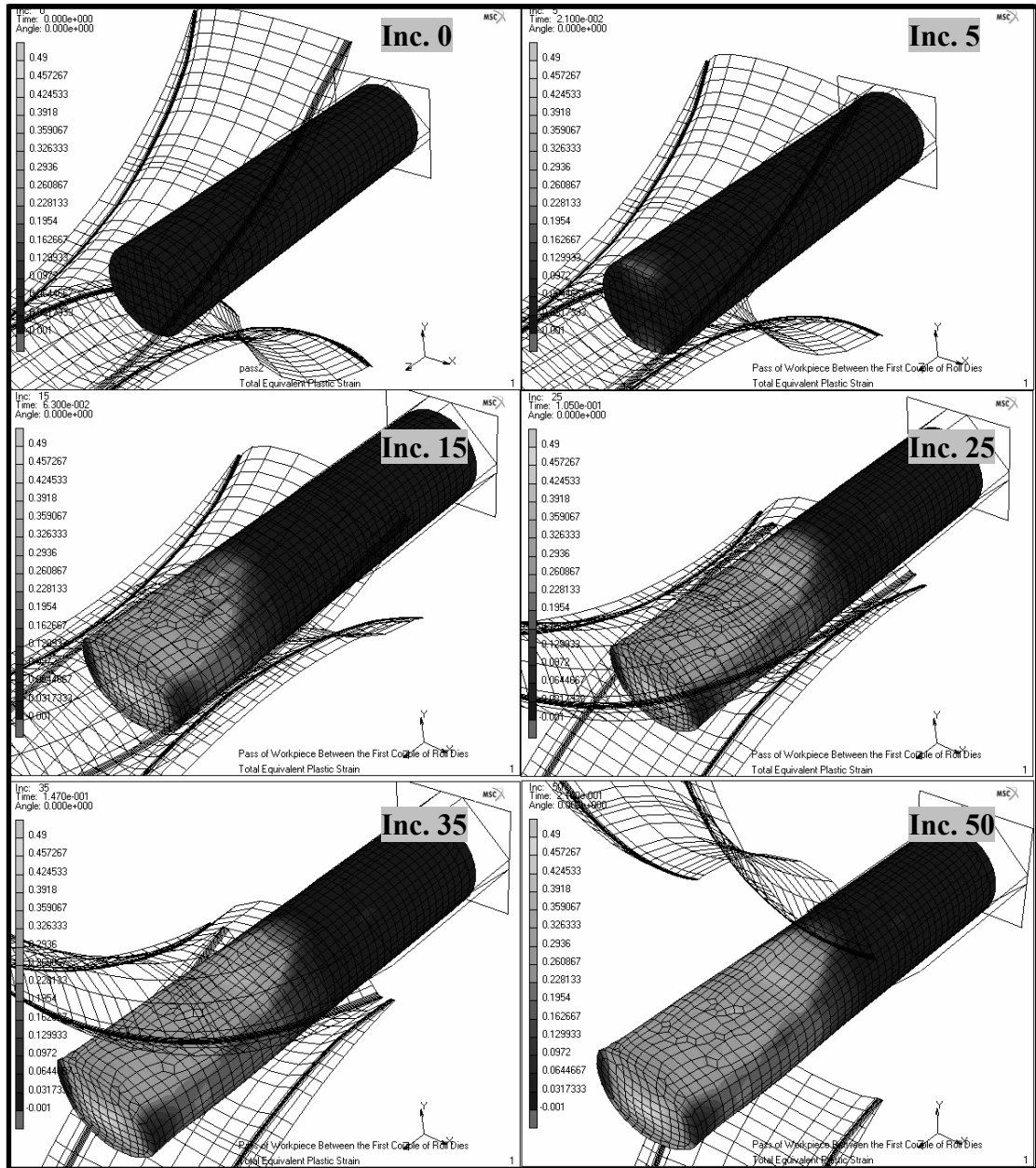


Figure 4.22 Equivalent plastic strain distribution on the workpiece in stage I

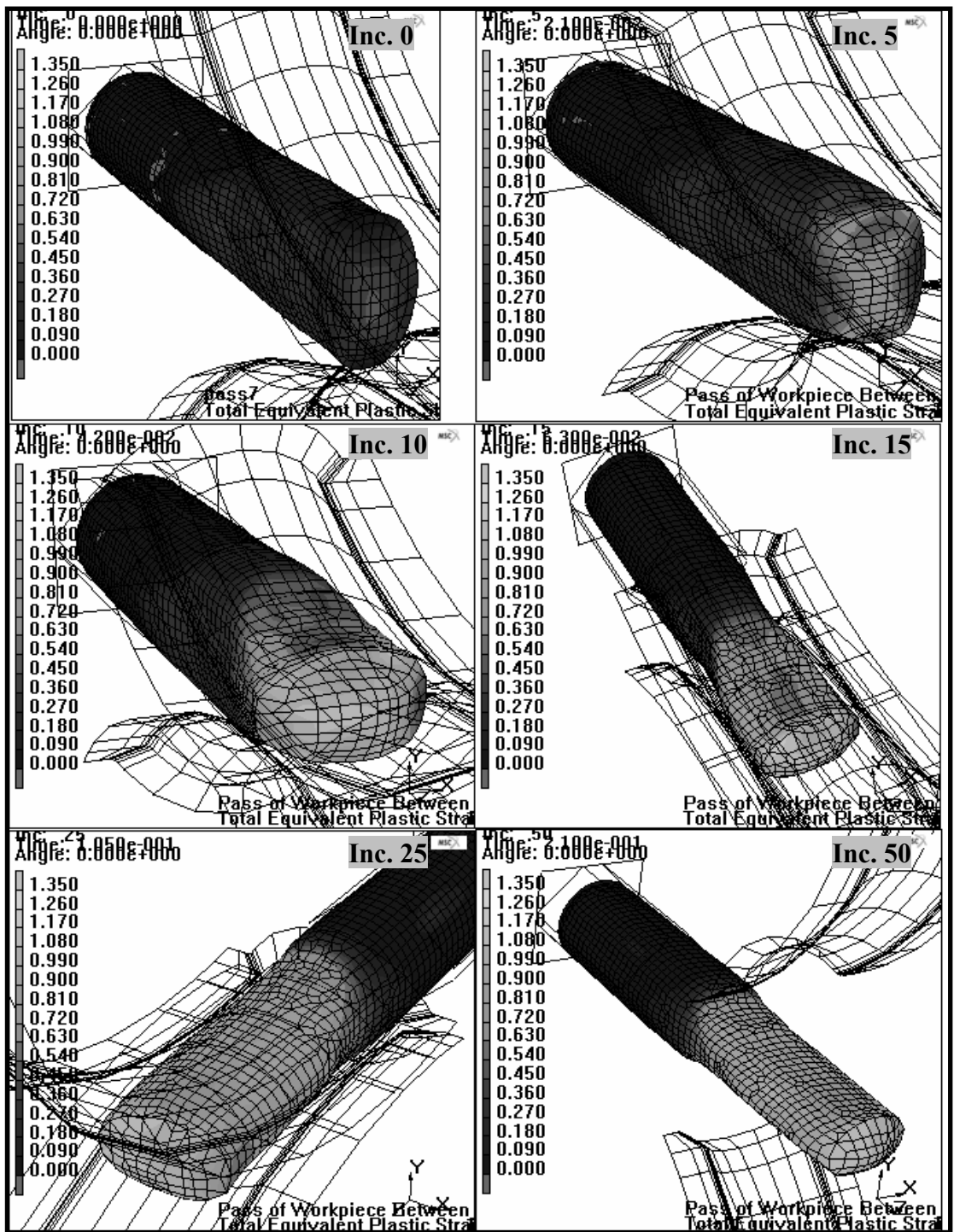


Figure 4.23 Equivalent plastic strain distribution on the workpiece in stage 2

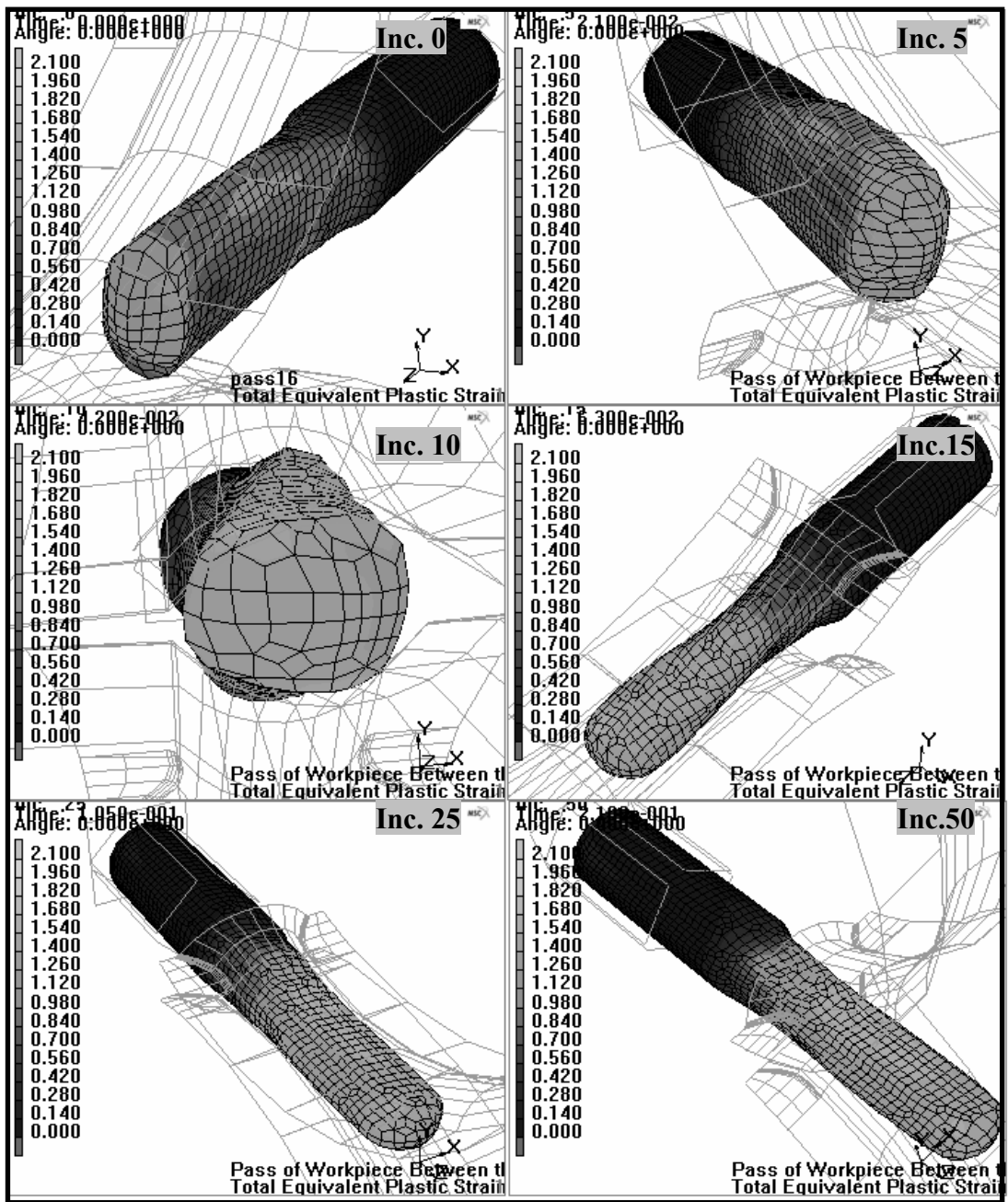


Figure 4.24 Equivalent plastic strain distribution on the workpiece in stage 3

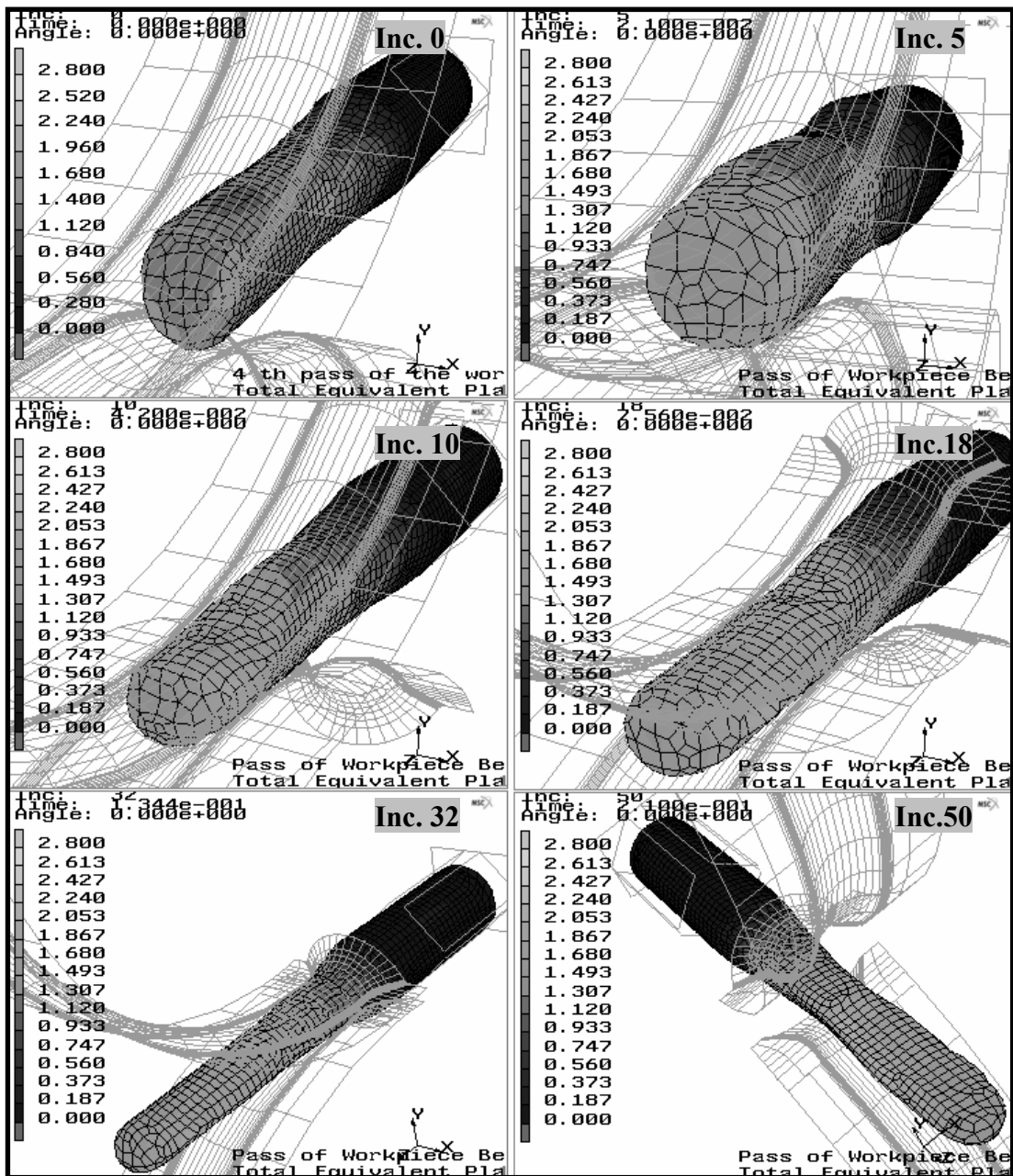


Figure 4.25 Equivalent plastic strain distribution on the workpiece in stage 4

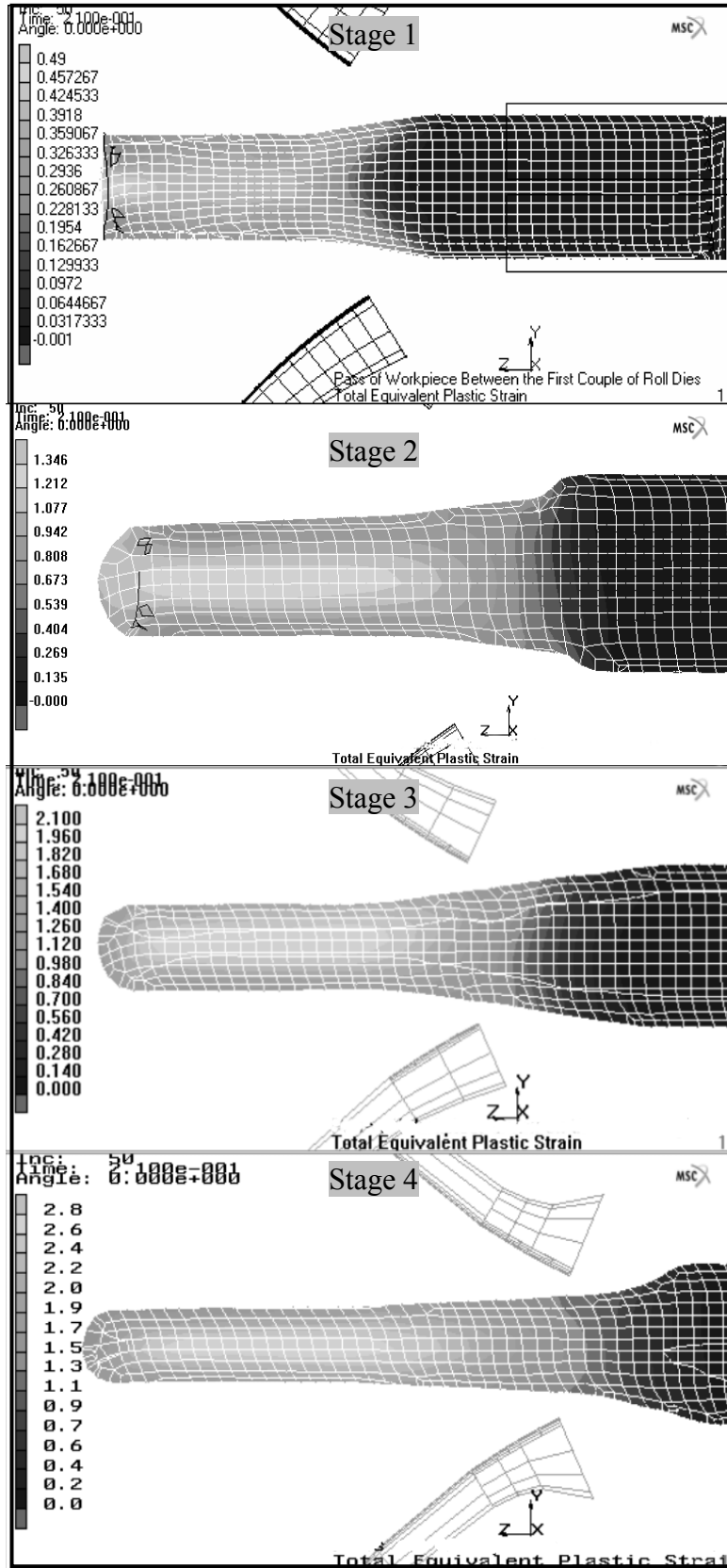


Figure 4.26 Equivalent plastic strain distribution inside the workpiece in stages 1-4

In Figures 4.27-4.30, the temperature distribution on the surface of the workpiece is shown. As seen, surfaces, which are in contact with tong and die grooves, cool faster. However, other surfaces cool very slowly and remain nearly constant. At the 10th increment in Figure 4.27, the front end of the workpiece cools to 1080 °C. At the subsequent increments, the minimum temperature is 950 °C on the surface. During the deformation, heat has been generated in deforming zone and transferred to the boundaries of deforming zone and atmosphere ambient (Figure 4.31). The decrease of the temperature from center to surface is seen in Figure 4.31 for the stages 1-4. The lowest temperature can be observed on the circumferential surface, which is in contact with side parts of the tong. This surface touches to tong at the beginning of the simulation and stays in contact during the whole deformation.

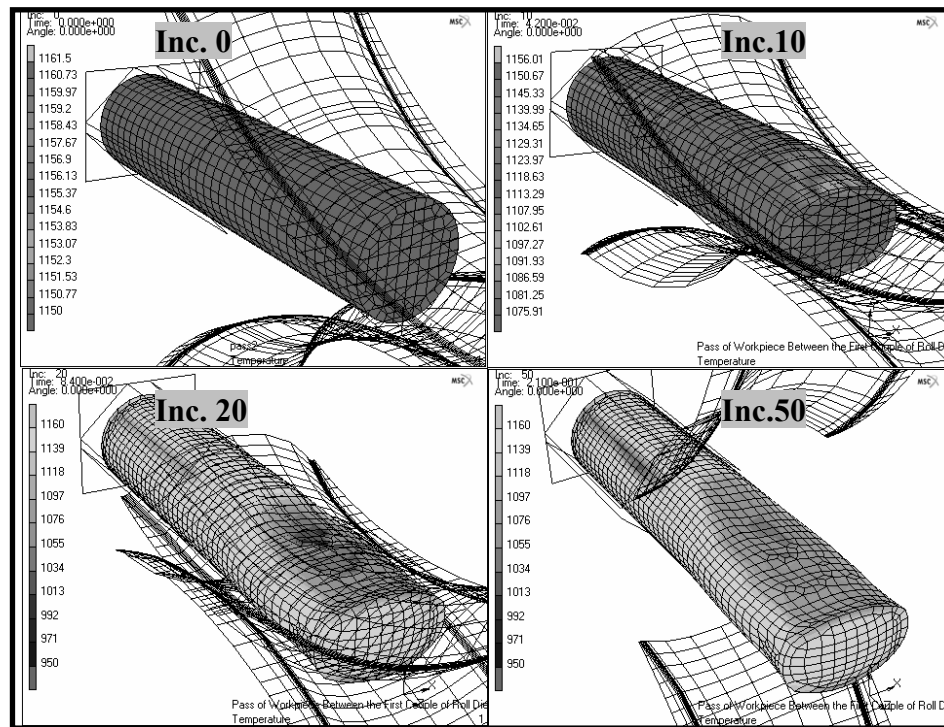


Figure 4.27 Temperature distribution on the workpiece in stage 1

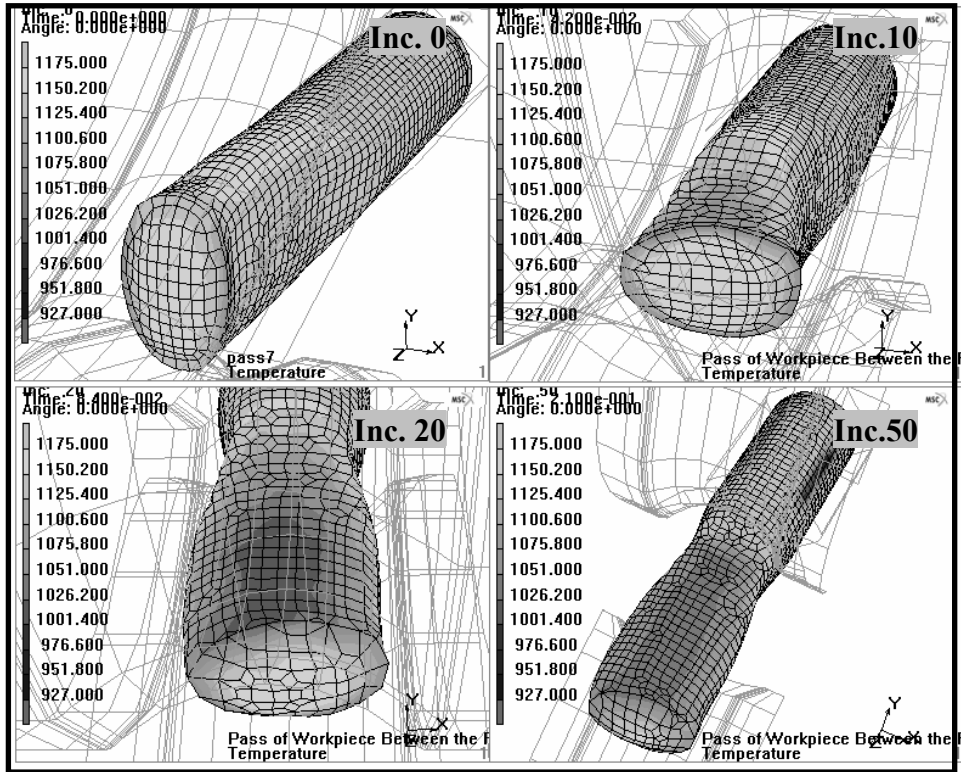


Figure 4.28 Temperature distribution on the workpiece in stage 2

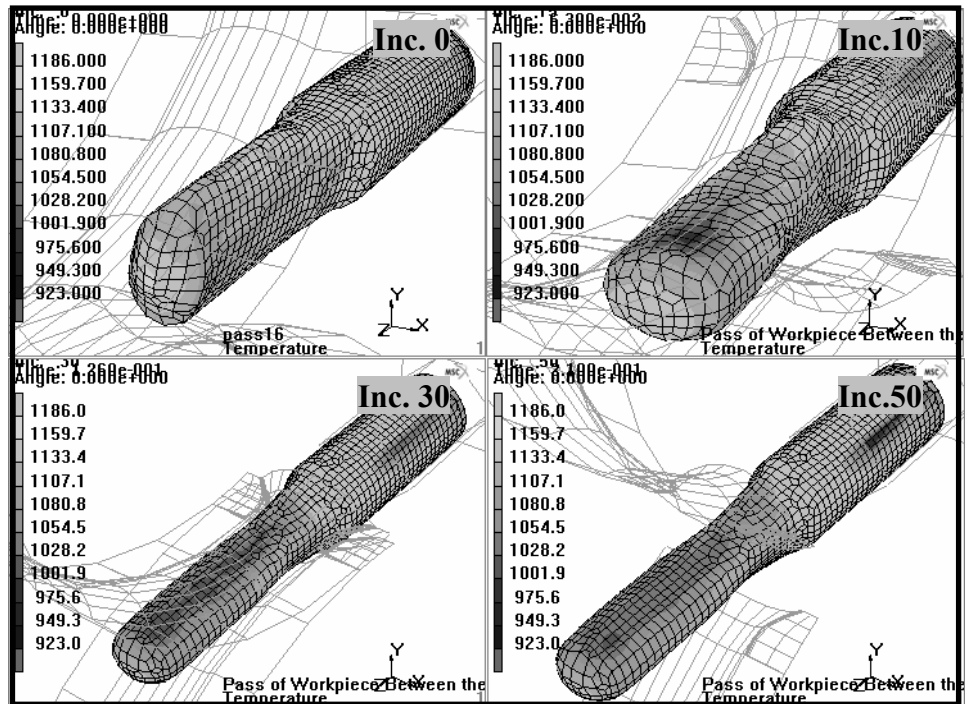


Figure 4.29 Temperature distribution on the workpiece in stage 3

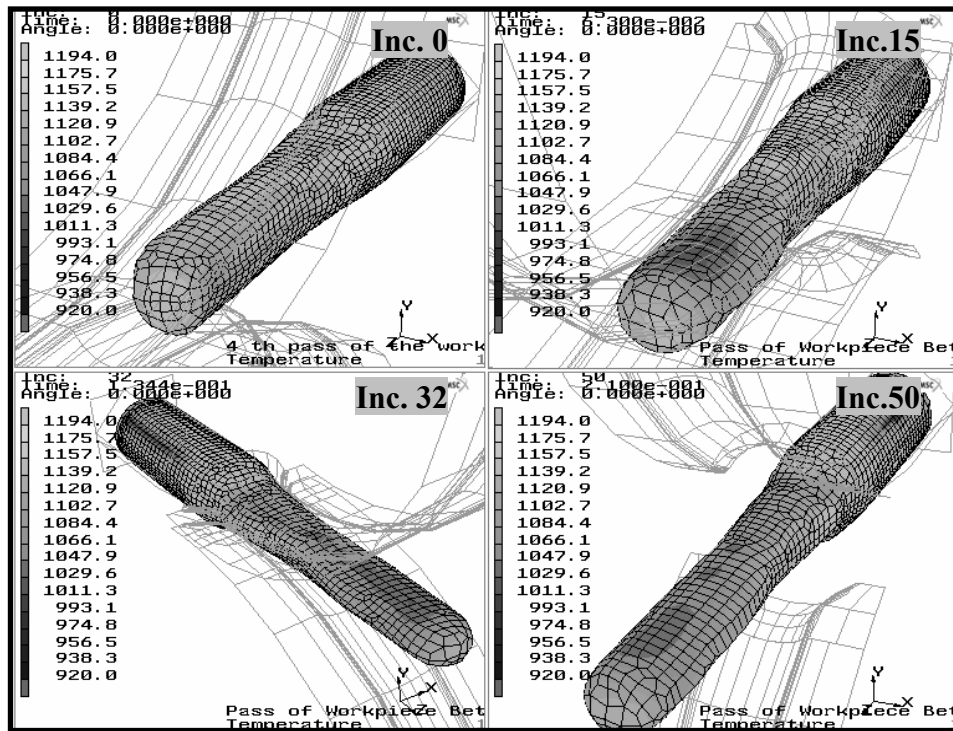


Figure 4.30 Temperature distribution on the workpiece in stage 4

The equivalent von Mises stress distributions on the surface of the workpiece are seen in Figures 4.32-4.35 for stages 1-4 at various increments, respectively. The maximum values of von Mises stress have been observed on the contact regions of the workpiece. The von Mises stress distributions in the interior of the workpiece are shown better in Figures 4.36-4.39.

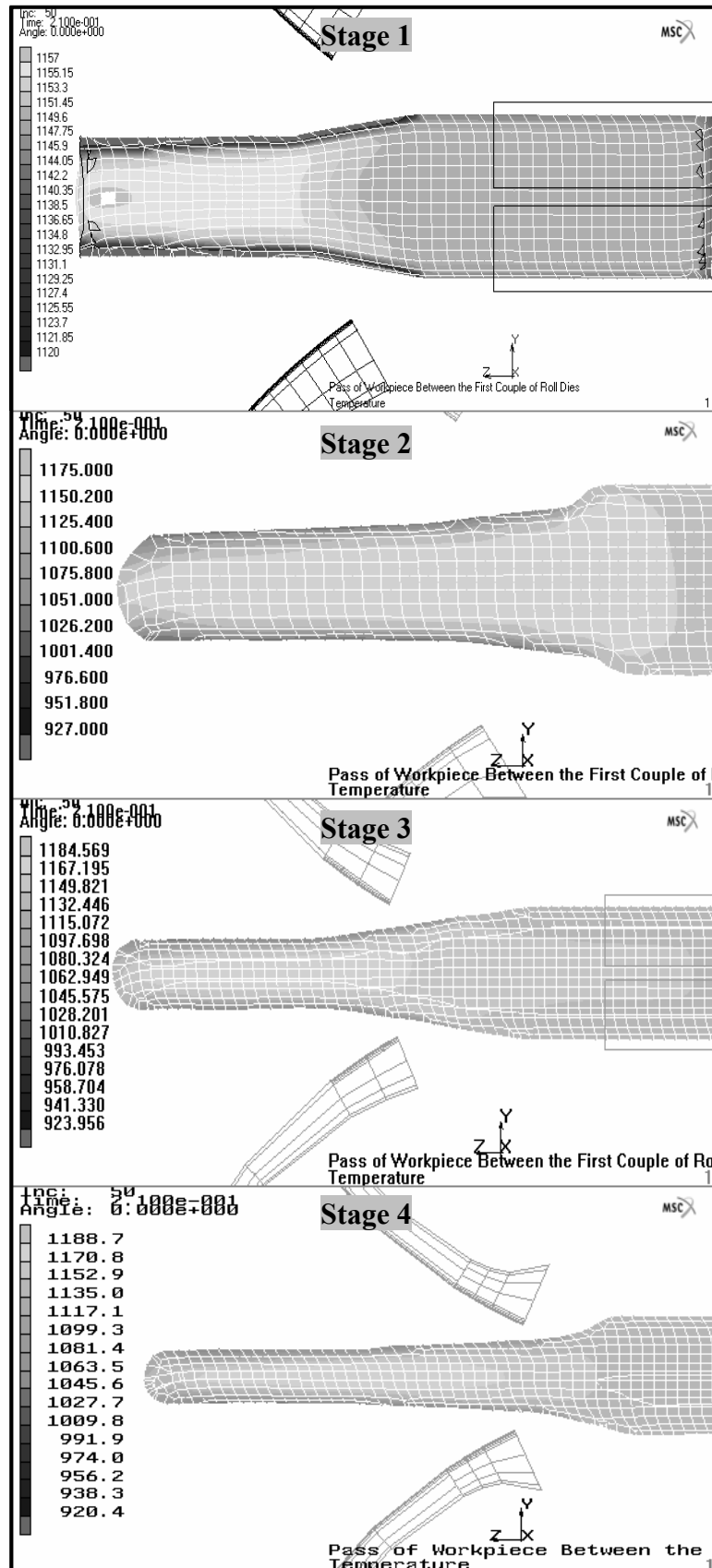


Figure 4.31 Temperature distribution inside the workpiece in stages 1-4

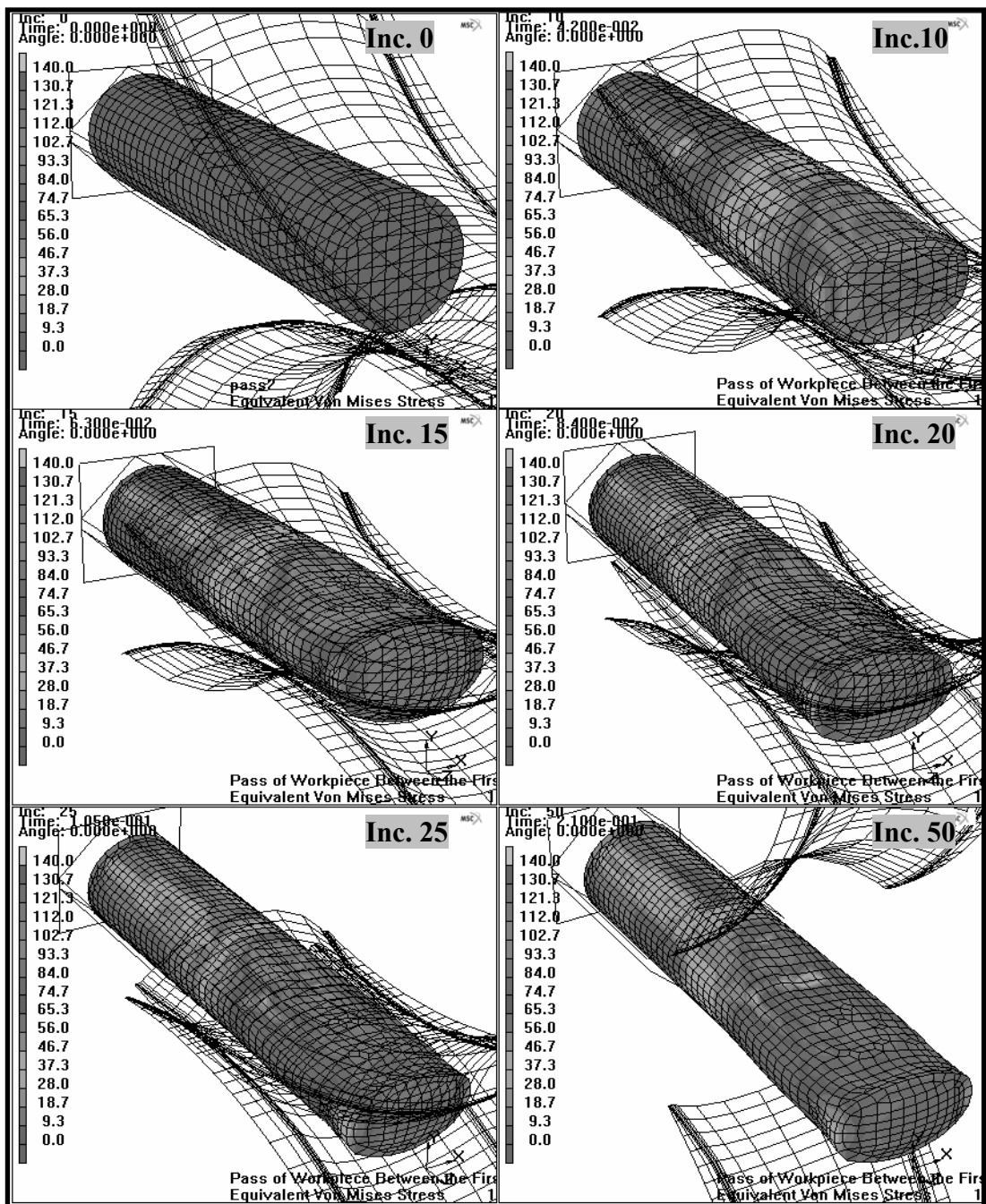


Figure 4.32 Equivalent von Mises stress distribution on the workpiece in stage 1

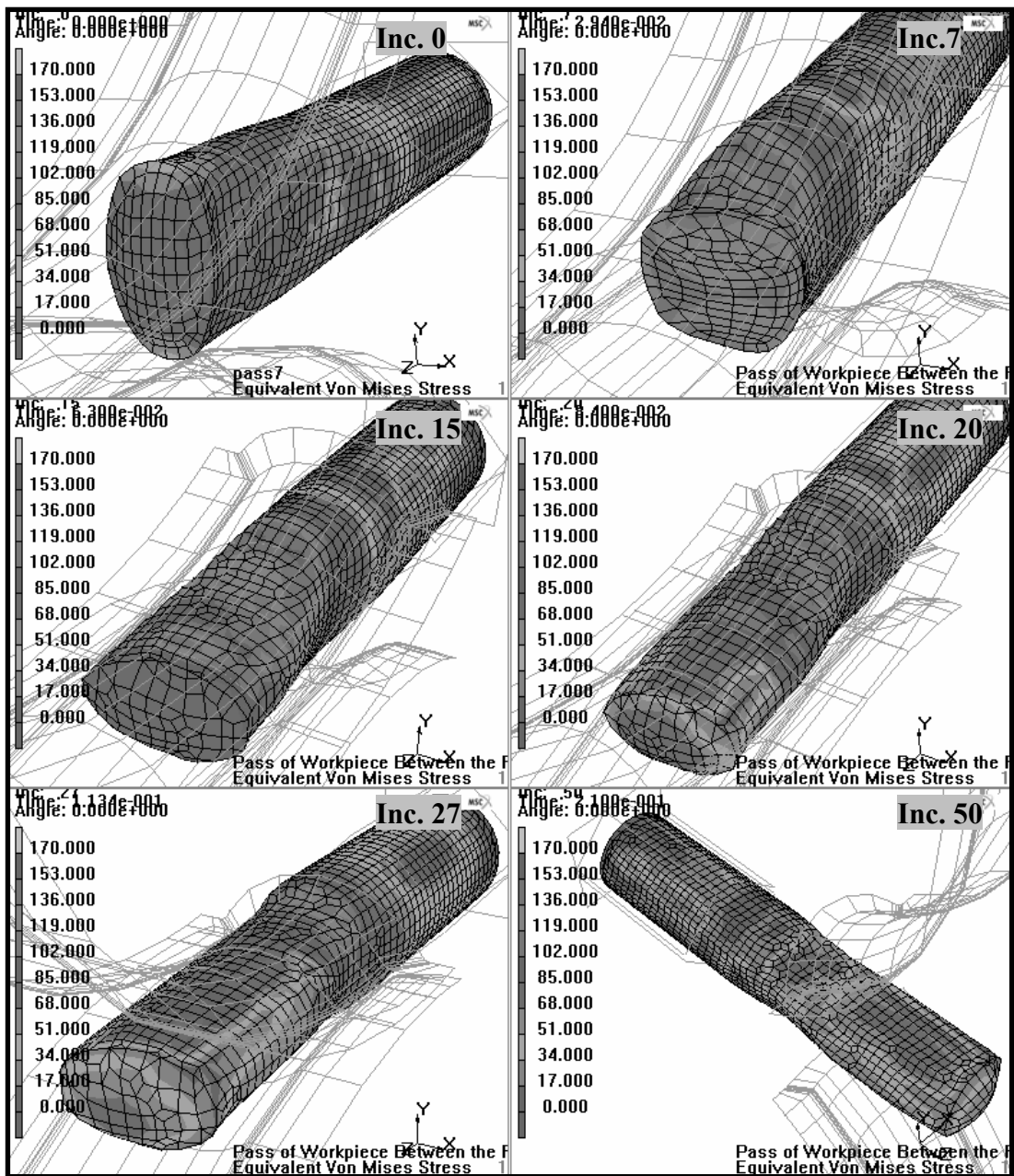


Figure 4.33 Equivalent von Mises stress distribution on the workpiece in stage 2

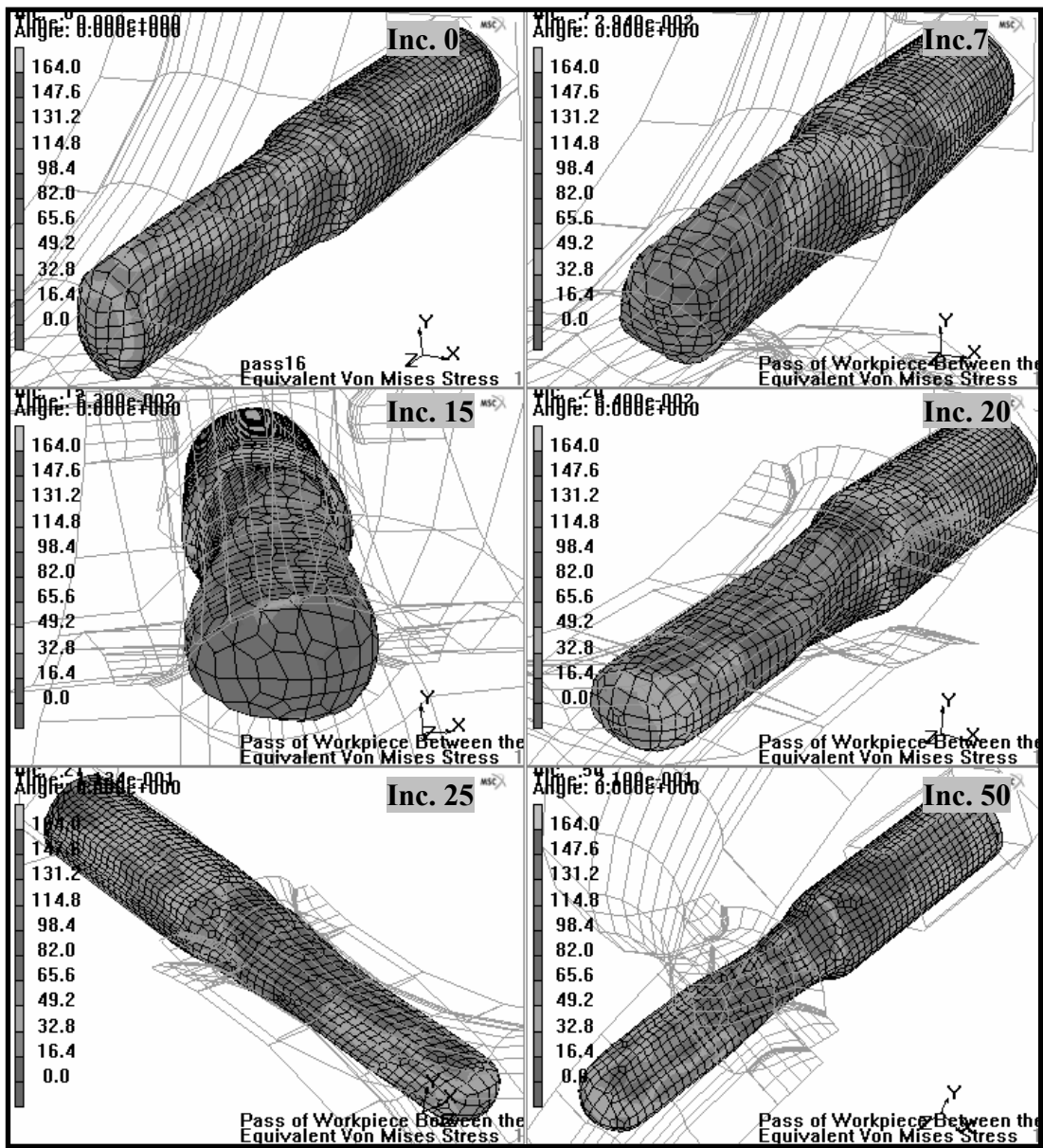


Figure 4.34 Equivalent von Mises stress distribution on the workpiece in stage 3

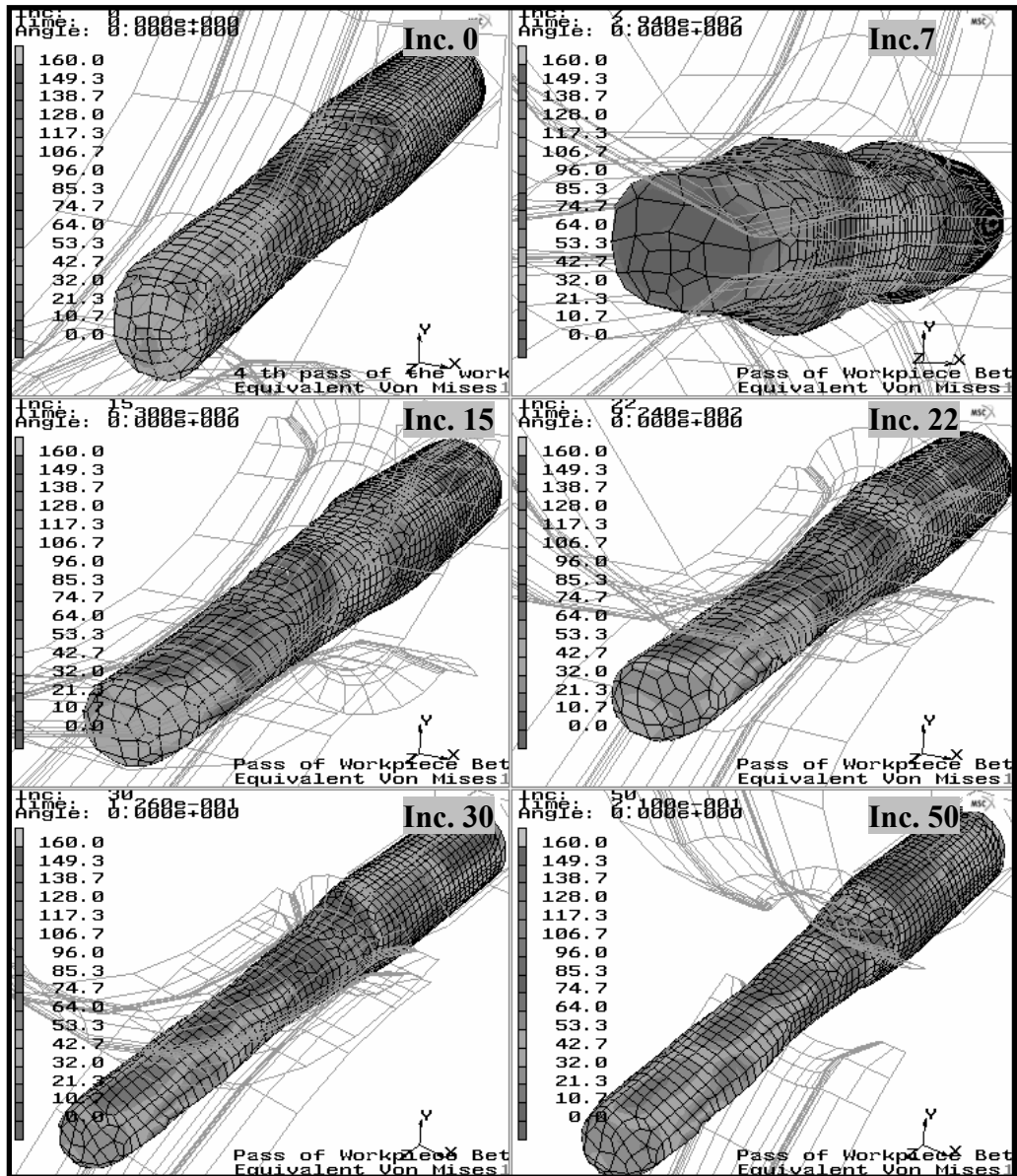


Figure 4.35 Equivalent von Mises stress distribution on the workpiece in stage 4

The highest value of von Mises stresses in stage 1 is 140 MPa. At the preliminary contact, the stress starts to propagate from corners to the centerline. At the progressive increments, the maximum stress zone remains at the contact of dies and workpiece. As the workpiece moves further, front end of the workpieces are released from the roll-forging dies. As a result, the stress decreases due to relaxation. Increment 50 shows the residual stress distribution on the workpiece at the end of stages. Residual stresses at center of workpiece are low. On the other hand, towards the surface, stresses are approximately two times the centers.

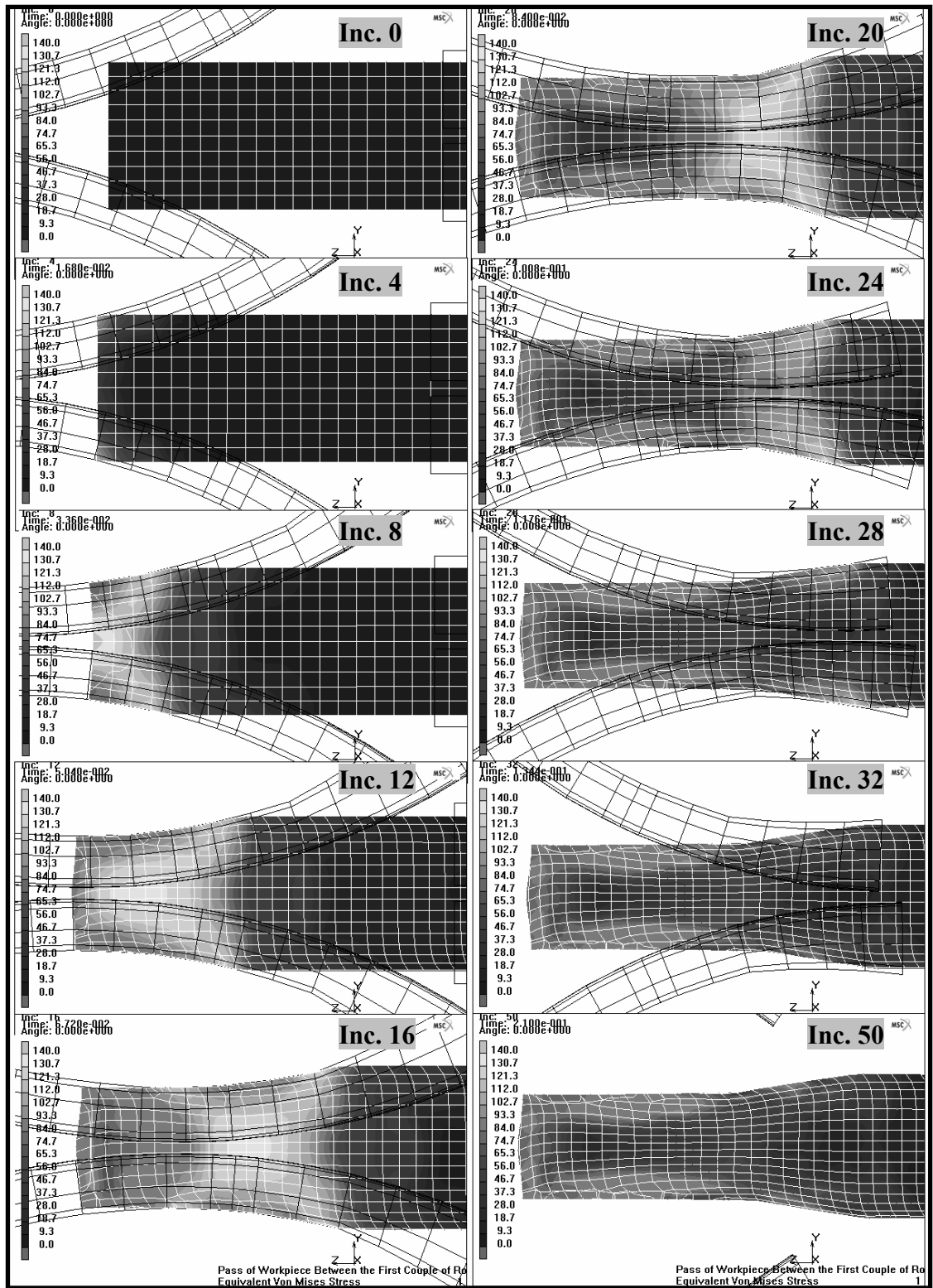


Figure 4.36 Equivalent von Mises stresses inside of workpiece in stage 1

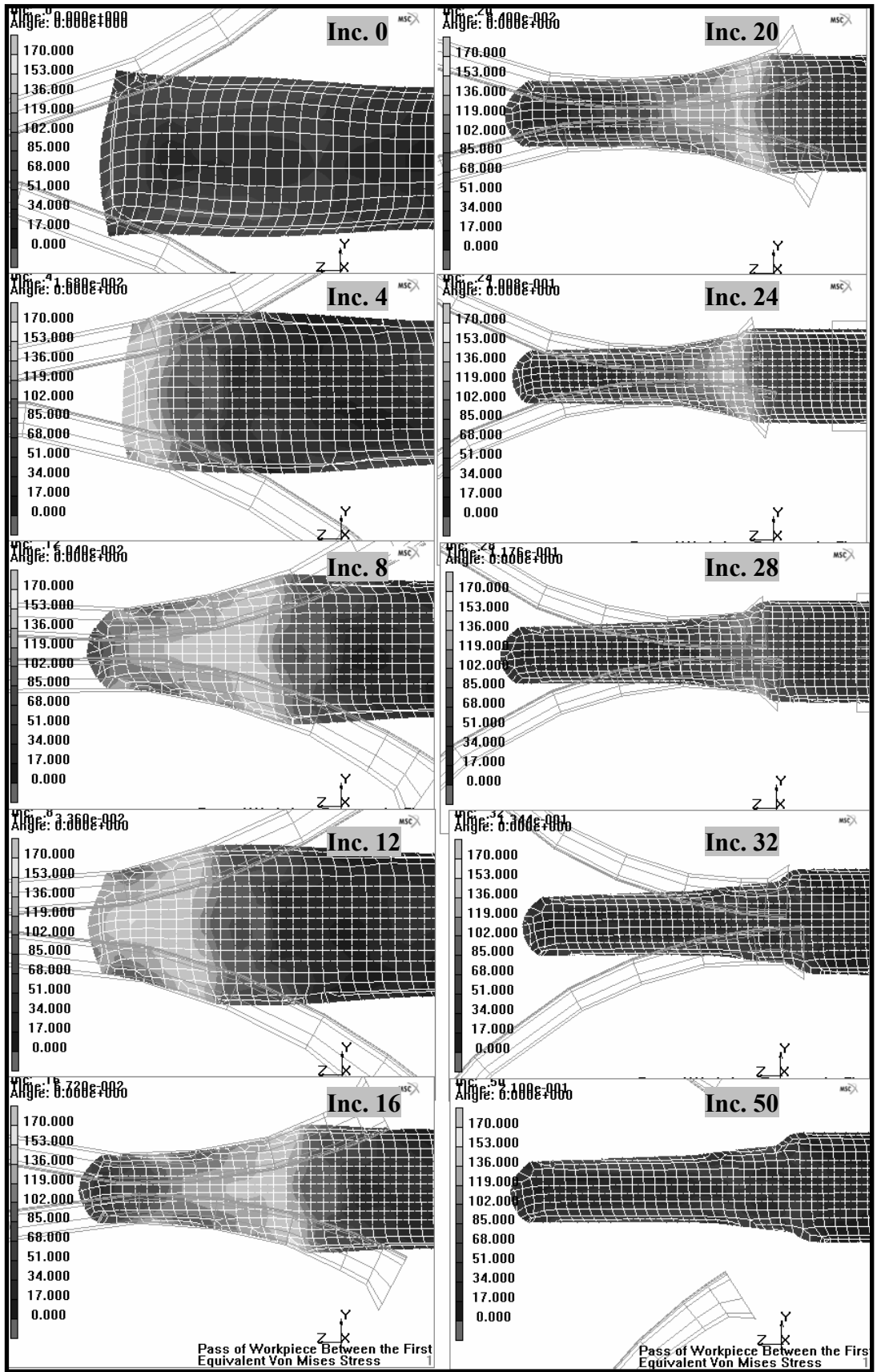


Figure 4.37 Distribution of von Mises stresses inside of workpiece in stage 2

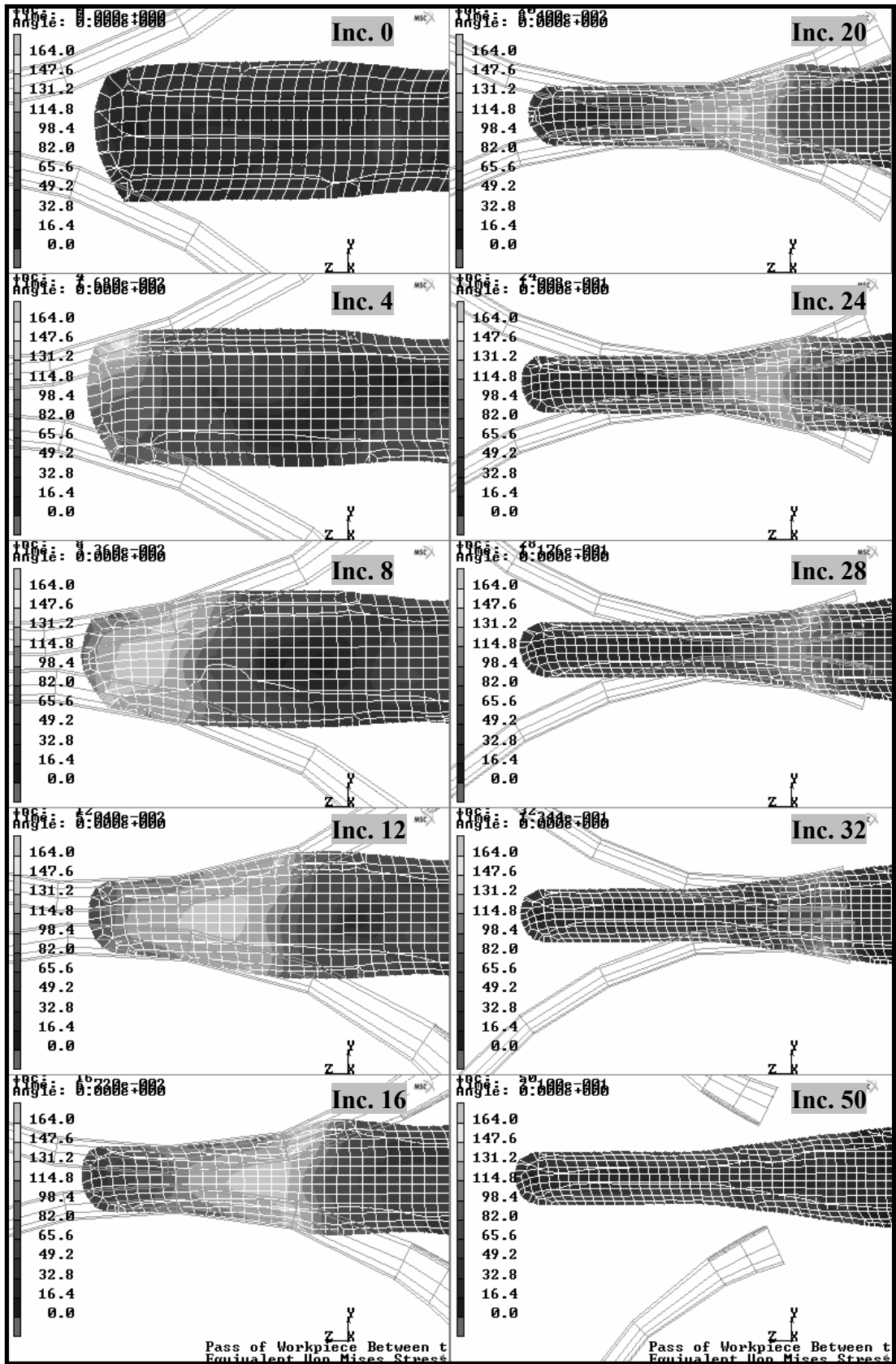


Figure 4.38 Distribution of von Mises stresses inside of workpiece in stage 3

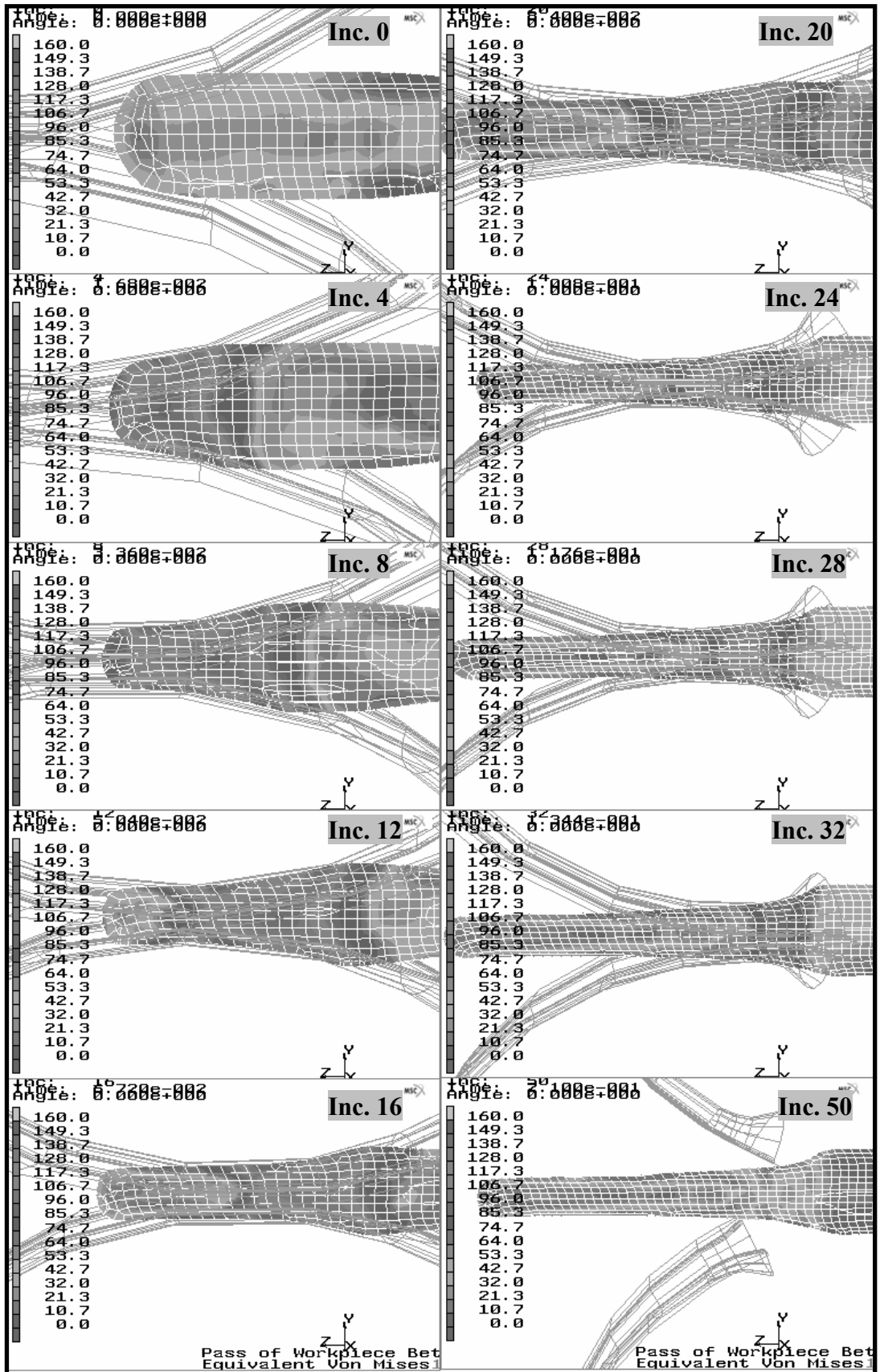


Figure 4.39 Distribution of von Mises stresses inside of workpiece in stage 4

The geometry of workpiece obtained at the end of the experiment and FEA simulation, for stages 1-4 have been compared in Figures 4.40-4.43. It is seen that almost the same geometries obtained in the stages 1-2. As seen in Figure 4.42 and Figures 4.43, there are some minor differences on the front end of the experimental and simulated workpieces although the results are in well agreement. Due to the remeshing and excessive deformation on the front end, edge lines on the end of the workpiece were lost.

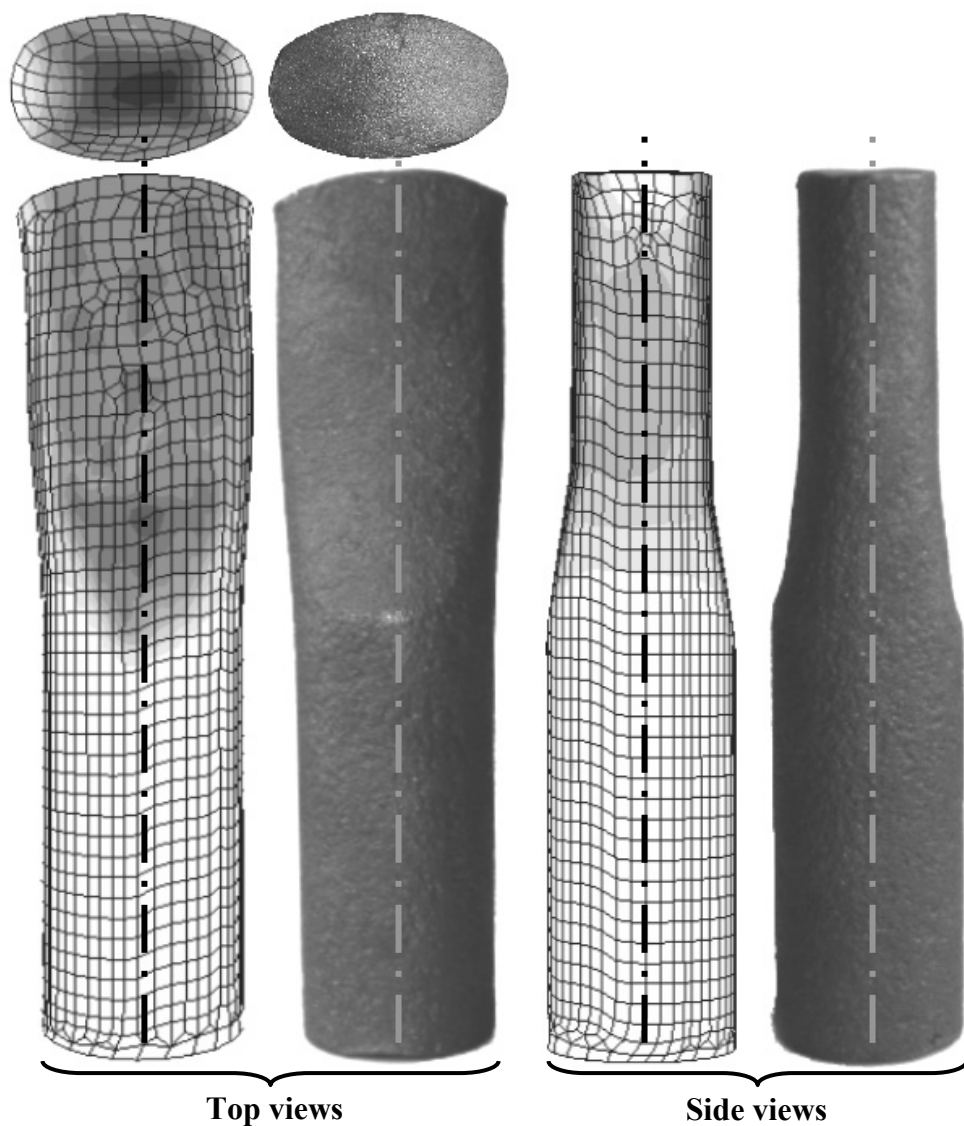


Figure 4.40 Comparison of experimental and simulated geometry of workpiece in stage 1

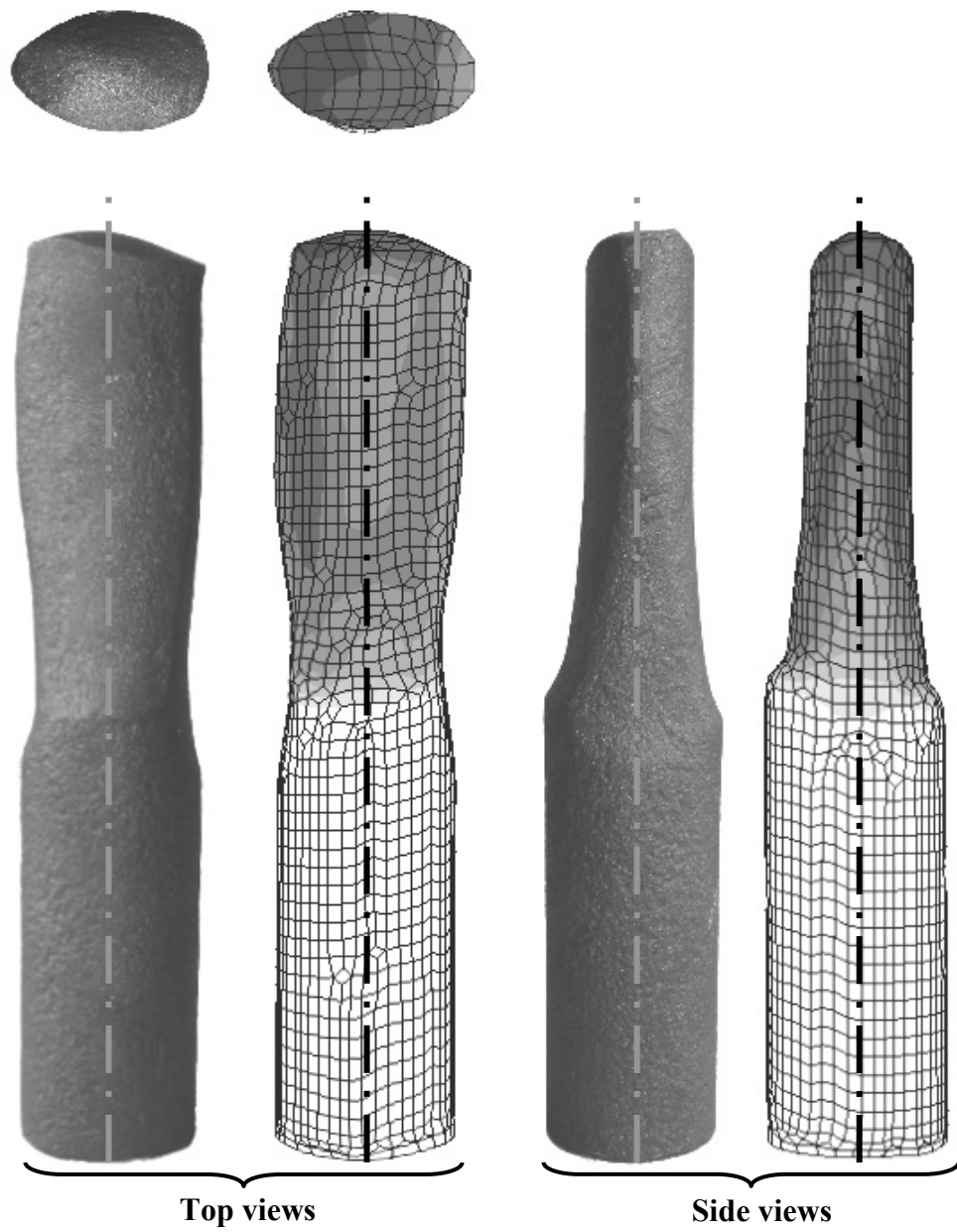


Figure 4.41 Comparison of experimental and simulated geometry of workpiece in stage 2

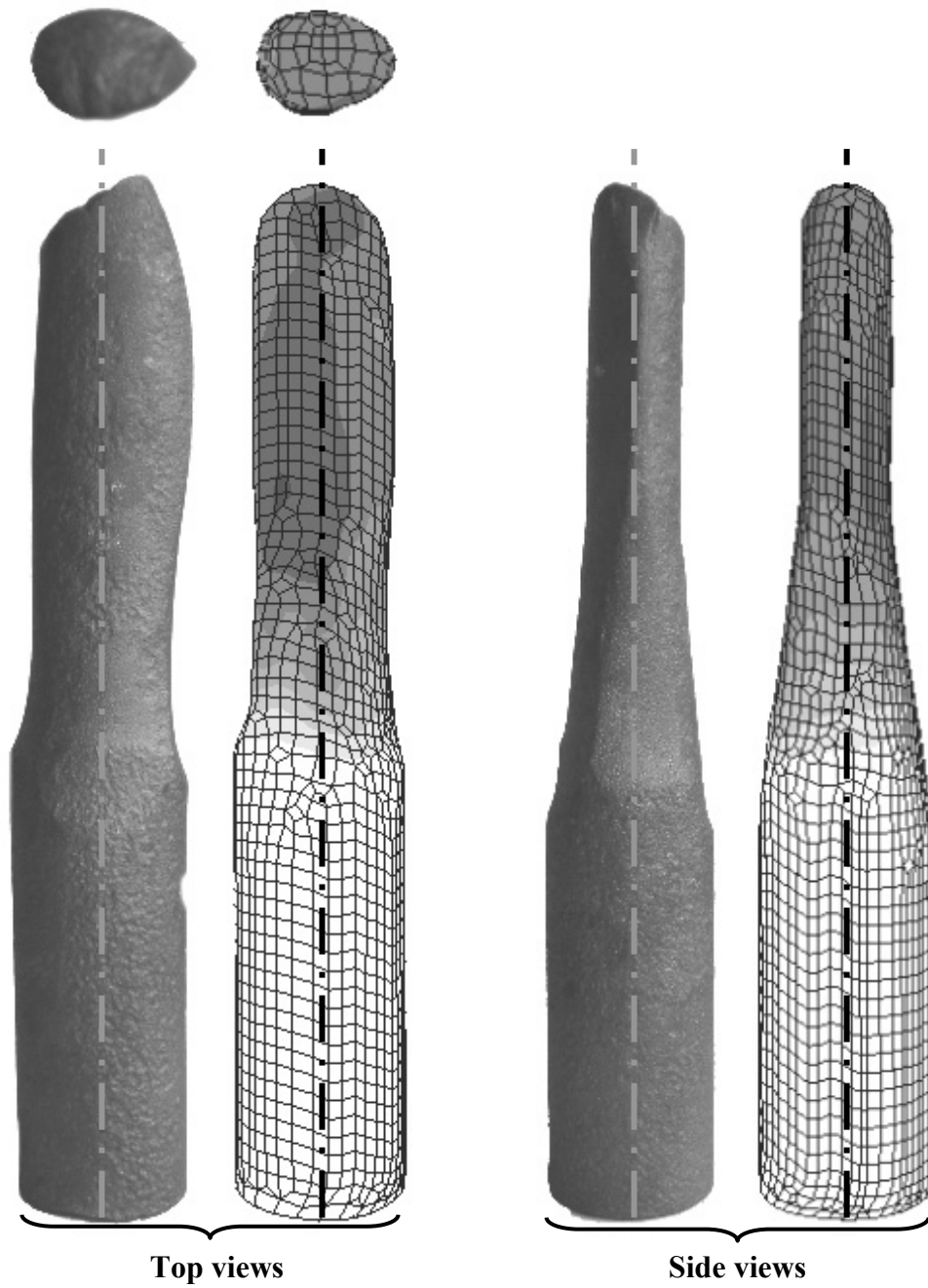


Figure 4.42 Comparison of experimental and simulated geometry of workpiece in stage 3

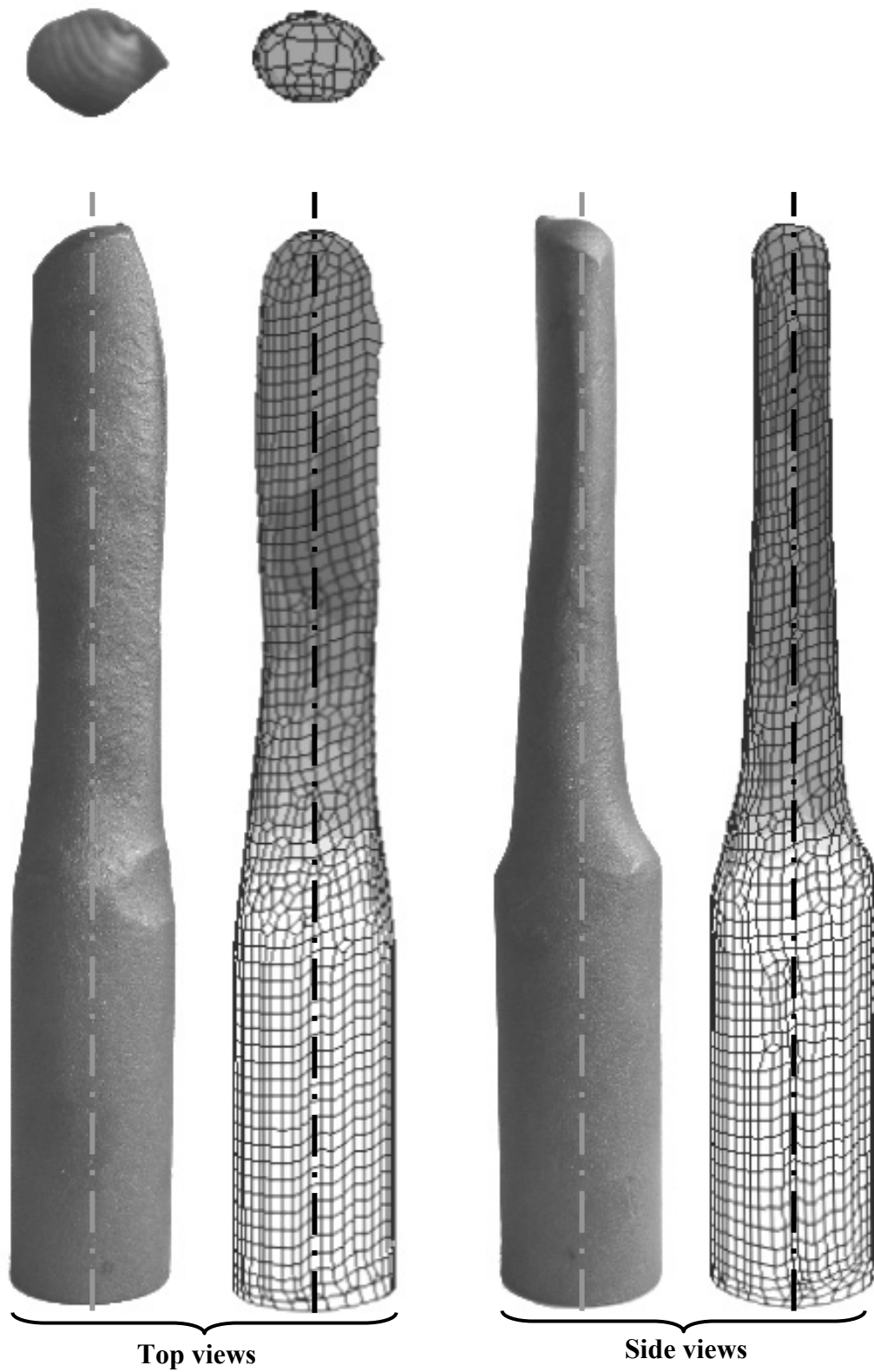


Figure 4.43 Comparison of experimental and simulated geometry of workpiece in stage 4

In Figure 4.44, the reduction of the cross section area of the workpiece through its length is given based on the simulation results. As seen in the figure, the vertical axis of the figure gives relative area with respect to initial cross sectional area of cylindrical billet, and the horizontal axis of the figure shows the distance from the rear end of the workpiece. The geometries of the workpieces at the end of each stage have also been given to show the material deformation. A length of about 50 mm is held by the tong and there is no deformation through the 80 mm distance from rear end of the billet but starts to reduce from this point. In the first stage reduction ratio is about 15 %. Similarly, the reduction ratio in the second stage in 80-115mm range is 35 %. In the 115-200mm range, reduction ratio further increases to 32 %. For the third stage, reduction ratios are 38 % and 55 % in the ranges 80-115mm and 115-200mm respectively. For the final stage, reduction ratio reaches to 65 % in the range 80-160mm. Further, 5 % percent reduction is observed after 160mm from the rear end of the billet. As seen from the figure that 70 % reduction in the cross section of the workpiece can be achieved in just four stages which takes less than 10 seconds.

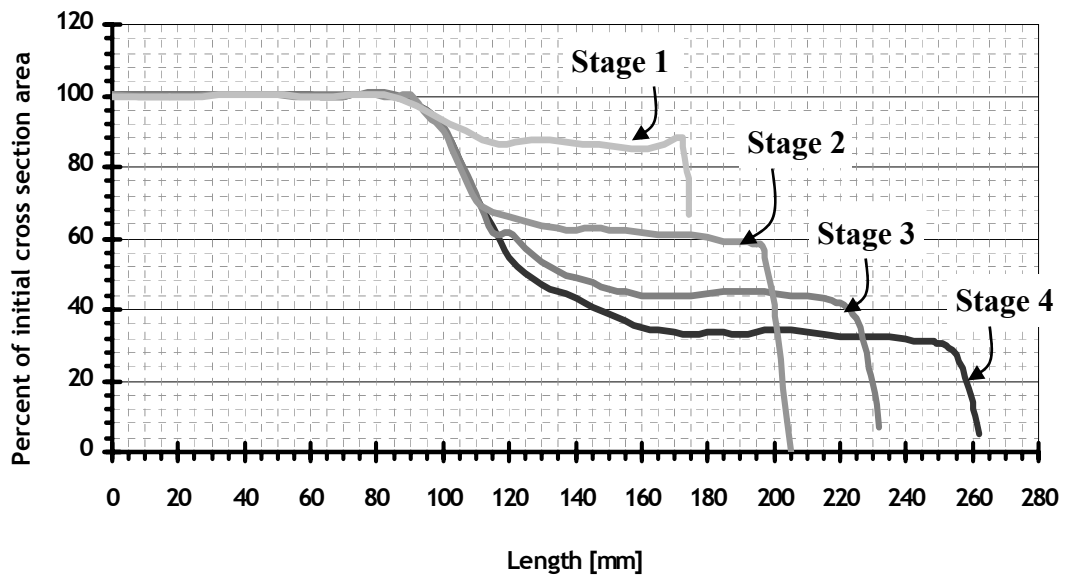
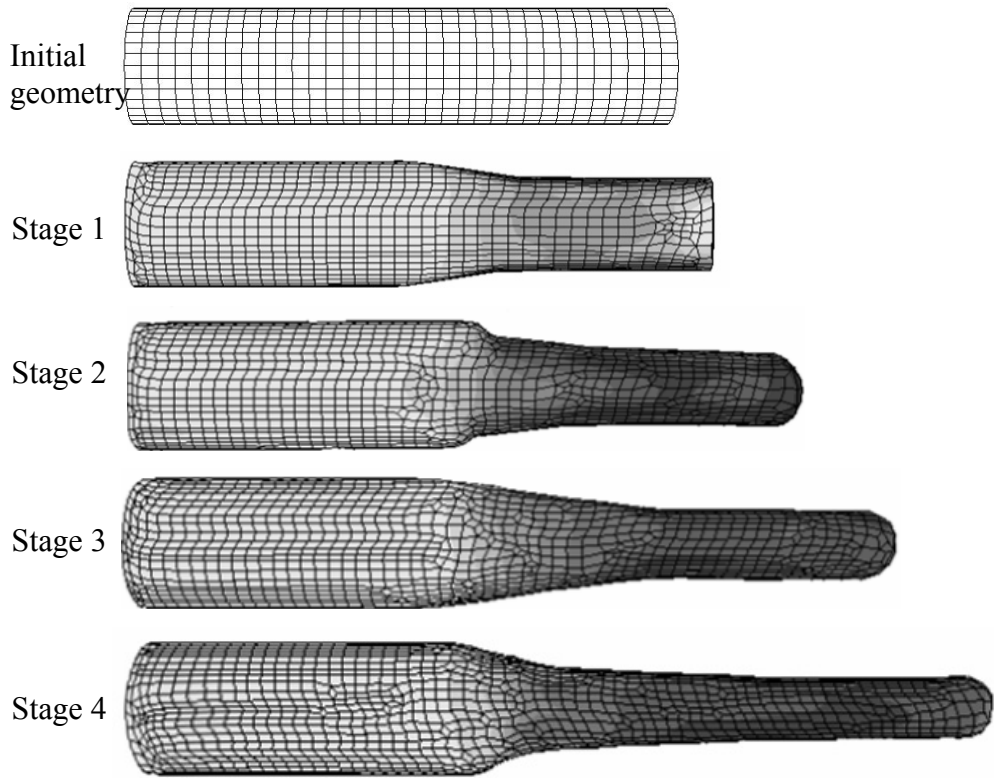


Figure 4.44 Volume distribution through the length of the workpiece at the end of each stage

CHAPTER V

CONCLUSIONS

In this study, multistage roll-forging process, which is mainly used for producing preforms in forging process, has been analyzed by Finite Element Method. A simplified and idealized finite element model by using symmetry assumption and a non-simplified finite element model of process have been used in the analyses. Four stages of the roll-forging of a particular part have been examined.

5.1 Conclusion

The following conclusions have been drawn from the current study;

1. When the symmetry assumption is used, it has been observed that the geometries obtained in experimental study mismatched to the geometry obtained in the finite element analysis. It has been determined that geometry of the workpiece at the end of the experiments did not have the symmetric material distribution along the longitudinal symmetry axis because of the misalignment of roll-forging dies used in experimental study. Consequently, the use of symmetry assumption has been found impractical for the particular case and it is necessary to model the actual case.
2. The finite element model has been revised by considering the misalignment of roll-forging dies. It was observed that the simulated geometries of the workpiece at the end of the first and second stages well agree with the geometries obtained in the experiments. For the third and fourth stages, some minor differences have been found on the front end of the workpiece due to loss of edges and details as the result of remeshing during FEA. However, it was seen that the spreading of material due to squeezing and the height reduction in the cross sections of part at experimental and simulation cases are similar to each other.

3. It has been observed from the temperature distribution in the workpiece that the temperature increases in inner sections of the workpiece due to heat generation and decreases on the contact surface due to the heat transfer to the roll-forging dies and tong as expected to be.
4. It was concluded that the FEA model in this study gives reasonable results and this approach can be used for the design of roll-forging process and related roll-forging dies.
5. According to the best knowledge of the author, this study is the first one successfully completed to simulate roll-forging process by using finite element analysis.

5.2 Recommendations for future work

The followings may be suggested as future works and extensions of this particular study;

1. A study may be conducted to design the roll-forging process by using the predetermined final geometry and optimize the amount of elongation at each roll pass to improve production efficiency and product quality.
2. The analysis may be performed considering different initial temperatures for the billets and roll-forging dies.
3. In addition, the analysis may be performed using different workpiece materials. Results may be compared with each other to understand the effect of workpiece material on the roll-forging process.
4. The finite element analysis for wear of roll-forging dies may be performed and compared with the roll-forging dies used in the forging industry.

5. Wedge rolling is another technique to produce preforms in forging. It may be valuable to analyze it and compare the wedge rolling and roll-forging in terms of productivity, geometric tolerances etc. by using computer simulation techniques.
6. Some studies may be done on the parts which can be entirely formed by using the roll-forging machine.
7. The results of the MSC.SuperForm, which is a finite element solver, may be compared to the results to be obtained by using other finite element programs such as FORGE3, QFORM3D, DEFORMTM-3D, ABAQUES or finite volume solver MSC.Superforge etc.

REFERENCES

- [1] T. Altan, Metal Forming Handbook, editor: New York, Springer-Verlag, 1998.
- [2] Engineers Edge, <http://www.engineersedge.com/forgings.htm> ,Last accessed; September 2005
- [3] ASM International, Metals Handbook Volume 14, Forming and Forging, Metal Park Ohio, 1988.
- [4] Vazquez, V. and Altan, T., 2000, “Die Design for Flashless Forging of Complex Parts,” Journal of Materials Processing Technology, Vol. 98, pp. 81-89.
- [5] Forging Industry Association (FIA), <http://www.forging.org/Design/toc.cfm>, Last accessed; September 2005
- [6] Mac-Hero-Grp, <http://www.mac-herogrp.com/strength.html>, Last accessed; September 2005
- [7] E.P. DeGARMO, Materials and Process in Manufacturing 6th ed., New York, Macmillan, 1984
- [8] Ali Fatemi and Mehrdad Zorouf, Fatigue Performance Evaluation of Forged versus Competing Manufacturing Process Technologies: A Comparative Analytical and Experimental Study, final report, The University of Toledo, 2004.
- [9] K. Lange, Hand Book of Metal Forming, McGraw-Hill Company, 1985.
- [10] Müller Weingarten,
http://www.muellerweingarten.de/web/produkte/index_p.cfm, Last accessed; September 2005
- [11] ULS70R Cross-rolling machine catalogue, Smeral catalogue
- [12] Zhong-Yi Cai, “Precision design of roll-forging die and its application in the forming of automobile front axles “ Journal of Material Processing Technology, 2005
- [13] ARWS documents, SMS Eumuco GmbH,

- [14] S.K. Biswas and W.A. Knight, 'Towards an Integrated Design and Product System for Hot Forging Dies' Int. J. Prod. Res., p23 (1976)
- [15] D.J.Joyce, 'Combination Die and Tool Design for Quantity Production', Metal Treatment, 32, p 3, (1965)
- [16] Y.K. Chan, W.A.Knight 'Computer Aided Design and Manufacture of Dies for Lonh Hot Forgings' 6th North American Metal Research Conference, Florida, p 455, 1978
- [17] S.K.Biswas, W.A. Knight, 'Computer Aided Preform Design for Long Hot Forgings' 17th Machine Tool Design and Research Conference, Birmingham, p 27, 1976
- [18] ERATZ-Engineering, http://www.eratz.de/index_e.htm, Last accessed; September 2005
- [19] Alper, E., "Computer Aided Design of Axisymmetric Press Forging", M. S. Thesis, Middle East Technical University, Ankara, 2001.
- [20] Kutlu, A., E., "Analysis and Design of Preforms for Non-axisymmetric Press", M. S. Thesis, Middle East Technical University, Ankara, 2001.
- [21] Karagözler, A., B., "Analysis and Preform Design for Long Press Forgings with Non-Planar Parting Surfaces", M. S. Thesis, Middle East Technical University, Ankara, 2003.
- [22] Gülbahar, S., "Preform Design for Forging of Heavy Vehicles Steering Joints", M. S. Thesis, Middle East Technical University, Ankara, 2005.
- [23] Doğan, Ö., "Finite Element Analysis of Effect of Tapered Preforms on Final Product in Cold Upsetting, M. S. Thesis, Middle East Technical University, Ankara, 2000.
- [24] Kazancı, E., "Analysis of Hot Upset Forging with Non-Circular Cross-Sections", M. S. Thesis, Middle East Technical University, Ankara, 2002.
- [25] S.-Y. Kim, Y. -T. Im, "Three dimensional finite element analysis of non-isothermal shape rolling", Journal of Material Processing Technology, 127(2002), pp:57-63
- [26] MSC.SuperForm Command Reference, Marc Analysis Research Corporation, 2004

- [27] MSC.Marc User's Guide Volume A: Theory and User Information, Marc Analysis Research Corporation, 2003
- [28] ASM international, Handbook of Workability and Process Design, Ohio, 2004
- [29] MSC.SuperForm User's Guide, Marc Analysis Research Corporation, 2004
- [30] Technical documents of Roll-forging machine
- [31] Civelekoğlu, B., "Analysis of Forging for Three Different Alloy Steels ", M Sc. Thesis, Middle East Technical University, 2003
- [32] MSC.SuperForm Database for friction coefficient,
- [33] MSC.SuperForm material database, Marc Analysis Research Corporation, 2004
- [34] SAM 5.0 User guide, ARTAS-Engineering Software, 2003
- [35] The DXF Reference, AutoDesk Inc. 2005

APPENDIX A

FEATURES OF THE ROLL-FORGING MACHINE USED IN THE STUDY

The features of the roll-forging machine that has been shown in Figure 1-7 and 3.2 is given in Table A.1

Table A.1 Features of Roll-Forging Machine used in the Study

Main Dimensions of Machine Body (LengthXHeightXWidth)	5.7x2x2.8 m
Roll Shaft Diameter	240 mm
Maximum Available Die Diameter	368 mm
Rotational Velocity of Roll Shaft	79 rpm
Maximum Diameter of Workpiece	55 mm
Power of motor which drives flywheel	15 kW
Rotational Velocity of Motor	1500 rpm
Power of oil pump motor	3 kW
Air Tank Capacity	30 Lt
Air Pressure	6 bar
Oil Tank Capacity	10 Lt
Oil Pressure	55 bar

APPENDIX B

MECHANISM ANALYSES OF SECOND ROBOT ARM

The position and velocity analyses of second robot arm of the Roll-forging machine are required for the thesis study. In the Finite Element Analysis of roll-forging process, it is important to correctly input the position of the tong of second robot arm with respect to the angular position of the roll-forging dies and velocity of the tong. The position and velocity analyses have been made to be able to realistically model the process and coincide the section of workpiece to die cavity as in the application.

In the analysis of robot arm mechanism, a mechanism design tool SAM 5.0 (Simulation and Analysis of Mechanisms)[34] has been used. This is an interactive PC-software for the design and analysis for motion and force at arbitrary planar mechanisms. The dimensions of mechanism are obtained from the technical drawings of the roll-forging machine. The joints and linkages of mechanism described in Figure 3.5 are drawn in CAD environment and saved in DXF [35] format to import to SAM 5.0. The results of mechanism analysis by using SAM 5.0, which includes displacement (U_x) and velocity (V_x) of the tong, absolute angle (A) of linkage A, position difference of tong and joint 1 (D_x) on x direction are given in Figure B.1. These are used in Finite Element Analysis as the motion and position of the tong.

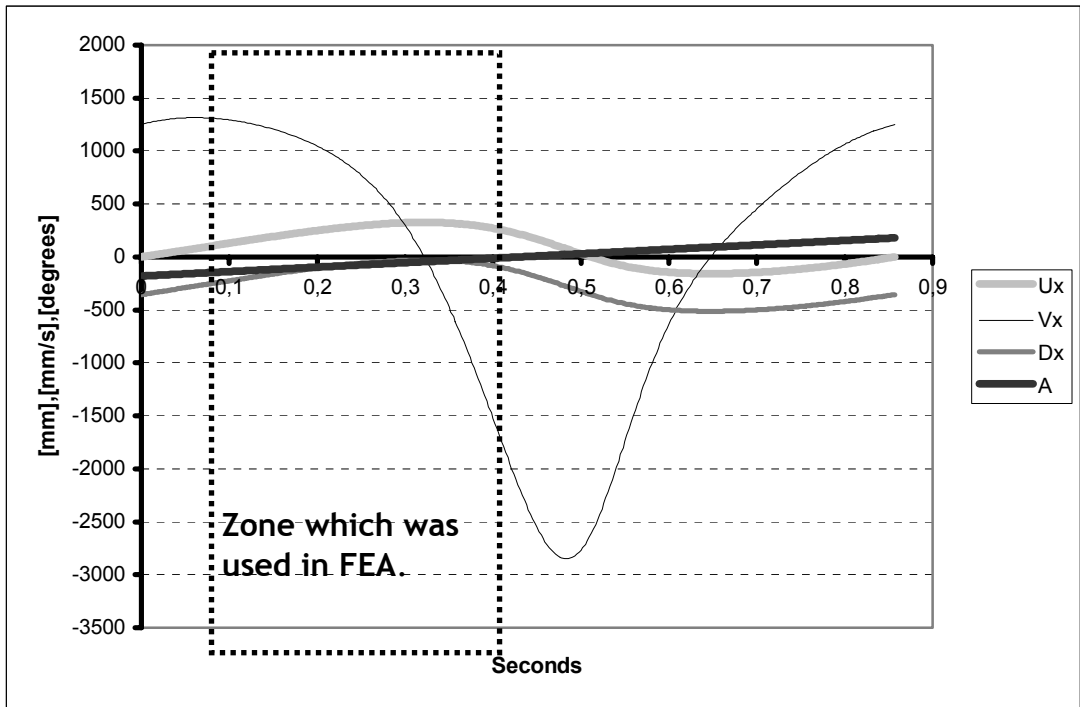


Figure B.1 Analysis result for one rotation of the roll shaft in 0.857 sec.